APPLICATION OF REMOTE SENSING (RS) AND GEOGRAPHIC INFORMATION SYSTEM (GIS) TECHNOLOGY TO DETERMINE YIELD PREDICTION IN MAIZE

Master of Science Thesis

Nghi Tan DO

Eskişehir, May 2019

APPLICATION OF REMOTE SENSING (RS) AND GEOGRAPHIC INFORMATION SYSTEM (GIS) TECHNOLOGY TO DETERMINE YIELD PREDICTION IN MAIZE

Nghi Tan DO

MASTER OF SCIENCE THESIS

Department of Remote Sensing and Geographical Information System

Supervisor: Assist. Prof. Dr. Zehra YİĞİT AVDAN

Eskişehir

Anadolu University

Graduate School of Science

May 2019

FINAL APPROVAL FOR THESIS

This thesis titled “APPLICATION of REMOTE SENSING (RS) and GEOGRAPHIC INFORMATION SYSTEM (GIS) TECHNOLOGY to DETERMINE YIELD PREDICTION in MAIZE” has been prepared and submitted by Nghi Tan DO in partial fullfillment of the requirements in “Anadolu University Directive on Graduate Education and Examination” for the Degree of Master of Science in Department of Remote Sensing and Geographical Information System has been examined and approved on 27/05/2019.

Committee Members		**Signature**
Supervisor	: Assist. Prof. Dr. Zehra YİĞİT AVDAN	………...
Member	: Assist. Prof. Dr. Emrah PEKKAN	………..
Member	: Assist. Prof. Dr. Resul ÇÖMERT	………...

Director

Graduate School of Science

ABSTRACT

APPLICATION OF REMOTE SENSING (RS) AND GEOGRAPHIC INFORMATION SYSTEM (GIS) TECHNOLOGY TO DETERMINE YIELD PREDICTION IN MAIZE

Nghi Tan DO

Department of Remote Sensing and Geographical Information System

Anadolu University, May 2019

Supervisor: Assist. Prof. Dr. Zehra YİĞİT AVDAN

In the 21st century, precision agriculture is becoming more and more common, increasing crop yield and reducing costs in agriculture. Advanced geographic technology (Geographic Information System-GIS, Remote Sensing-RS technology, Global Navigation Satellite System-GNSS) played an important role in determining input variables of precision agriculture system. In particular, remote sensing technology with higher-end image processing techniques (spatial, spectral, temporal, and radiometric resolution) enhanced the accuracy of the crop yield models. This thesis has two main purposes: the first one presented an overview of the capabilities of remote sensing technology in maize yield forecast from its beginning time up to now through the many specific studies. It also reviewed a variety of vegetation indices (VIs) derived from remote sensing data that had a high correlation with corn yield measured. Furthermore, the literature proved that the remarkable development of remote sensing technology at each different platforms have improved significantly the accuracy of maize yield prediction before harvest. The other goal determined the correlation of the vegetation indices (NDVI, EVI, SAVI, WDRVI, GNDVI) derived from Landsat-8 and Sentinel-2 images and building the maize yield predicting models for the study area based on the Bayesian Model Averaging (BMA) method. This research determined 2 optimal models which were validated with RMSE = 9.38 t/ha for Landsat-8 and RMSE = 12.33 t/ha for Sentinel-2. The QGIS and R software were used throughout the process of spatial analysis and statistical data analysis. In the near future, remote sensing and open-source software will definitely become an absolutely necessary component of precision agriculture.

Keywords: *remote sensing, precision agriculture, vegetation indices, maize yield forecasting model, open-source software*

ÖZET

UZAKTAN ALGILAMA (UA) VE COĞRAFİ BİLGİ SİSTEMİ (CBS) TEKNOLOJİSİ KULLANILARAK MISIR BİTKİSİNİN VERİMİNİN TAHMİN EDİLMESİ

Nghi Tan DO

Uzaktan Algılama ve Coğrafi Bilgi Sistemleri Anabilim Dalı

Anadolu Üniversitesi, Mayıs 2019

Danışman: Dr. Öğr. Üyesi Zehra YİĞİT AVDAN

21. yüzyılda, hassas tarım gitgide yaygınlaşmakta, ürün verimi artmakta ve tarım maliyetleri azalmaktadır. İleri teknoloji (Coğrafi Bilgi Sistemi-CBS, Uzaktan Algılama-UA Teknolojisi, Global Navigasyon Uydu Sistemi-GNSS), hassas tarım sisteminin giriş değişkenlerinin belirlenmesinde önemli bir rol oynamıştır. Özellikle, ileri görüntü işleme teknikleriyle (mekansal, spektral, zamansal, ve radyometrik çözünürlük) uzaktan algılama teknolojisi ürün verim modellerinin doğruluğunu arttırmıştır. Bu tezin birinci amacı, başlangıç zamanından bugüne kadar ki birçok özel çalışma vasıtasıyla mısırın verim tahmininde uzaktan algılama teknolojisinin kabiliyetlerine genel bir bakış sunulmasıdır. Ayrıca, ölçülen mısır verimi ile yüksek korelasyonu olan uzaktan algılama verilerinden elde edilen çeşitli bitki örtüsü indisleri (VIs) de hesaplanmıştır. Bunun yanında, literatür çalışmaları kapsamında her bir farklı platformda uzaktan algılama teknolojisi ile ilgili çalışmalar derlenmiştir. Bu teknolojilerin gelişmesiyle birlikte, hasattan önce mısır verim tahmininin ilişkisini önemli ölçüde geliştirdiği gözlenmiştir. Tezin ikinci amacı ise Landsat-8 ve Sentinel-2 görüntülerinden elde edilmiş vejetasyon indekslerinin (NDVI, EVI, SAVI, WDRVI, GNDVI) korelasyonunun belirlenmesi ve Bayesian Model Averaging (BMA) metodu baz alınarak çalışma alanı için mısır verimini ön gören modellerin oluşturulmasıdır. Mekansal analiz ve istatistiksel veri analizi süresince QGIS ve R yazılımı kullanılmıştır. Mekansal ve spektral çözünürlüğe bakarak yakın gelecekte, uzaktan algılama ve açık-kaynak yazılımı kuşkusuz hassas tarım için mutlak gerekli bir bileşen ve güçlü bir ürün verimi tahmin aracı olacaktır.

Anahtar Sözcükler: *Uzaktan Algılama, Hassas Tarım, Vejetasyon İndeksi, Mısır Verim Tahmin Modeli, Açık-Kaynak Yazılımı*

STATEMENT OF COMPLIANCE WITH ETHICAL PRINCIPLES AND RULES

I hereby truthfully declare that this thesis is an original work prepared by me; that I have behaved in accordance with the scientific ethical principles and rules throughout the stages of preparation, data collection, analysis and presentation of my work; that I have cited the sources of all the data and information that could be obtained within the scope of this study, and included these sources in the references section; and that this study has been scanned for plagiarism with “scientific plagiarism detection program” used by Anadolu University, and that “it does not have any plagiarism” whatsoever. I also declare that, if a case contrary to my declaration is detected in my work at any time, I hereby express my consent to all the ethical and legal consequences that are involved.

27/05/2019

Nghi Tan DO

ACKNOWLEDGEMENTS

Firstly, I would like to express my sincere gratitude to my supervisor Assistant Professor Dr. Zehra YİĞİT AVDAN for the continuous guidance and support of my master study and related research with her patience, enthusiasm, and expert knowledge. Besides my advisor, special thanks to Associate Professor Dr. Uğur AVDAN who gave advice, guidance, valuable feedback so that I could complete my thesis in the best way.

I would like to thank my friends and colleagues at the Earth and Space Sciences Institute who helped, supported, encouraged, motivated and created favourable conditions throughout the time of my master course.

I would like to thank the Turkish government funded the scholarship and supported me during 3 years of studying and living in Turkey.

Finally, my thesis would not have been possible without the support and encouragement of my family and friends. I would like to express my very profound gratitude to my parents, my sisters, and my girlfriend for standing by me all the time.

Thank you all.

TABLE OF CONTENTS

Page

Page

Page

LIST OF TABLES

LIST OF FIGURES

Page

LIST OF ABBREVIATIONS

AVHRR	: Advanced Very High-Resolution Radiometer
BMA	: Bayesian Model Averaging
BIC	: Bayesian Information Criterion
CASI	: Compact Airborne Spectrographic Imager
CERES	: Crop Environment Resource Synthesis
CHRIS	: Compact High-Resolution Imaging Spectrometer
CIMMYT	: International Maize and Wheat Improvement Center
CRAN	: Comprehensive R Archive Network
CSM	: Cropping System Model
DEM	: Digital Elevation Model
EC	: European Commission
ESA	: European Space Agency
fAPAR	: The fraction of Absorbed Photosynthetically Active Radiation
FAO	: Food and Agriculture Organization of the United Nations
GBAO	: Ground-Based Active Optical sensors
GDAL	: Geospatial Data Abstraction Library
GIS	: Geographic Information System
GNSS	: Global Navigation Satellite System
GPS	: Global Positioning System
GRASS	: Geographic Resources Analysis Support System
GYURI	: General Yield Unified Reference Index
IDE	: Integrated Development Environment
IFAD	: International Fund for Agricultural Development
LIDAR	: Light Detection and Ranging
MCRM	: Maize and the Markov Chain Canopy Reflectance Model
MMS1	: Monolithic Miniature Spectrometer
MODIS	: Moderate Resolution Imaging Spectroradiometer
NASA	: National Aeronautics and Space Administration
NASS	: National Agricultural Statistics Service
NOAA	: National Oceanic and Atmospheric Administration
OSGeo	: Open Source Geospatial Foundation

PAR	: Photosynthetically Active Radiation
PostGIS	: Geographic Database Management System
PRISM	: Parameter-Elevation Relationships on Independent Slopes Model
QGIS	: Quantum Geographic Information System
RADAR	: RAdio Detection and Ranging
RMSE	: Root Mean Square Error
RS	: Remote Sensing
RS–P–YEC	: Remote Sensing–Photosynthesis–Yield Estimation for Crops
SAGA	: System for Automated Geoscientific Analyses
SARs	: Synthetic Aperture Radars
SONAR	: Sound Navigation and Ranging
UAV	: Unmanned Aerial Vehicle
UNICEF	: United Nations Children's Fund
USDA	: United States Department of Agriculture

1. INTRODUCTION

1.1. Context and Background

After the first aerial imagery was taken in 1858 by Gaspaed Felex Tournachon from a balloon (Slonecker et al., 1999), the earliest application of aerial photographs in agriculture was done by the Agricultural Adjustment Administration of the United States for precise measurements of cropland in the 1930s (Monmonier, 2002). According to Colewell, 1956, remote sensing technology has been used in agriculture since the 1950s. Moreover, some researchers argued that satellites remote sensing have been used in agriculture since the early 1970s when Landsat 1 was launched in 1972 (Bauer & Cipra, 1973; P. C. Doraiswamy et al., 2003; Jewel, 1989; National Agricultural Statistics Service, 2005). Nowadays, with the boom of remote sensing (ground-based, UAV, airborne, and satellite), reflectance data are increasingly being used in agriculture. Furthermore, many new technologies have been developed for agricultural use such as low-cost positioning systems (Global Positioning System-GPS and Global Navigation Satellite System-GNSS), geographic information systems (GIS), geophysical sensors, low-cost or open remote sensing data, tractor mounted sensor platforms, crane systems and variable-rate technologies.

Remote sensing has played an important role in agriculture since its foundation. Some reviews have clarified this role in each agriculture application such as Atzberger, 2013; FAO, 2017; Global Strategy to Improve Agricultural and Rural Statistics, 2015; Jin et al., 2018; Kasampalis et al., 2018; Nellis et al., 2009; Paul J. Pinter et al., 2003; Tenkorang & Lowenberg-doboer, 2008; Wójtowicz et al., 2016. In precision agriculture, the remote sensing technology is an essential component crop classification (Zhang & Kovacs, 2012), crop health (Mulla, 2013; Seelan et al., 2003), crop growth (Stafford, 2000) and yield prediction (Awan, 2016; Khanal et al., 2018) that was mentioned in the following studies. It has provided imagery data timely with the return visit frequency from 16 days to less than 1 day; the spatial resolution from low resolution (1 km, 500 m, 250 m), medium resolution (100, 80, 30, 20 m) to high and very high resolution (10, 5, 0.31 m); the diverse spectral resolution included the region of the spectrum (visible, near infrared (NIR), infrared, short wave infrared (SWIR), and microwave), the number and width of the spectral bands (panchromatic, multispectral, hyperspectral); the radiometric resolution (6, 8, 12, and 16 bits); the type of sensor such as optical, thermal, RADAR

(RAdio Detection And Ranging), SARs (Synthetic Aperture Radars), LIDAR (Light Detection and Ranging), SONAR (Sound Navigation and Ranging). The optical sensor or the optical remote sensing is most commonly used in the agricultural industry, which utilizes visible, NIR, and SWIR sensors to obtain information of land surface, land cover or vegetation through imagery data (Khanal et al., 2018; Prasad et al., 2011). These regions of the electromagnetic spectrum are used to detect vegetation indices (VIs) based on spectral reflectance properties of leaves and soil that were presented by Basso, B., Cammarano, D., & Carfagna, 2013; Mulla, 2013; Paul J. Pinter, 2003; Xue & Su, 2017. Vegetation indices are mathematical combinations or ratios of different wavebands and it has been developed to estimate and evaluate various plant and soil characteristics, e.g., crop health, growth, vigour, stress; leaf area, leaf chlorophyll content; biomass, vegetation productivity; temperature, moisture and erosion of soil, etc. The validation process is through direct or indirect correlations between VIs derived from remote sensing and the plant, soil characteristics of interest measured in situ, such as biomass, leaf area index (LAI), the fraction of Absorbed Photosynthetically Active Radiation (fAPAR), crop height. A detailed list of the common VIs was shown in Table 2 of Basso, B., Cammarano, D., & Carfagna, 2013 and Table 1 of Xue & Su, 2017. In addition, Atzberger, 2013; Khanal, 2018; Mulla, 2013; Nellis, 2009; Paul J. Pinter, 2003; Seelan, 2003; Wójtowicz, 2016 were synthesized the studies that used VIs in many agricultural sectors such as crop classification, condition; crop yield prediction; water management; nutrient management; detection of disease and pest damage; and weed control. Especially, from that evidence showed that the NDVI is the most used index in agriculture in general and in precision agriculture in particular. Moreover, remote sensing has become a simple and effective method in modern agriculture. Today, in order to satisfy the increasingly accurate requirements of precision agriculture, UAV technology (Candiago et al., 2015; Sankaran et al., 2015; Senthilnath et al., 2017; Wójtowicz, 2016; Yang et al., 2017) and ground-based monitoring tools (Bu et al., 2017; Wójtowicz, 2016) have been developed and applied effectively. Nevertheless, these technologies require users and farmers to be master of them and have to invest a large amount of money in equipment and software.

Crop yields play an important key for developing agriculture system in each country. Thus, crop yield monitoring and forecasting are the first steps in precision agriculture for many farmers, agricultural organizations and government. Its final product is a crop yield prediction map before harvest that provides necessary information to help farmers and managers make reasonable decisions. The simplest method for estimating crop yields is to determine the correlation between ground-based yield measures and VIs derived from remote sensing platform among the growing season. Some early studies Lewis et al., 1998; Quarmby et al., 1993; Shanahan et al., 2001; Tucker et al., 1980; Unganai & Kogan, 1998; Wiegand et al., 1990 were tested with wheat and maize proved that VIs can explain over 80% of the observed crop yields (David B. Lobell, 2013). On the other hand, the remote sensing data provided input parameters into crop models to improve the estimation accuracy of crop yields and this method was presented in detail in the reviews of FAO, 2017; Jin, 2018; Kasampalis, 2018.

In the context of current climate change, the food insecurity situation is at an alarming level. In 2017, almost 124 million people across 51 countries and territories faced “crisis” levels of acute food insecurity or worse due to climate variability and climate extremes are already undermining the production of major crops (wheat, rice and maize) in tropical and temperate regions (FAO, IFAD, UNICEF, 2018). Similar to rice and wheat, maize is one of the most important food crops and has gained enormous importance in tropical and temperate regions as food, fodder, and energy crop (Liebisch et al., 2015). Cassman, 1999 suggested that annual-average corn yields must reach 70%–80% of their potential ceiling (~24 T/ha) within the next 30 years to keep pace with the growing global population.

With the capacity of remote sensing technology mentioned above, it has been applied in corn yield forecasts for a few previous decades and provided the predicting results timely and accurately. The review article of Chivasa et al., 2017 continued to reinforce and expand the power of remote sensing in maize yield prediction. Moreover, the outstanding progress of the sensor technology in the spatial, temporal, and spectral resolution that impact directly on the increased accuracy of corn yield estimate in recent years. This significant development was sufficiently demonstrated in much research, e.g., Aguate et al., 2017; Battude et al., 2016; Bu et al., 2017; Cai et al., 2017; Franzen et al., 2014; Gao et al., 2018; D. M. Johnson, 2016; M. D. Johnson et al., 2016; Kern et al., 2018; Lambert et al., 2018; Maresma et al., 2016, 2018; Mladenova et al., 2017; Ngie & Ahmed, 2018; Peralta et al., 2016; Petersen, 2018; Shao et al., 2015; Sharma et al., 2018; Yao et al., 2015. Nowadays, the free-cost satellite image data such as MODIS, Landsat, Sentinel combined with the boom of open source software, big data analytics, and machine learning will create a great approach in precision agriculture in general and corn yield forecast in specific, which help the farmers approach new and free technologies easily and keep pace with the fourth industrial revolution.

1.2. Research Objectives

In order to achieve the research objectives of the thesis, the research results must answer the following research questions:

1. How is the capacity of remote sensing technology in predicting corn yield?
2. Which one of the following vegetation indices (NDVI, EVI, SAVI, WDRVI, GNDVI) has the closest relationship with the actual yield of the study area?
3. What are the optimal models for predicting maize yield in the study area from the Landsat-8 and Sentinel-2 data?
4. How is the capacity of open-source software (QGIS, R) in spatial analysis, statistical data analysis and building an interactive web application?

1.3. Thesis Outline

This thesis is arranged into 5 chapters as follows:

- Chapter 1: Introduction
- Chapter 2: Literature review
- Chapter 3: Materials and Method
- Chapter 4: Results and Discussion
- Chapter 5: Conclusion and Recommendation

The research questions of this thesis are clarified in each chapter step by step.

2. LITERATURE REVIEW

2.1 Using Remote Sensing Technology for Crop Yield Forecast

Remote Sensing (RS) is defined as the science of acquiring information about an object through the analysis of data obtained by a device that is not in contact with the object (Lillesand & Kiefer, 1994)). Another definition, remote sensing is the science and the art of acquiring information about an object by observing it from a distance (Fischer et al., 1976). It uses a variety of platforms to get the data such as ground-based, UAV, airborne, and satellite which employs such specialized sensors as the radiometers, scanners, camera, lasers, radar systems, seismographs, radio frequency receivers, sonar, magnetometers, and gravimeters. In addition, collecting data (imagery) base on the wavelengths from ultraviolet to radio regions.

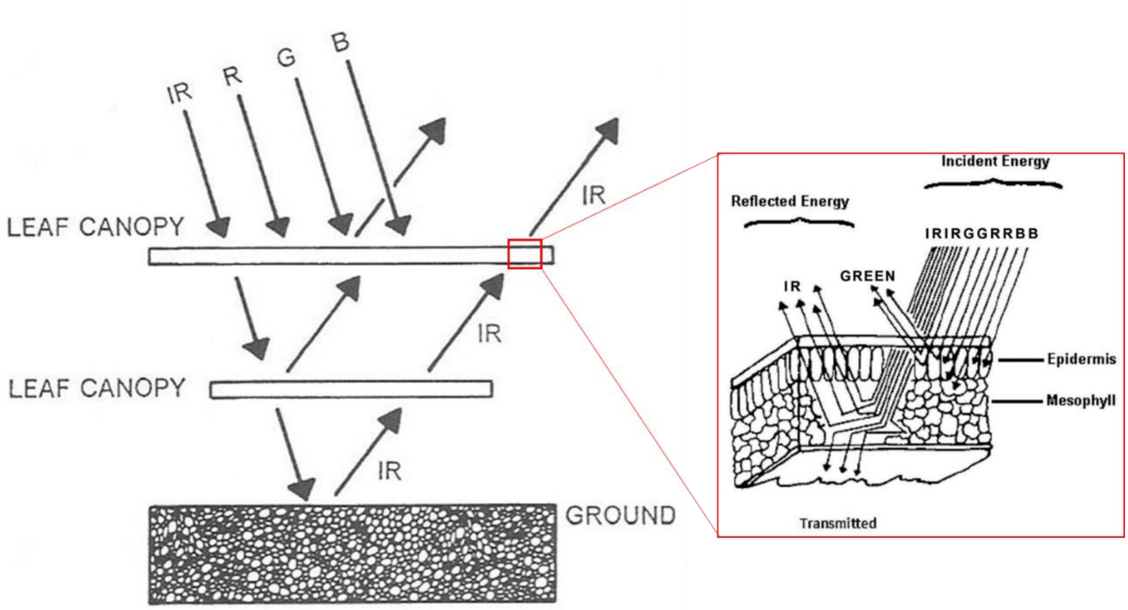

Figure 2.1. *The interactive process of visible and NIR radiation with the healthy leaf layers and leaf structure (adapted from Campbell, 1996, 2007)*

For healthy vegetations, Chlorophyll of green leaves strongly absorbs the blue and red lights and reflects the green light (Campbell, 1996). The leaves' internal mesophyll structure highly reflects and transmits the near-infrared (NIR) wavelength region. On the other hand, NIR radiation can show canopy density because it can transmit through the first leaf layer and then reflect on the leaf layer below, then continue to pass back through the canopy above (Figure 2.1). According to Lillesaeter, 1982, the NIR wavelength can see through roughly eight leaf layers, while the red radiation sees only one leaf layer or less.

Figure 2.2 shows that the healthy leaf typically absorbs blue and red spectrum, and reflects green spectrum and near-infrared waves. For most crops, the reflection ratio of the blue light is about 2%, the green light is 5%, and the red light is 3%, whereas the NIR waves are about 50% to 60%. The high ratio between the NIR and visible radiations helps to distinguish the properties, conditions of the crop.

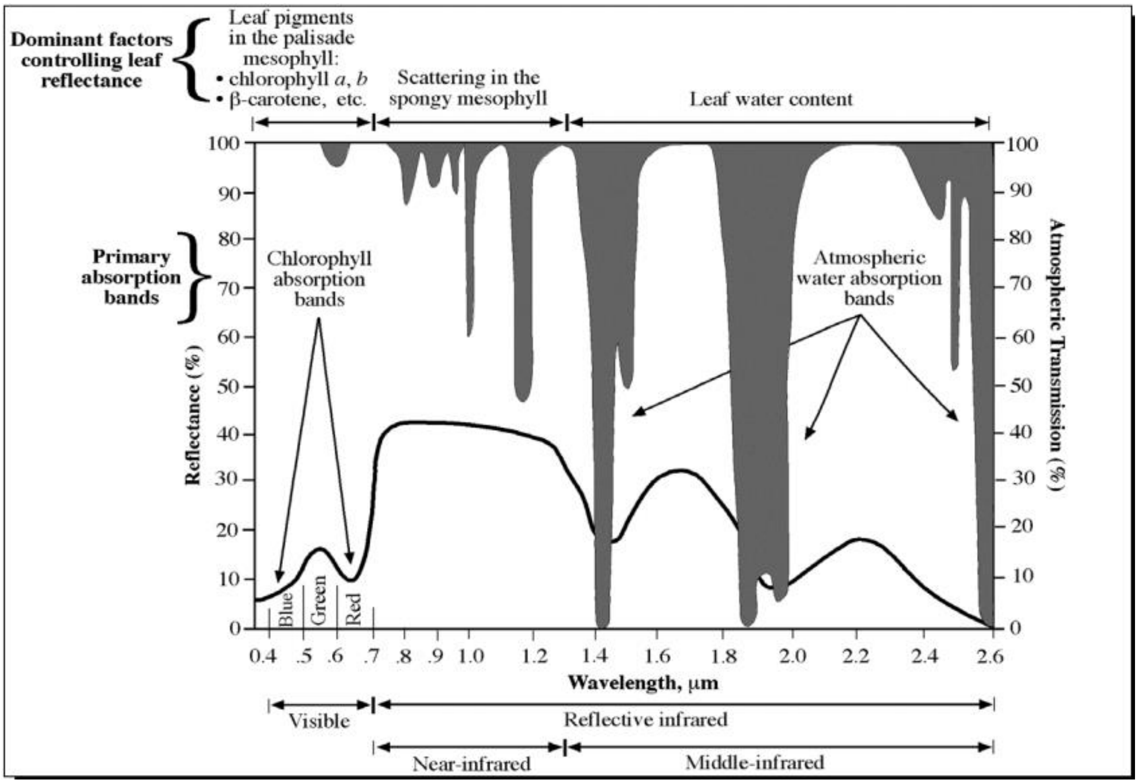

Figure 2.2. *Typical visible and NIR reflectance of the healthy leaf (Jensen, 2009)*

Thus, arithmetic combinations of these two wavelength regions define a number of helpful vegetation indices that can provide information about the crop’s health and productivity. The relationships between crop characteristics and remote sensing data are proved through the vegetation indices.

For a few decades ago, many crop yield forecast models were built from RS data. Hatfield, 1983, classified them into three main types: Spectral models (C.J. Tucker, 1980); Albedo models (S B Idso et al., 1978), and Thermal models (Sherwood B Idso et al., 1977; Walker & Hatfield, 1979). On the other hand, Horie et al., 1992, also divided into three types: the empirical regression model, the biomass production model as a function of absorbed or intercepted solar radiation, and the stress degree day model. In addition, data derived from RS was used for crop yield estimation directly or integrated into crop simulation models.

2.2. Vegetation Indices for Monitoring the Crop Yield of Maize

Vegetation indices (VIs) began to be used in agricultural monitoring system from the mid-20th century and nowadays it is a very important index in precision agriculture. VIs provide a very simple yet elegant method for extracting the green plant quantity signal from complex canopy spectra (Paul J. Pinter, 2003). Vegetation information from remotely sensed images is mainly interpreted by differences and changes of the green leaves from plants and canopy spectral characteristics. The most common validation process is through direct or indirect correlations between VIs obtained and the vegetation characteristics of interest measured in situ, such as vegetation cover, LAI, biomass, growth, and vigour assessment (Xue, 2017).

Biophysical features of plants can be characterized spectrally by vegetation indices defined as unitless radiometric measures that are calculated as ratios or differences of two or more bands in the VIS, NIR and SWIR wavelengths. In 1956, a pioneering study of Colwell pointed out that infrared aerial photography could be used to determine loss of vigour from the disease in wheat. The first use of a ratio between red and NIR radiance was developed by Jordan in 1969, named Ratio Vegetation Index (RVI), which is based on the principle that leaves absorb relatively more red than infrared light. RVI was created by dividing NIR reflectance and red reflectance. Since the RVI, a number of vegetation indices have been developed and can be used to interpret aerial imagery.

Table 2.1. *List of indices used to directly or indirectly estimate vegetation biomass*

Short Name	Radiometric Index Name	Reference
RVI (SR)	Ratio VI or Simple Ratio	Jordan, 1969
NDVI	Normalized Difference VI	Rouse et al., 1974
TVI	Transformed VI	Rouse et al., 1974
TVI	Triangular Vegetation Index	Broge and Leblanc, 2001
MTVI1,2	Modified Triangular Vegetation Index 1,2	Haboudane et al., 2004
PVI	Perpendicular VI	Richardson & Wiegand, 1977
SAVI	Soil-Adjusted VI	Huete, 1988
WDVI	Weighted Difference VI	Clevers, 1989
SAVI2	2^{nd} version of Soil-Adjusted VI	Major et al., 1990

TSAVI	Transformed Soil-Adjusted VI	Baret & Guyot, 1991
ARVI	Atmospherically Resistant VI	Kaufman & Tanre, 1992
GEMI	Global Environmental Monitoring Index	Pinty & Verstraete, 1992
NDVIc	Corrected NDVI	Nemani et al., 1993
SARVI	Atmospherically Resistant SAVI	Huete et al., 1994
MSAVI	Modified Soil-Adjusted VI	Qi et al., 1994
OSAVI	Optimised SAVI	Rondeaux et al., 1996
GARI	Green Atmospherically Resistant VI	Gitelson et al., 1996
GNDVI	Green NDVI	Gitelson et al., 1996
NDVIre	Red-edge NDVI	Gitelson & Merzlyak, 1994
NDWI	Normalized Difference Water Index	B. Gao, 1996
EVI	Enhanced VI	Huete et al., 1997
EVI2	Enhanced VI 2	Jiang et al., 2008
PRI	Photochemical Reflectance Index	Gamon et al., 1997
MGVI	MERIS Global VI	Gobron et al., 1999
GESAVI	Generalised Soil-Adjusted VI	Gilabert et al., 2002
VARI	Visible Atmospherically Resistant Index	Gitelson et al., 2002
LVI	Linearised VI	Unsalan & Boywer, 2004
WDRVI	Wide Dynamic Range VI	Gitelson, 2004
VARIgreen	Visible Atmospherically Resistant Index	Gitelson, 2002
VARI700	Visible Atmospherically Resistant Index - 700 nm	Gitelson, 2002
MTCI	MERRIS Terrestrial Chlorophyll Index	Dash & Curran, 2007
CAR	Chlorophyll Absorption Reflectance	Kim et al., 1994
CARI	Chlorophyll CARI	Kim et al., 1994
MCARI	Modified CARI	Daugthry et al., 2000
MCARI 1,2	Modified CARI 1,2	Haboudane et al., 2004
TCARI	Transformed CARI	Haboudane et al., 2002
NDRE	Normalized Difference Red Edge	Barnes et al., 2000
CCCI	Canopy Chlorophyll Content Index	Fitzgerald et al., 2006

Numerous spectral vegetation indices (VIs) have been developed to characterize vegetation canopies. Plant canopy reflectance factors and derived multispectral VIs are receiving increased attention in agricultural research as they are considered robust surrogates for traditional agronomic parameters. Spectral reflectance and the thermal emittance properties of soils and crops have been used extensively, to predict ecological variables such as the percentage of vegetation cover, plant biomass, green LAI and other biophysical characteristics (FAO, 2017). Vegetation indices have served as the basis for many applications of remote sensing to crop management because they are well correlated with green biomass and leaf area index of crop canopies (Paul J. Pinter, 2003). The normalized difference vegetation index (NDVI) was originally proposed to estimate green crop biomass by Compton J Tucker, 1979. Moreover, other researches proved that the vegetation indices such as SAVI, OSAVI, TSAVI, PVI, EVI, and GNDVI were more useful for determining and estimating crop biomass, leaf area index (LAI), absorbed photosynthetically active radiation (APAR), and crop yield in agriculture. Until now, there is no doubt that NDVI is the basic VI and the most common used VI in agriculture which is a kind of foundation index for developing new VIs. The importance of NDVI comes from it has a close correlative relationship with the canopy LAI and fAPAR (fraction of Absorbed Photosynthetically Active Radiation).

The definitions of Leaf area index (LAI) have been provided by scientists from many disciplines for a range of purposes, such as determination of forest community succession, simulation of potential biological activities, and solar radiation regimes within plant canopies (Zheng & Moskal, 2009). The first concept of LAI is proven by Watson, 1947 that is the total one-sided area of photosynthetic tissue per unit ground surface area (Table 2.2). LAI is a very important parameter in studies that research about terrestrial vegetation, land cover, land surface. It clearly shows the growth, health, and productivity of vegetation because leaf surfaces are the primary sites of metabolism of plants with the surrounding environment, with important processes such as canopy interception, evapotranspiration, and gross photosynthesis. Furthermore, it is closely related to the amount of radiation that can be absorbed by the canopy.

Table 2.2. *Brief and comparison of LAI definitions (Zheng & Moskal, 2009)*

Type	Definition	Application	Reference
Total Leaf Area Index (ToLAI)	Total one-sided area of photosynthetic tissue per unit ground surface area.	Applicable to broad leaves.	Watson, 1947; Myneni et al., 2002
Projected Leaf Area Index (PLAI)	The area of horizontal shadow that is cast beneath a horizontal leaf from light at the infinite distance directly above it.	The maximum area of leaves from the overhead orbital view – varies depending on the zenith angle of sensor.	Myneni et al., 2002; Ross, 1981
Silhouette Leaf Area Index (SLAI)	The area of leaves inclined to the horizontal surface.	Investigates the radiation interception for different shapes of leaves.	Smith et al., 1991
Effective Leaf Area Index (ELAI)	One half of the total area of light intercepted by leaves per unit horizontal ground surface area – assume the foliage spatial distribution is random.	Precisely describes the radiation interception and radiation regime within and under the canopy.	Black et al., 1991
True Leaf Area Index (TLAI)	One half the total green leaf area per unit horizontal ground surface area.	Quantitatively characterizes radiation regime within and under the canopy, and simulates leaf controlled ecological process.	J. M. Chen & Black, 1992; Lang, 1991

There are two methods to estimate the LAI: direct and indirect. The direct method includes destructive harvest and litter traps. The indirect method can be divided into three categories: hemispherical photography, PAR (photosynthetically active radiation)-inversion, and spectral reflectance. In the review article of Liang et al., 2012, spectral reflection method also known as remote sensing method or statistical method was discussed. According to Qi et al., 2000, there are two common approaches to estimating LAI using remote sensing imagery: a vegetation index approach and a modelling approach. In addition, The LAI depends on many factors such as species composition, growth stage, seasonality, and conditions to take care of crops (irrigation, fertilizer). During past decades, many studies (Asrar et al., 1985; Baret, 1995; Best & Harlan, 1985; Curran, 1983; Peterson et al., 1987; Price & Bausch, 1995) proposed to estimate the LAI from the interrelations between LAI and VI following to the formulas (Qi et al., 2000).

$LAI = ax^3 + bx^2 + cx + d,$

$LAI = a + bx^c,$

$LAI = -1/2a \ln(1-x),$

$LAI = f(x).$

where x is either the vegetation index or the reflectances derived from remotely sensed data. The coefficients a, b, c, and d are empirical parameters that vary by vegetation type.

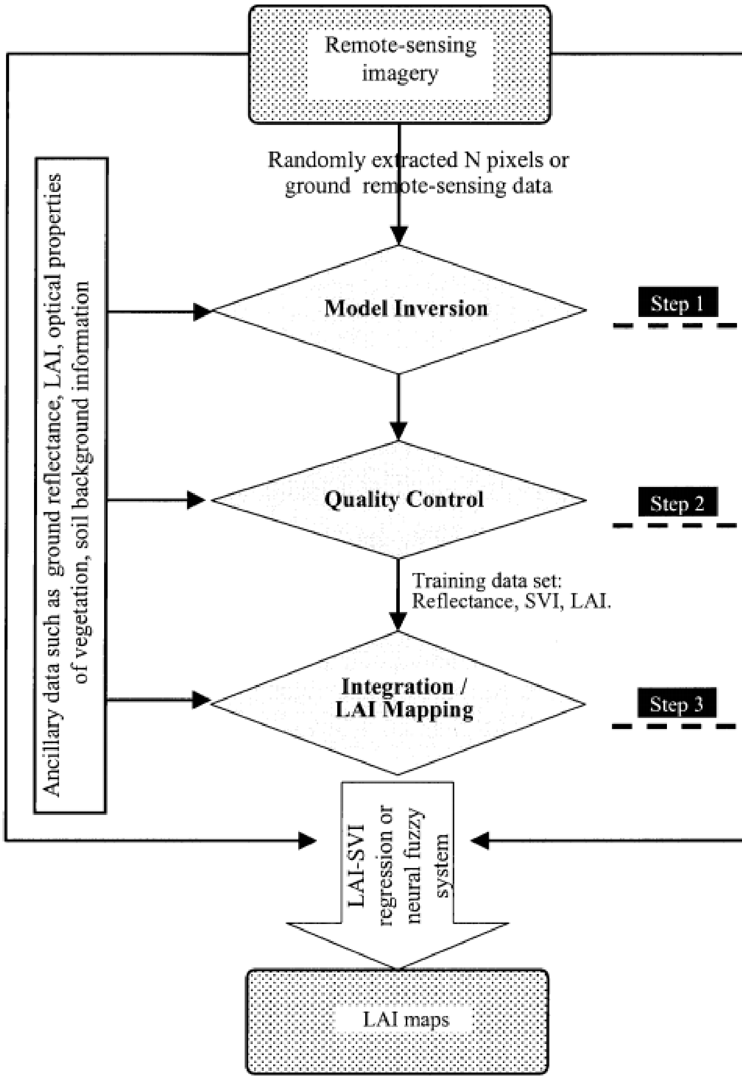

Figure 2.3. *The graphic shows the proposed approach to estimating leaf area index with remote sensing imagery (Qi et al., 2000)*

The photosynthetically active radiation (PAR) is defined as the amount of light available for photosynthesis, which ranges between 400 and 700 nm (McCree, 1971). In this visible region the vegetation pigments absorb energy that is actually absorbed is called absorbed PAR and when this energy is absorbed as a fraction of the total incident radiation, it is known as the fraction of APAR (fAPAR). The VIs and greenness are linearly related to the PAR absorption rate of crop canopies (Asrar, 1985; Jerry L. Hatfield et al., 1984; L. Wiegand & J. Richardson, 1990; Wiegand et al., 1979). For example, the study of Compton J Tucker et al., 1981 showed that both simple ratio and NDVI were closely related to the dry accumulation. The evidence of Asrar, 1985 pointed out a strong correlation between NDVI and PAR. Moreover, Wiegand et al, 1990 found that the estimate of fAPAR by combining GVI and PVI had the most accurate with $r^2 = 0.94$. Casanova et al., 1998 used VIs and PAR to estimate the LAI and biomass and its result was more reliable than the estimation of the LAI.

Beyond the estimation of LAI, fAPAR, and biomass, VIs were used to predict crop yield with high accuracy that was proved some studies about crop/grain yield of maize (Ferencz et al., 2004), wheat (Aase & Siddoway, 1981; Ferencz, 2004; Pearson et al., 1976; Pinter, Jr. et al., 1981; Reginato et al., 1978; Song et al., 2010; Compton J Tucker, 1981), sugar beet (Ferencz, 2004), cotton (Paul J. Pinter, 2003; Thomas et al., 1967), soybean (C.J. Tucker et al., 1979; You et al., 2017), alfalfa (Paul J. Pinter, 2003; Ferencz, 2004), cabbage (Thomas & Gerbermann, 1977), grape (Zarco-Tejada et al., 2005). The simplest approach to estimating crop yields is to establish empirical relationships between ground-based yield measures and VIs measured on a single date or integrated over the growing season (David B. Lobell, 2013). Early applications with wheat and maize indicated that variations in VI can explain over 80% of the observed variation in crop yields within individual fields (L. Wiegand, 1990; Shanahan, 2001; C.J. Tucker, 1980). This approach has been successfully implemented and applied in several studies with corn (Baez-Gonzalez et al., 2005; Battude, 2016; Bognár et al., 2011; Bu, 2017; Delia Báez-González et al., 2002; Fang et al., 2008; Ferencz, 2004; Guindin-Garcia, 2011; D. M. Johnson, 2014; Y. Li et al., 2014; D B Lobell & Asner, 2003; David B Lobell et al., 2015; Peralta, 2016; A. K. Prasad et al., 2006; Sakamoto et al., 2014; Shanahan, 2001; Sibley et al., 2014). Finally, VIs, LAI, fAPAR, and biomass is strongly correlated with corn yield and they are provided from remote sensing data that can be obtained from these main platforms: ground-based, UAV, airborne, and satellites.

2.3. Advanced Remote Sensing Technologies for Maize Yield Forecast

In the world and each zone, maize production may experience different kinds of constraints such as weather and management practices over the entire season. Thus, the factors to estimate crop yield are diverse. Maize crop could be monitored to assess its phenology and growth traits using remote sensing (Vina et al., 2004). Those cited above, using remote sensing to predict corn yield has been brought high efficiency in agricultural production, furthermore, nowadays it became a key component of precision agriculture. This section gives details of each available satellite/sensors and their applicability in predicting maize grain yield. The available platforms are National Oceanic and

Atmospheric Administration (NOAA)'s Advanced Very High-Resolution Radiometer (AVHRR), Moderate Resolution Imaging Spectroradiometer (MODIS), Landsat, Sentinel, Drones, or Unmanned Aerial Vehicles (UAVs), and the others platform (Spot, QuickBird, RapidEye, RADARSAT, Terra ASTER, Formosat). Each platform offers specific features that generate some different advantages and disadvantages for forecasting maize yields.

Most of them were used in studies to monitor and predict maize yield but depending on spatial resolution, temporal resolution, and spectral resolution, they were applied in different aims and regions. The higher the spatial resolution, the better the estimating corn yield's capability is. Besides, in recent years, the application of UAV in precision agriculture has become popular because of saving cost and time. The next part gives details of each the available satellite that is commonly applied in maize yield forecast.

2.3.1. Using NOAA-AVHRR in monitoring the crop yield of maize

Satellite imagery data obtained from the National Oceanic and Atmospheric Administration's Advanced Very High-Resolution Radiometer (NOAA-AVHRR) has been used to monitor large-scale cropping systems and to forecast yield since the 1980s (C.J. Tucker et al., 1985). NOAA-AVHRR data provides a spatial resolution of 1.1 km^2 for local coverage and 4 km^2 for global coverage. It's sensing in the visible (0.58 –0.6 µm), near-infrared (0.725–1.1 µm) and offers a short temporal repeat cycle of one take every 12 hours.

NOAA-AVHRR satellite is one of the earliest and most popular used satellites in corn yield forecast. In 1993, Quarmby et al. used vegetation index profiles from AVHRR data to monitor crop yield for wheat, cotton, rice and maize crops. The results showed that the crop yield has been estimated to a high degree of accuracy using a simple linear relationship between NDVI and yield. In a large area, using the Vegetation Condition Index derived from NOAA/AVHRR satellite data to estimate the maize production for the United States Corn Belt (Hayes & Decker, 1996). NDVI was applied in a simple regression model as the only independent variable was encouraging with r=0,75; p=0,05 and pointed out that NDVI can be a responsive indicator of maize production (Lewis, 1998). Using NDVI from NOAA's AVHRR images in Mexico to develop and validate a maize yield estimating model that accounts for 89% of the variability in yields under irrigated conditions and 76% under nonirrigated conditions (Delia Báez-González, 2002). The results of Mkhabela et al., 2005 proved that NDVI data from NOAA-AVHRR can be used to rapidly forecast maize yield in the Middleveld, Lowveld and Lubombo Plateau agro-ecological regions of Swaziland. The models developed for forecasting maize yield in the three regions are as follows:

Middleveld: $Y = 5.7045(\sum AveNDVI) - 3.8171$;
Lowveld: $Y = 4.0224(\sum AveNDVI) - 4.4442$;
Lubombo Plateau: $Y = 1.9695(\sum AveNDVI) - 4.5591$.
where Y is maize yield (t/ha) and $\sum$AveNDVI is cumulative average NDVI.

In addition, many studies showed that using linear regression models with multiple parameters had higher accuracy. The study of Unganai, 1998 was found that usable corn yield scenarios can be constructed from the VCI and TCI at approximately 6 (in some regions up to 13) weeks prior to harvest time. Combining NDVI, VCI, and TCI from NOAA-AVHRR data as input variables into the maize yield prediction model was applied in the study of A. K. Prasad, 2006 (with R^2 values are 0.78 for Corn and 0.86 for Soybean). Soria-Ruíz & Fernández-Ordoñez, 2003; Soria-Ruíz et al., 2004 based on the multi-temporal analysis of NOAA-AVHRR satellite images, and used parameters such as NDVI, LAI, and degree-days to predict corn occurrence and yield in Guanajuato, Mexico. Yield prediction for corn resulted in a 9.6 % overestimation compared with the average field-measured value. Bognár, 2011; Ferencz, 2004 used a new vegetation index (General Yield Unified Reference Index-GYURI) was deduced using a fitted double-Gaussian curve to the NOAA-AVHRR data during the vegetation period to estimate the corn yield. The results showed that the correlation between GYURI and the field level yield data for corn was high (R^2 = 84.6–87.2) and the forecast for corn can be made 70 days before harvest.

Finally, the use of low-resolution satellite images, along with their high temporal frequency, broad geographical coverage, the price of the data is low and also the accessibility of the NOAA-AVHRR data seems hopeful in the long run, thus, the NOAA-AVHRR satellite imageries become a good choice for predicting maize yield.

Table 2.3. *Vegetation indices for monitoring crop yield of maize by AVHRR*

Index	Formula	References
Normalized Difference Vegetation Index	$\mathrm{NDVI} = \frac{Channel1 - Channel2}{Channel + Channel2}$ *Channel1: 580 – 680 nm* *Channel2: 725 – 1100 nm*	Quarmby et al., 1993; Hayes J. M. & Decker W. L., 1996; Lewis et al., 1998; Unganai & Kogan, 1998; Soria-Ruiz, J. & Y. Fernandez-Ordonez, 2003, 2004; Mkhabela, M. S., et al., 2005; Kogan et al., 2005; Ferencz et al., 2004; Prasad et al., 2006; A. Li et al., 2007; Salazar et al., 2008; Bognár et al., 2011; Kogan et al., 2012; M. D. Johnson, 2016
General Yield Unified Reference Index	$\mathrm{GYURI} = \int_{t01}^{t02} GN(t)dt$	Ferencz et al., 2004; Bognár et al., 2011
Leaf Area Index	LAI	Baez-Gonzalez et al., 2002; Soria-Ruiz, J. & Y. Fernandez-Ordonez, 2003, 2004

2.3.2. Using MODIS in monitoring the crop yield of maize

Another frequently used satellite in maize yield forecast is the National Aeronautics and Space Administration's Moderate Resolution Imaging Spectroradiometer (MODIS). Both NOAA-AVHRR and MODIS have high-frequency observations of 12 hours and 8, 16 days, respectively but MODIS's spatial and spectral resolution are better than NOAA-AVHRR that include resolutions of 250 m, 500 m, and 1000 m, along with depending on its products such as MOD09A1, MOD12Q1, MOD13Q1, MOD13A1, and MOD15A2. Therefore, using MODIS data for predicting maize yield is more accurate than AVHRR data.

Many studies have used VIs that were created from MODIS products to develop corn yield forecasting models. Bolton & Friedl, 2013 used NDVI, EVI2, and NDWI to develop empirical models estimating maize and soybean yield in the Central United States and proved that EVI2 and NDWI performed better than NDVI for estimating maize yield. The result of Johnson's study (2014) shows that both corn and soybean yields were positively correlated with NDVI and negatively correlated to daytime LST with high coefficients of determination ($R^2 = 0.93$). In 2013 and 2014, Sakamoto and colleagues completed a method for near real-time yield prediction of U.S. corn by using WDRVI was calculated from MODIS-250m products (MOD09Q1, MYD09Q1) that were collected 7 days before the corn silking stage and this corn-yield prediction method estimated national-level U.S. corn yield of 9.59 t/ha in 2013, which was 3.8% lower than the U.S. Department of Agriculture (USDA) National Agricultural Statistics Service (NASS) statistical data (9.97 t/ha). A multiple linear regression model was developed by Kern et al. (2018) with meteorological data and remote sensing based vegetation index (MODIS-NDVI) as input variables to estimate crop yield in Hungary for the 2000–2016 time period. This model results in high accuracy with the variance of 81% for maize.

In addition, based on the correlation between LAI and crop yield, P. Doraiswamy, 2004; P. C. Doraiswamy et al., 2005 used the MODIS derived LAI at 250 m resolution and 8-days cycle to predict corn and soybean in the U.S. Corn Belt. According to the researches of Fang et al., 2008, 2011, the Cropping System Model (CSM)–Crop Environment Resource Synthesis (CERES)–Maize and the Markov Chain canopy Reflectance Model (MCRM) were applied to estimate maize yield for each county of Indiana, USA and the MODIS derived LAI, EVI and NDVI were parameters of the coupled model. The estimated corn yield outcome was very close with USDA-NASS data that was less than 3.5%. Guindin-Garcia, 2011 found a linear relationship between maize grain final yield and average estimates of maize green leaf area index ($R^2 > 0.70$) in Nebraska, Iowa, and Illinois (USA), which was estimated from MODIS-250 m products derived WDRVI. Using LAI derived from MODIS product MOD15A2 as an input parameter of the Ensemble Kalman Filter model to predict maize yields in Story County, Iowa, USA. The result showed that the yield correlation improved more when both soil moisture and LAI were assimilated ($R = 0.65$) (Ines et al., 2013). Zhao et al., 2013 used the crop model - PyWOFOST (the EnKF based coupled WOFOST and MODIS LAI model) to simulate maize growth and yield in Northeastern China with a high correlation. Shao et al., 2015 developed corn yields forecasting models for the entire Midwestern United States that used MODIS-NDVI, digital elevation model (DEM) and parameter-elevation relationships on independent slopes model (PRISM) climate data as variables inputs and resulted in an average R^2 of 0.75 and an RMSE value of 1.10 t/ha. Yao et al., 2015 also used a model combination that named the Remote-Sensing–Photosynthesis–Yield estimation for Crops (RS–P–YEC) model to estimate the yield of maize in the Northeast China Plain. This model includes 2 parameters that were derived from MODIS products (MCD12Q1 and MOD09A1) are LAI data and Land cover data. Leaf area duration (LAD) - a new variable was used as an independent variable in the simple linear regression to predict maize yield, which is the integral of MODIS-LAI over time. The result shows that the errors for predicting maize yield in the Y_P (using LAD Accumulated from the Estimated Emergence Date) and Y_F (using LAD Accumulated from an Arbitrarily Fixed Date) models, namely, the Y_P model exhibited RMSE values of 0.68–0.69 t/ha in Illinois (USA) and 0.66–0.96 t/ha in Heilongjiang (China), while the Y_F model had RMSE values of 1.0–1.1 t/ha and 0.82–0.84 t/ha, respectively (Ban et al., 2017). The researches were summarized in the table below (Table 2.4).

The evidence in this section have proven the special benefits of MODIS for corn yield prediction for the large farms but the estimating yield of small areas is a big challenge because its area is often smaller than the spatial resolution of the MODIS data (250 m).

Table 2.4. *Vegetation indices for monitoring crop yield of maize by MODIS*

Index	Formula	Product types	References
Normalized Difference Water Index	$\frac{Green - NIR}{Green + NIR}$	MOD09Q1(A1) MYD09Q1(A1)	Bolton & Friedl, 2013; Petersen, 2018
Normalized Difference Vegetation Index	$\frac{NIR - RED}{NIR + RED}$	MOD13Q1(A1) MYD13Q1(A1) MOD09GQ MOD09GA MYD11A2	A. Li, 2007; Funk & Budde, 2009; Peng & Gitelson, 2011; Bolton & Friedl, 2013; Jovanovic et al., 2014; D.M. Johnson, 2014, 2016; M.D. Johnson et al., 2016; Shao et al., 2015; Cai et al., 2017; Mladenova et al., 2017; Gao et al., 2018; A. Kern et al., 2018; Petersen, 2018
Wide dynamic range vegetation index	$\frac{\alpha NIR - RED}{\alpha NIR + RED}$ $0.1 \leq \alpha \leq 0.2$	MOD09Q1(A1) MYD09Q1(A1)	Peng & Gitelson, 2011; Sakamoto, 2013, 2014; Sibley, 2014
Enhanced Vegetation Index	$2.5\frac{NIR - RED}{(NIR + 6RED - 7.5BLUE) + 1}$	MOD13Q1(A1) MYD13Q1(A1)	M.D. Johnson et al., 2016; Guan et al., 2017;

		MOD13C1	Mladenova et al., 2017; Petersen, 2018
Enhanced Vegetation Index 2	$2.5\frac{NIR - RED}{NIR + 2.4RED + 1}$	MOD13Q1(A1) MYD13Q1(A1) MOD09GQ MOD09GA	Peng & Gitelson, 2011; Bolton & Friedl, 2013; Jaafar & Ahmad, 2015; Gao et al., 2018
Leaf Area Index	LAI	MOD15A2 MCD15A3	P. Doraiswamy, 2004; P. C. Doraiswamy et al., 2005 Baez-Gonzalez et al., 2005; Fang et al., 2008, 2011; Guindin-Garcia, 2011; Guindin-garcia et al., 2012; Sakamoto et al., 2013; Ines et al., 2013; Zhao et al., 2013; Xin et al., 2013; Yao et al., 2015; D.M. Johnson, 2016; Ban et al., 2017

2.3.3. Using Landsat in monitoring the crop yield of maize

Landsat satellite series (e.g. Landsat 5, 7, 8) is a platform was developed to solve the spatial resolution limitations of AVHRR and MODIS satellite with its spatial resolution from 15 m to 120 m. However, the orbit period of Landsat is longer than AVHRR and MODIS (16 days), which severely limits frequent observations at crop growth term. In addition, the Landsat imagery was provided for free by National Aeronautics and Space Administration (NASA) of U.S., that why it was applied in many majors, especially in agriculture.

A publication of Bach, 1998 used LAI derived from Landsat and daily meteorological data as parameters to determine the corn yield for the upper Rhine valley (Germany) in 1995. The comparison of the results with Special Yield Estimation (for 23 corn fields) shows a relative error of 2.3%. Lobell, 2003 predicted the crop yield (maize, wheat, soybean) by using Landsat data in an intensive agricultural region in northwest Mexico and their study showed that the incorporation of fAPAR from SR and NDVI offered a distinct advantage over yield models that require estimates of leaf area index. Comparative research between Earth Observing 1 (EO-1) Advanced Land Imager (ALI) and Landsat-7 Enhanced Thematic Mapper Plus (ETM+) in crop identification and yield prediction in Mexico was carried out by Lobell and Asner (2003). For comparison of predicted maize yields, the root means square error difference between ALI and ETM+ was 0.30 ton/ha, which is roughly 5% of average yields. The study of Liu et al., 2010 pointed out the relationship between corn yield and fAPAR that the cumulative APAR accounted for 72% of the yield variability, which was estimated from hyperspectral data acquired by the Compact Airborne Spectrographic Imager (CASI) and from multi-spectral data acquired by the Landsat-5/7.

To enhance the accuracy of forecasting corn yields, some recent researchers combined both higher spatial resolution data from Landsat with higher temporal resolution data from MODIS, AVHRR or the other platforms, crop models. According to the study of Baez-Gonzalez, 2005, the LAI derived from Landsat ETM+ data and AVHRR data that was used to predict maize yield in large areas in Sinaloa, Mexico with a mean error of -11.2% (from 71 corn fields). Jégo et al., 2012 used green LAI that was obtained from airborne hyperspectral data or multispectral satellite data (Landsat TM and SPOT) for yield and biomass predictions. The estimated crop yields were good for corn and soybean with RMSE about 15–20%. Sibley, 2014 used the VIs and APAR derived from Landsat and MODIS as input parameters of three methods (the APAR approach, the crop model curve selection, and the crop model-based regression) to estimate corn yield for 134 irrigated and 94 rainfed maize (*Zea mays L.*) fields in Nebraska, USA. The result has proved that the combination of a well-tested crop model and the predictions from Landsat were considerably more accurate, with up to 20% of rainfed and 50% of irrigated yield. In the study of Y. Li, 2014, the ensemble Kalman filter (EnKF) algorithm was developed to integrate regional LAI derived from Landsat ETM+ data into a fully coupled hydrology-crop growth model (World Food Study - WOFOST and hydrology model HYDRUS-1D) to estimate the regional variation for maize yield in the Zhangye Oasis, an arid region in northwest China. This method obtained good results, namely, the coefficient of variations of the regional maize yield estimates was 8.7%. Gao et al. (2018) used the vegetation index time-series (NDVI, EVI2) retrieved from Landsat data, MODIS data, and Landsat-MODIS fused data to test the correlation between VIs and maize yield in central Iowa (part of the U.S. Corn Belt). It proved that the fused data had a better relationship, namely, for maximum NDVI, the coefficient of determination (R^2) was 0.33 (Landsat data), 0.55 (MODIS data), and 0.62 (Landsat-MODIS fused data), for maximum EVI2, was 0.46, 0.56, 0.62, respectively. Those mentioned above showed the positive points of the Landsat with 30 m spatial resolution in corn yield forecasts are summarized in Table 2.5.

Table 2.5. *Vegetation indices for monitoring crop yield of maize by Landsat*

Index	Formula	References
Normalized Difference Water Index	$\frac{NIR}{RED}$	David B Lobell et al., 2003; Lobell & Asner (2003); Pan et al., 2009
Normalized Difference Vegetation Index	$\frac{NIR - RED}{NIR + RED}$	Bach, 1998; Lobell & Asner (2003); David B Lobell et al., 2003; Pan et al., 2009 Jovanovic et al., 2014; Gao et al., 2018
Wide Dynamic Range Vegetation Index	$\frac{\alpha NIR - RED}{\alpha NIR + RED}$ $0.1 \leq \alpha \leq 0.2$	Sibley et al., 2014
Enhanced Vegetation Index 2	$2.5\frac{NIR - RED}{NIR + 2.4RED + 1}$	Gao et al., 2018
Leaf Area Index, Green Area Index	LAI, GAI*	Bach, 1998; Doraiswamy, 2004; Baez-Gonzalez et al., 2005; Jégo et al., 2012; Y. Li, 2014; David B Lobell, 2015; Battude et al., 2016*
Modified triangular vegetation index	$1.5\frac{1.2(NIR - GREEN) - 2.5(RED - GREEN)}{\sqrt{(2NIR + 1)^2 - (6NIR - 5\sqrt{RED}) - 0.5}}$	Liu et al., 2010; Jégo et al., 2012

** Spectral wavelengths: RED: 630 – 692 nm; NIR: 760 – 900 nm; Green: 519 – 601 nm.*

2.3.4. Using Sentinel in monitoring the crop yield of maize

The current Sentinel series includes Sentinel-1, Sentinel-2, and Sentinel-3, which was designed and developed by the European Space Agency (ESA) and funded by the European Commission (EC). All its data was provided for free by the Copernicus – Sentinels Scientific Data Hub portal. Sentinel-1 is the European Radar Observatory, which is composed of two satellites: Sentinel-1A and Sentinel-1B, with enhanced revisit frequency (6 days), medium and high-resolution (5-40 m) in all-weather conditions.

Sentinel-2 is a multispectral operational imaging mission, which consists of twin polar-orbiting satellites in the same orbit (Sentinel-2A, 2B). Its data provides the high spatial resolution (10m/20m/60m) multi-spectral (13 bands) imagery with a high revisit capability: ten days with one satellite, five days with two satellites at the Equator, and two to three days at mid-latitudes. The Sentinel-3 mission is designed multispectral, radar, and microwave sensors with a medium spatial resolution (300m/500m/1000m), and 27 days for 1 repeat cycle. With the characteristics mentioned above. Sentinel 1 and 2 offer good potential for forecasting corn yield.

The results of Veloso et al., 2017 showed that, for maize crops, the Sentinel-1and Sentinel-2 data are correlated to Greeb area index (GAI) and fresh biomass. It found correlations R^2 of 0.91 between NDVI and VH/VV and 0.89 between NDVI and VH (N=13), which were used to estimate biomass and GAI. Schwalbert et al., 2018 used yield data collected from 19 maize fields located in Brazil and in the United States, and normalised vegetation indices (NDVI, green NDVI and red edge NDVI) obtained from Sentinel-2 data. The VIs showed high accuracy for predicting maize yield in both the Rio Grande do Sul and the Mato Grosso regression model with R^2 = 0.68 and R^2 = 0.59, respectively. Lambert, 2018 combined Sentinel-2 time series and ground data to carry out a comparison of maize yield estimators based on the various spectral VIs and derived LAI from Sen2-Agri system in Koningue, Mali. The result showed that the Sen2-Agri estimates of LAI achieve better prediction of final grain yield than various VIs, reaching R^2 of 0.62 for maize. Similar to Landsat data, the fused data method of multi-satellites or platforms was applied for Sentinel data in corn yield forecast. In 2018, Gao and colleagues proved that high temporal and spatial resolution data from the fused daily Landsat/Sentinel-2/MODIS results explain crop yield variability better than Landsat, Sentinel-2, or MODIS data alone.

Table 2.6. *Vegetation indices for monitoring crop yield of maize by Sentinel*

Index	Formula	References
Normalized Difference Vegetation Index	$\frac{NIR - RED}{NIR + RED}$	Veloso et al., 2017; Schwalbert et al., 2018; Gao et al., 2018
Enhanced Vegetation Index 2	$2.5\frac{NIR - RED}{NIR + 2.4RED + 1}$	Gao et al., 2018

Leaf Area Index, Green Area Index	LAI, GAI*	Veloso et al., 2017*; Lambert et al., 2018

** Spectral wavelengths: RED: 665 nm; NIR: 842 nm.*

2.3.5. Using other satellite platforms, airborne in monitoring maize yield

Besides the freely available remote sensing data (NOAA-AVHRR, MODIS, Landsat, and Sentinel), there are various other platforms that support agricultural applications in general and predicting maize yield in particular. Most of them provide a high and very high spatial resolution (less than 10 m) usually have a low temporal resolution due to their narrow swath (coverage of a single image). Moreover, these satellites (optical or SAR) such as QuickBird, RapidEye, SPOT, WorldView, Formosat, RADARSAT are commercial platforms that usually provide on demand, namely, their data are not acquired unless a customer or application orders them with a certain fee.

Very high-resolution and super-spectral imagery provided by DigitalGlobe, for precision agriculture, DigitalGlobe imagery supports various activities, such as discrimination of weeds and field crops, the monitoring of effects of irrigation on crop health, and the calculation of yield by mapping crop health. Bausch et al., 2008 used QuickBird high-resolution multispectral images for estimating yield (biomass and grain) of irrigated maize (Zea mays L.) and the results showed that the relative green waveband DN had the highest correlations with grain yield (R^2 =0.81) than the other vegetation indices i.e. NDVI (R^2 =0.53), GNDVI (R^2 =0.63), and Normalised Chlorophyll Index Green Model (R^2 =0.67). The research of Pan, 2009 pointed out that QuickBird imagery can improve the accuracy of predicted results relative to the Landsat TM image by comparing the predicted crop yield derived from them. The crop yield forecast was near with the harvested yield that was collected from the farmers. The RapidEye satellites are a product of Planet Labs/BlackBridge, which are the first commercial satellites to include the Red-Edge band. Studies show that this band play an important role in monitoring agriculture such as vegetation health, crop stress, crop yield. Peralta, 2016 carried out a test on yield monitor data and RapidEye satellite imagery obtained for 22 corn fields located in five different counties of Kansas, USA. Their results proved that the VIs that better explained the variation in yield was the NDVIre because the NDVIre was the most appeared variable in all of the regression models. This evidence presents the potential of the Red-Edge band in enhancing accuracy for predicting corn yields.

The SPOT satellite family was launched by the French Space Agency that provides the multispectral resolution (Visible & Infrared), very high-spatial resolution (20 - 1.5 m), and revisit capacity for anywhere in the world, about 2-3 days. Thus, it offers high accuracy in monitoring vegetation, land use planning, environment, agriculture, military and natural resource management. In the context of the maize yield forecast, the SPOT data increased the accuracy of corn yield models, e.g., an R^2 of 0.92 for the Agnes field and for Cairo the R^2 was 0.9 in South Africa (Ngie & Ahmed, 2018) and according to Fernandez-Ordonez & Soria-Ruiz, 2017, the model Y = f(LAI) reported a value of 5.96 ton/ha and the model Y = f(NDVI) value of 5.04 ton/ha was obtained. Their accuracy compared to the average yield of cornfield sampling were 114% and 97% respectively. Especially, the VEGETATION Programme is developed by France, Belgium, Italy, Sweden, and the European Commission, which consists two observation instruments, namely, VEGETATION 1 is aboard the SPOT-4 and VEGETATION 2 is aboard SPOT-5 satellite. It can obtain almost all the Earth's surface in a day because of its swath size of 2250 km. Hence, many studies used NDVI derived from SPOT-VEGETATION for monitoring agriculture in general and corn yield forecast in specific, e.g., Abiy & Suryabhagavan, 2016; Durgun et al., 2016; Rojas, 2007. The HJ-1A/1B satellites were developed by China for the environment and disaster monitoring, which have a high temporal resolution (four days revisit period) and mid-high spatial resolution (30 m). The NDVI derived from the HJ-1A/1B satellites was used in mapping crop (Z. Pan et al., 2015) and identifying the species of salt marshes (Sun et al., 2016). Moreover, the study of B. Yu & Shang, 2017 indicated that the vegetation and phenology-based classifier using HJ-1A/1B data could effectively identify the multi-year distribution of maize and sunflower in Hetao, China and crop identification played an important role in crop yield prediction. A Compact High-Resolution Imaging Spectrometer (CHRIS) instrument is on board the PROBA satellite was applied by Wang et al., 2013 for regional corn yield estimations that provide up to 150 channels over the spectral range of 400-1050 nm and high spatial resolution of 17 m. The results showed that the assimilation of remote sensing data (CHRIS-LAI) into the crop growth model can predict the regional corn yield with high accuracy (RMSE of 339.14 kg/ha). Furthermore, the FORMOSAT-2 (formerly known as ROCSAT-2) satellite was developed by the National Space Organization (NSPO) of Taiwan (K. Chen et al., 2010) and the Deimos-1, owned and operated by Deimos Imaging were combined with SPOT-4-Take5 and Landsat-8 in the research of Battude et al. (2016) that also showed high accuracies for predicting maize yield in the South-West of France (R = 0.81; RRMSE = 8.9% for local yield and R = 0.96; RRMSE = 4.6% for regional yield).

On the other hand, in the recent three decades, the Synthetic Aperture Radar (SAR) remote sensing has been widely used in agriculture because the active sensors use microwave wavelengths to get data that is not hindered by cloud cover and is not dependent on solar energy. Moreover, many experimental results indicated that the radar backscatter coefficient is sensitive to vegetation parameters (Ulaby & Dobson, 1989). After the first operational SAR sensor onboard ERS-1 was launched in 1991, various technologies of SAR sensors used for remote sensing in monitoring crops, i.e., basic SAR sensor, SAR interferometry, SAR polarimetry and polarimetric interferometry SAR were developed to get crop characteristics (Sivasankar et al., 2018). Moreover, the availability of the multipolarization data from a number of SAR sensors operating at different frequencies has significantly advanced the use of SAR for agriculture such as X-Band (TerraSAR-X), C-Band (ENVISAT-ASAR and RADARSAT-2), and L-Band (ALOS-PALSAR) that provide more information relating to crop structure and crop condition (FAO, 2017). Thus, based on the advantages of SAR above, integration of optical and radar remote sensing is an attractive option and accuracy can be increased by combining both data. Soria-Ruiz et al., 2007 used RADARSAT-2 data and SPOT-5 data to determine different corn condition for enhancing the accuracy of corn yield forecast in Central Mexico. Germany's TerraSAR-X and Canada's RADARSAT-2 were launched in 2007 and their data was used in the research of Fieuzal et al., 2017 along with optical satellite images (Formosa-2 and SPOT-4,5) to estimate maize yield in an agricultural region in southwestern France. The results showed that the combined use of both red reflectance and C-VH or red reflectance and C-HH provided very good corn yield estimation performances, with an R^2 of 0.69 and an RMSE of 7.0 q/ha. In addition, Europe Space Agency launched Sentinel-1A in 2014 and Sentinel-1B in 2016, which carry a C Band-SAR sensor and imagery in all-weather conditions. Hence, Sentinel-1 is very useful for monitoring crop, yield forecast as some studies mentioned in the previous section.

However, compared to optical data, the use of SAR data in agricultural applications has not been well developed, partly due to the complexity, diversity and availability of SAR data, and partly due to the difficulty of data interpretation (Veloso, 2017).

Finally, compared with satellite platforms, airborne remote sensing imagery can substantially improve the accuracy of corn yield forecasting models. The RMSE decreased from 20% to nearly 10% (Wójtowicz et al., 2016). Some studies have demonstrated this assertion, e.g., Shanahan et al., 2001; Chang et al., 2003; Panda et al., 2010; Aguate et al., 2017; Khanal et al., 2018; Maresma et al., 2018.

Table 2.7. *VIs for monitoring maize yield by using other satellite, airborne platforms*

Index	Formula	Spectral wavelengths (nm)	Platforms/Sensors	References
Normalized Difference Vegetation Index	$\frac{NIR - RED}{NIR + RED}$	520-900	QuickBird	Bausch et al., 2008; G. Pan et al., 2009
		520 - 850	RapidEye	Jovanovic et al., 2014; Peralta et al., 2016; Bu et al., 2017
		610 - 890	SPOT-4 SPOT-5	O. Rojas, 2007; Durgun et al., 2016; Abiy & Suryabhagavan, 2016 Fernandez-Ordonez & Soria-Ruiz, 2017; Ngie and Ahmed, 2018
		450 - 900	Formosat-2	Fieuzal et al., 2017
		C-VH/C-HH	RADARSAT-2; TerraSAR-X	Fieuzal et al., 2017
		550 - 1750	Daedalus Enterprises Model 1260 Instrument	Senay et al., 1998
		400 - 900	Nikon SLR 35 mm camera	Panda et al., 2010
		520 - 900	IKONOS and Multispectral Digital Camera	Chang et al., 2003
		392 - 850	Piper PA-16 Clipper/Headwall	Aguate et al., 2017

			Photonics Micro-Hyperspec ARS3	
		420 - 920	Leica ADS80 digital camera	Khanal et al., 2018
		450 - 780	DMSC-2k System sensor	Maresma et al., 2018
		630 - 900	HJ-1A/1B satellites	Yu & Shang, 2017
Green Normalized Difference Vegetation Index	$\frac{NIR - GREEN}{NIR + GREEN}$	520 – 900	QuickBird	Bausch et al., 2008
		520 - 900	IKONOS and Multispectral Digital Camera	Chang et al., 2003
		450 - 900	SpecTerra Mark III; Vision One	Shanahan et al., 2001
		450 - 780	DMSC-2k System sensor	Maresma et al., 2018
Normalised Chlorophyll Index Green Model	(NIR/Green)-1	520 - 900	QuickBird	Bausch et al., 2008
Wide Dynamic Range Vegetation Index	$\frac{\alpha NIR - RED}{\alpha NIR + RED}$ $0.1 \leq \alpha \leq 0.2$	450 - 780	DMSC-2k System sensor	Maresma et al., 2018
Enhanced Vegetation Index	$2.5\frac{NIR - RED}{(NIR + 6RED - 7.5BLUE) + 1}$	450 - 780	DMSC-2k System sensor	Maresma et al., 2018
Leaf Area Index, Green Area Index	LAI, GAI*	400 - 1050	CHRIS-PROBA satellite	J. Wang et al., 2013
		500 - 1750	SPOT-4; SPOT-5	Soria-Ruiz et al., 2007; Battude et al., 2016*; Fernandez-Ordonez & Soria-Ruiz, 2017;
		450 - 900	Formosat-2	Battude et al., 2016*
		520 - 900	Deimos-1	Battude et al., 2016*
		HV/VH	RADARSAT-2	Soria-Ruiz et al., 2007
Soil-Adjusted Vegetation Index	$\frac{NIR - RED}{NIR + RED + L}(1 + L)$ L = 0.5	610 - 890	SPOT-5	Ngie & Ahmed, 2018
		450 - 780	DMSC-2k System sensor	Maresma et al., 2018
		400 - 900	Nikon SLR 35 mm camera	Panda et al., 2010

2.3.6. Using UAV and ground-based platform in the corn yield forecast

Satellite remote sensing technologies have become an extremely useful platform to provide data and images for various agricultural crop yield applications, especially, for maize yield prediction. However, there exist many limitations such as the high cost, the risk of cloud cover, the long revisit periods, and the insufficient polarization or frequency. To overcome the drawbacks above, the UAVs and ground-based platforms are good alternatives that offer low-cost, higher spatial and spectral resolutions (Candiago, 2015, Table 1). In the context of precision agriculture, the image data derived from UAV's sensors have recently been applied. In particular, for estimating corn yield, according to Link et al., 2013, the analysis of collected data presented small correlations between corn yield and indices derived from the monolithic miniature spectrometer (MMS1), namely, the coefficient of determination was less than 0.20. Geipel et al., 2014 combined UAS-based RGB imagery with three different linear regression models to estimate corn yield in early- to mid-season crop growth stages with determination coefficients R^2 of up to 0.74 and RMSEP ranging from 0.67 to 1.28 t/ha. The study of Zaman-Allah et al., 2015 showed a good correlation between NDVI obtained from the UAV-platform and grain yield, with coefficients of correlation was 0.63. Whereas the result of Vergara-Díaz et al., 2016 was lower with R^2 of 0.452 for all trial and 0.543 for 6 hybrids at the CIMMYT Harare station in Southern Africa. Furthermore, Maresma, 2016 found the relationship between different multispectral vegetation indices (NDVI, WDRVI, GRVI) derived from the VEGCAM-Pro camera mounted on the drone and maize yield. The WDRVI was the best spectral index to explain final maize yield (R^2 = 0.92 and RMSE = 0.87 Mg/ha). Wahab et al., 2018 also proved that GNDVI was a good parameter in predicting corn yield model, which obtained from UAV imagery. The correlations were r of 0.372 and r of 0.393 for mean and maximum GNDVI respectively. With the above evidence, there is no doubt that the development of UAVs in recent time plays an important key in precision agriculture and enhances the accuracy for estimating crop yield at small fields.

On the other side, many non-destructive measuring techniques are ground-based or stationary using fixed, handheld or motorized systems (e.g. tractor mounted sensor platforms, crane systems or variable-rate technologies) were also used for crop monitoring (Liebisch, 2015). This technology provides better temporal, spectral, and spatial resolutions in comparison to UAV, airborne and satellite remote sensing. Jackson

R.D., 1986 pointed out that the handheld remote sensing instruments are very useful for small-scale operational field monitoring of biotic and abiotic stress agents. However, there are limitations such as small measurement scale, labour-intensive and time-consuming. Ground-based active optical sensors (GBAO) based on red and near-infrared ratios or NDVI to explain leaf density and chlorophyll status of the crop. Thus, many studies have applied GBAO in predicting crop yield (K. Sharma et al., 2015, 2018). The GreenSeeker sensor was used to collect NDVI in many study and field experiment, which showed the relationship between NDVI and corn grain yield with a good correlation. (Martin et al., 2005; Teal et al., 2006, with $R^2 = 0.77$; Martin et al., 2007, with $R^2 = 0.56$ to 0.66; Inman et al., 2007, with $R^2 = 0.65$; Spitkó et al., 2016). The Holland Scientific Crop Circle ACS Sensor was also used by Solari et al., 2008 that determined vegetation indices (GNDVI and CIgreen) with the greatest sensitivity in assessing corn grain yield. Furthermore, many recent studies have used both the GreenSeeker and Crop Circle ACS sensor along with In-season estimated yield (INSEY) that have better correlation with corn yield (Franzen, 2014; L. K. Sharma, Bu, & Franzen, 2016; L. K. Sharma, Bu, Franzen, et al., 2016; L. K. Sharma & Franzen, 2014; L.K. Sharma, 2018; Lakesh K. Sharma, 2015; Shaver et al., 2015).

Table 2.8. *Typical VIs used for monitoring corn yield by UAV, Ground-based platform*

Vegetation index	Formula	Platforms/Sensors	Spectral wavelengths [nm]	References
Green Normalized Difference Vegetation Index (GNDVI)	$\frac{NIR - GREEN}{NIR + GREEN}$	Enduro quadcopter/ GoPro Hero 4 cameras	460 - 900	Wahab et al., 2018.
		Holland Scientific Crop Circle ACS Sensor	Green: 590 NIR: 880	Solari et al., 2008
Normalized Difference Vegetation Index (NDVI)	$\frac{NIR - RED}{NIR + RED}$	Airelectronics (Madrid, Spain) /ADC-Lite multispectral camera	520 - 900	Zaman-Allah et al., 2015; Vergara-Diaz et al., 2016;
		Atmos-6 UAV/ VEGCAM-Pro camera	525 - 805	Maresma et al., 2016
		GreenSeeker	Red: 660 ± 15 NIR: 770 ± 15	Martin et al., 2005, 2007; Teal et al., 2006; Inman et al., 2007; Freeman et al., 2007; Martin et al., 2012;

				Cairns et al., 2012; Shaver et al., 2015; Spitkó et al., 2016; Sharma et al., 2018
		Holland Scientific Crop Circle ACS Sensor	Red: 650 ± 20 Red-Edge: 730± 10 NIR: 760 ± 10	Shaver et al., 2015; Sharma et al., 2018
In-season estimated yield (INSEY)	NDVI/GDD GDD: Growing Degree Days	GreenSeeker	Red: 660 ± 15 NIR: 770 ± 15	Teal et al., 2006; Inman et al., 2007; Martin et al., 2012; Sharma & Franzen 2014; Sharma et al., 2015; Franzen et al., 2014; Sharma et al., 2016; Sharma, Bu, & Franzen, 2016
		Holland Scientific Crop Circle ACS Sensor	Red: 650 ± 20 Red-Edge: 730 ±10 NIR: 760 ± 10	Sharma & Franzen 2014; Sharma et al., 2015; Franzen et al., 2014; Sharma et al., 2016; Sharma, Bu, & Franzen, 2016
Green Ratio Vegetation Index (GRVI)	$\frac{NIR}{GREEN}$	Atmos-6 UAV/ VEGCAM-Pro camera	525 - 805	Maresma et al., 2016
Wide Dynamic Range Vegetation Index (WDRVI)	$\frac{\alpha NIR - RED}{\alpha NIR + RED}$ $0.1 \leq \alpha \leq 0.2$	Atmos-6 UAV/ VEGCAM-Pro camera	525 - 805	Maresma et al., 2016
Vegetation Index Green (Vig)	$\frac{GREEN - RED}{GREEN + RED}$	MikroKopter Hexa XL/Canon Ixus 110 IS RGB consumer camera	380 – 700 Red-Green-Blue	Geipel et al., 2014
Excess Green Index (ExG)	2GREEN – RED – BLUE			
Plant Pigment Ratio(PPRb)	$\frac{GREEN - BLUE}{GREEN + BLUE}$			
Chlorophyll Index Green (CIgreen)	$\frac{NIR}{GREEN} - 1$	Holland Scientific Crop Circle ACS Sensor	Green: 590 NIR: 880	Solari et al., 2008
Infra-Red Index (IRI)	IRI 1 = R_{740}/R_{730} IRI 2 = R_{740}/R_{720} IRI 3 = R_{760}/R_{730}	E-Trainer 182 /MMS1	310 - 1100	J. Link et al., 2013

Dark Green Color Index (DGCI)	[(Hue – 60)/60 + (1 – Saturation) + (1 – Brightness)]/3	Olympus C3030 camera and Canon Power Shot S51S	380 – 700 Red-Green-Blue	Rorie et al., 2011

2.4. Crop Simulation Models (CSMs) for Crop Yield Forecast

CSMs are computerized representations of crop growth, development and yield, simulated through mathematical equations as functions of soil conditions, weather and management practices (Hoogenboom et al., 2004). There are many CSMs around the world and depending on the design of the model, CSMs can be divided into two general groups: Empirical models (statistical models) and Dynamic models (process-based models). The empirical models are formulated as regression equations (with simple or multiple input parameters) and are based on direct descriptions of the observed data. The dynamic models are rooted in a process-based understanding of crop development (require more input parameters than the empirical models) (Kasampalis, 2018). After over 40 years, the development of the CSMs has achieved outstanding results from simple to complex. The development process was summarized in Figure 2.5, with typical CSMs such as the WOFOST, ORYZA, DSSAT, APSIM, STICS, MONICA, DAISY, and AquaCrop models.

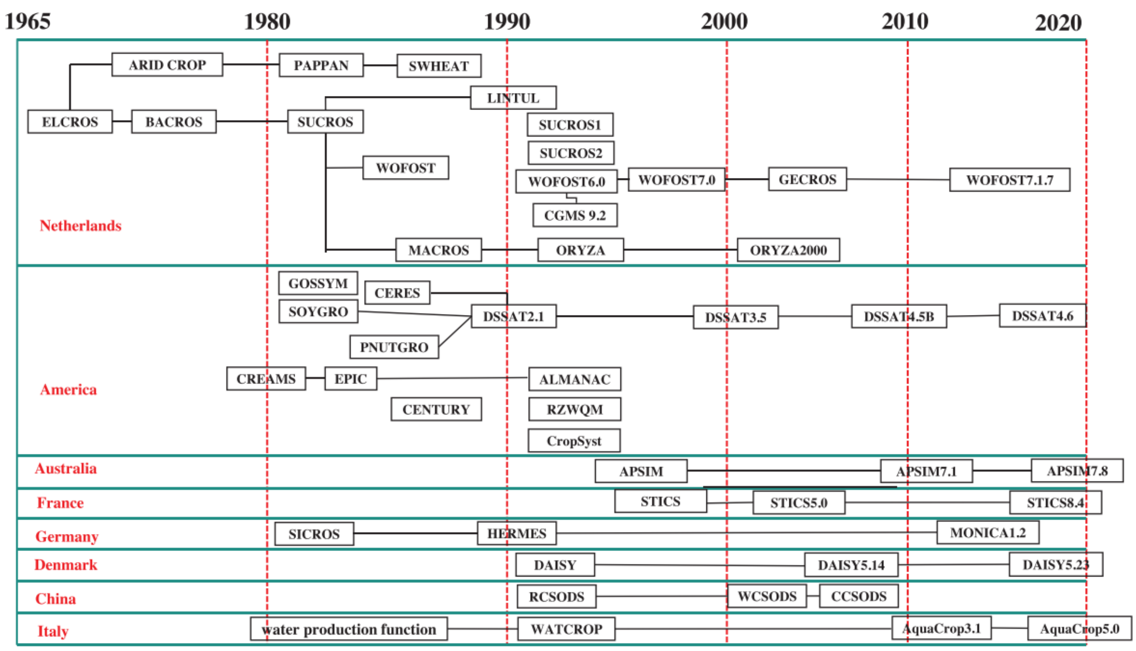

Figure 2.4. *Development process over time of typical CSMs (Jin, 2018)*

The experimental process of CSMs for crop yield prediction pointed out that the main limitations of them are the cost of obtaining the necessary input data to run the model, along with the lack of spatial information in some cases, and the input data quality (Basu & Kumar, 2014). Hence, the integration of RS and CSMs for crop yield forecast is essential to improve the accuracy.

2.5. Integration of Remote Sensing and CSMs

In the 1970s, Wiegand and colleagues stated that information derived from remote sensing data may increase the accuracy of crop modelling and the combination of RS and CSMs has been a subject of research for almost three decades. RS is capable of obtaining and providing data about crop status during the growing season through VIs directly or LAI, fAFAR, biomass indirectly, whereas CSMs can show the growth of crops day by day. The integration models generally are carried out with three basic steps: (i) estimate canopy variables with RS; (ii) run the CSM; and (iii) use a proper integration method to adjust model runs (FAO, 2017). In the first step, canopy variables are estimated from RS through the statistical/empirical models and the Physical Reflectance Models (PRMs). And then researchers use data assimilation methods to integrate, both in space and time, canopy state variables with various information using remote sensing methods for optimizing crop parameters in crop models. According to Jin et al., 2018, the current main data assimilation algorithms include Kalman Filter (KF), Ensemble Kalman Filter (EnKF), Three-Dimensional Variational Data Assimilation (3DVAR), Four-Dimensional Variational Data Assimilation (4DVAR), Particle Filter (PF) and Hierarchical Bayesian Method (HBM).

3. MATERIALS AND METHOD

3.1. Study Area

Erzurum is a province of Turkey and located in the Eastern Anatolia Region. The total area of Erzurum province is 25.066 km^2 (the fourth biggest in Turkey). It is situated 1.859 meters above sea level and has 20 districts. The study area is located in the Pasinler district that belongs to Erzurum province and has 72 communes (Figure 3.1). The location of Pasinler town is about 40 km east from the Erzurum city and situated 1.740 meters above sea level, between 39°58′N and 39°97′N and between 41°40′E and 41°67′E. The Pasinler district has an area of 1.134 km^2 and a population of 28.961 people in 2018.

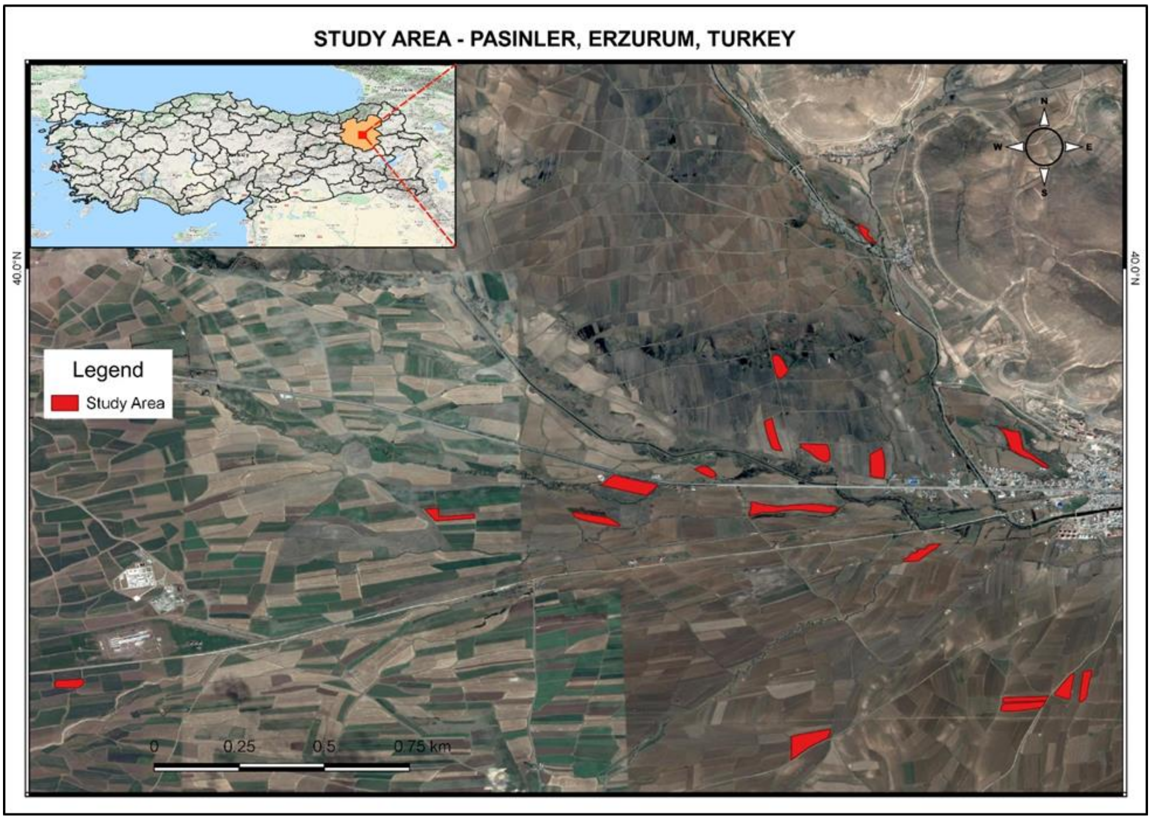

Figure 3.1. *The study area of the research*

The main topographies are mountains, plateaus and hills, along with plains and deep valleys intermingle between them. The Pasinler Plain was formed from the Pasinler river basin with an area of approximately 350 km^2. It is alluvial plain separated from Erzurum plain. There are 5 main types of soil that are alluvial soil, colluvial soil, reddish-brown soil, chestnut soil, and basalt soil and are suitable for agriculture. The climate of Pasinler is the continental climate of East Anatolia. Specifically, the winter is long with cold, slightly rainy and snowy; the spring is short and rainy, the summer is hot and dry. The average annual temperature is 5.6ºC, with an average temperature of 19.7°C in the warmest month (July) and - 6.3°C in the coldest month (January). The average annual rainfall is 458 mm and the rainiest month is May with the mean rainfall of 69 mm, whereas the driest month is August with a mean rainfall of 19 mm (Http-1). For these reasons, the climate in Pasinler is very severe and the dominant vegetation is grassland without forest or negligible forests. Most of the area of Pasinler is covered with snow from November to April annually.

3.2. Maize Phenology

The growth cycle of corn is divided two the phenological stages: the vegetative stage and the reproductive stage (Table 3.1). The vegetative stage is the appearance of leaves or leaf collars that starts when the emergence of the first internode on the corn plant above the soil surface (VE) and ends when the last branch of the tassel is completely visible and the corn plant has reached full height (VT). And then the reproductive stage starts when pollination occurs (R1) and ends with full maturity (R6), i.e. all kernels have attained maximum dry weight.

Table 3.1. *Phenological stages of the corn plant (Ransom & Enders, 2013)*

VEGETATIVE STAGES	REPRODUCTIVE STAGES
VE (emergence)	R1 (silking)
V1 (first leaf)	R2 (blister)
V2 (second leaf)	R3 (milk)
V3 (third leaf)	R4 (dough)
V(n) (nth leaf)	R5 (dent)
VT (tasseling)	R6 (physiological maturity)

The climate factors play an important role in the developmental stages of the corn plant, especially temperature and moisture. During the vegetative stage, the range of temperature is typically from 8 to 38ºC with an optimum of 34ºC (Badu-Apraku et al., 1983; Kiniry & Bonhomme, 1991) while for the reproductive stage, the range is from 8 to 30ºC (Muchow et al., 1990). The study of Dupuis & Dumas, 1990 and Herrero & Johnson, 1980 proved that the temperature exceeds 35ºC will be harmful to the pollen of corn plant. On the other hand, the relationship of corn phenology to the temperature which has been described through the use of growing degree days was summarized in the research of Jerry L Hatfield & Dold, 2018. Besides, the moisture also affects the growth cycle, e.g., maize seed begins germination when the seed contains at least 30% moisture (Ransom & Enders, 2013); the quality of movement from the tassel to the silk will decrease when the moisture comes down (Fonseca & Westgate, 2005). Knowledge of the plant growth process helps the farmer to determine the cause and effect of the disease or other crop problem and take appropriate and timely solutions (fertilizer, irrigation, cultivation, harvest) to improve yields significantly. However, this study is only concerned about the planting and harvest dates. In Turkey, the crop calendar of maize depends on each region and in the study area of this work, maize is planted from 1st to 15th of May and the harvest period starts on the 1st of September and ends on 30th of September.

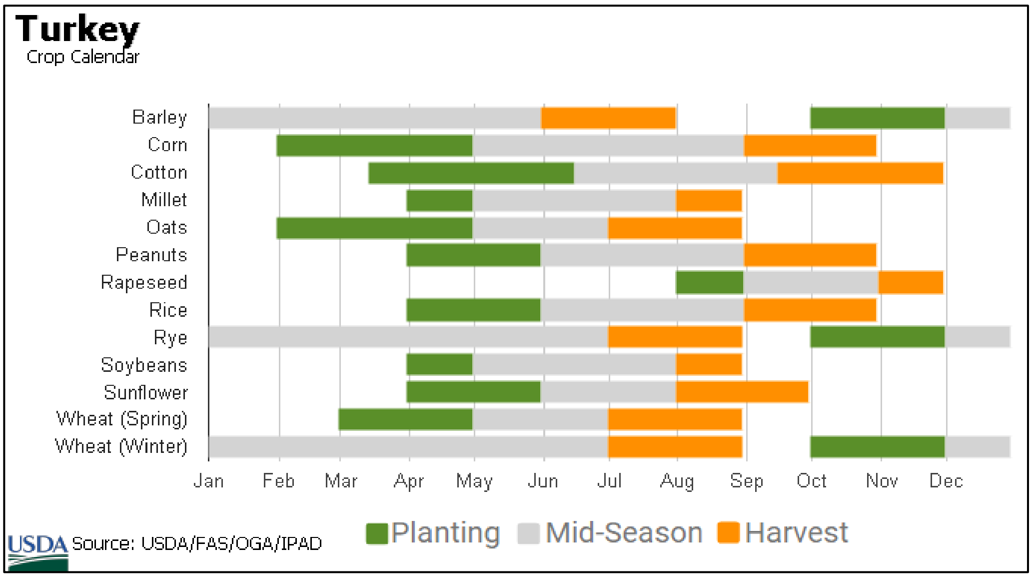

Figure 3.2. *Crop calendar of the food crops in Turkey (Http-2)*

3.3. Software

Nowadays, with the trend of open sharing, integration and access, open source software is becoming more and more powerful along with the support of a wide community of scientists and developers over the world. In the industry of research on remote sensing and GIS, open source software will completely replace commercial software in the near future. Thus, QGIS and R were used for analyzing the data in this study.

3.3.1. QGIS

The full name of QGIS software is Quantum Geographic Information System software which is a free, open-source and cross-platform (Windows, Android, Linux, Mac OS X, GNU/Unix) software. Besides, it can develop and expand through the plugin in Python and C++ languages. QGIS is proposed by Gary Sherman in 2002 as data visualization a tool for Geographic Resources Analysis Support System (GRASS) and Geographic Database Management System (PostGIS). In 2007, QGIS became the official projects of the Open Source Geospatial Foundation (OSGeo) and its first version 1.0 was launched in 2009, version 2.0 in 2013, version 3.0 in 2018 and the newest version is 3.6.1 - Noosa that was used in this study. QGIS integrates Geospatial Data Abstraction Library (GDAL), GRASS, System for Automated Geoscientific Analyses (SAGA), Orfeo ToolBox and supports a variety of vector data formats such as PostgreSQL-PostGIS, Shapefiles, GPX, GeoJSON, SQLite, KML, MapInfo, Autocad DXF, ESRI Personal Geodatabase, Oracle Spatial, Erdas, ENVI, and so on (Moyroud & Portet, 2018).

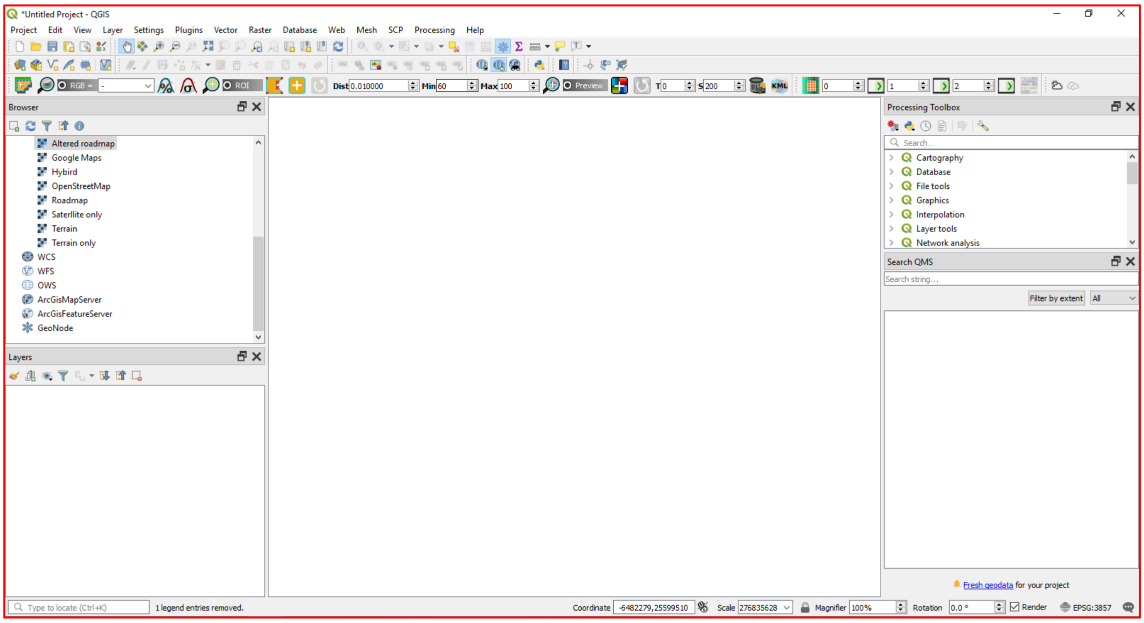

Figure 3.3. *The standard interface of QGIS software version 3.6.1*

3.3.2. R and Rstudio

R is a free, open-source software and programming language that is an environment for data analysis and graphics (Ihaka & Gentleman, 1996). It was developed by two statisticians Ross Ihaka and Robert Gentleman based on the S language, developed by

John Chambers and colleagues (Becker et al., 1988). R provides many functions to solve and build statistical models such as linear and nonlinear regression models, time-series analysis, classification, clustering, classical statistical tests and so on (R Development Core Team, 2013). Moreover, R is a versatile language that can be used for many different purposes through building specific packages that are free to download via the Comprehensive R Archive Network (CRAN) portal (https://cran.r-project.org/). Up to 20th April 2019, there were 14086 available packages in the CRAN and the rgdal, raster, shiny, shinydashboard, plotly, datasets, dplyr, leaflet, psych, BMA, reshape packages were used in this research.

RStudio is an integrated development environment (IDE) that integrates help and documentation, provides a workspace browser and data viewer and supports syntax highlighting code completion, and smart indentation in order to R users interact more readily. It is also free and similar to the standard RGui (see https://www.rstudio.com). The R version 3.5.1 and RStudio version 1.1.456 were used in this topic.

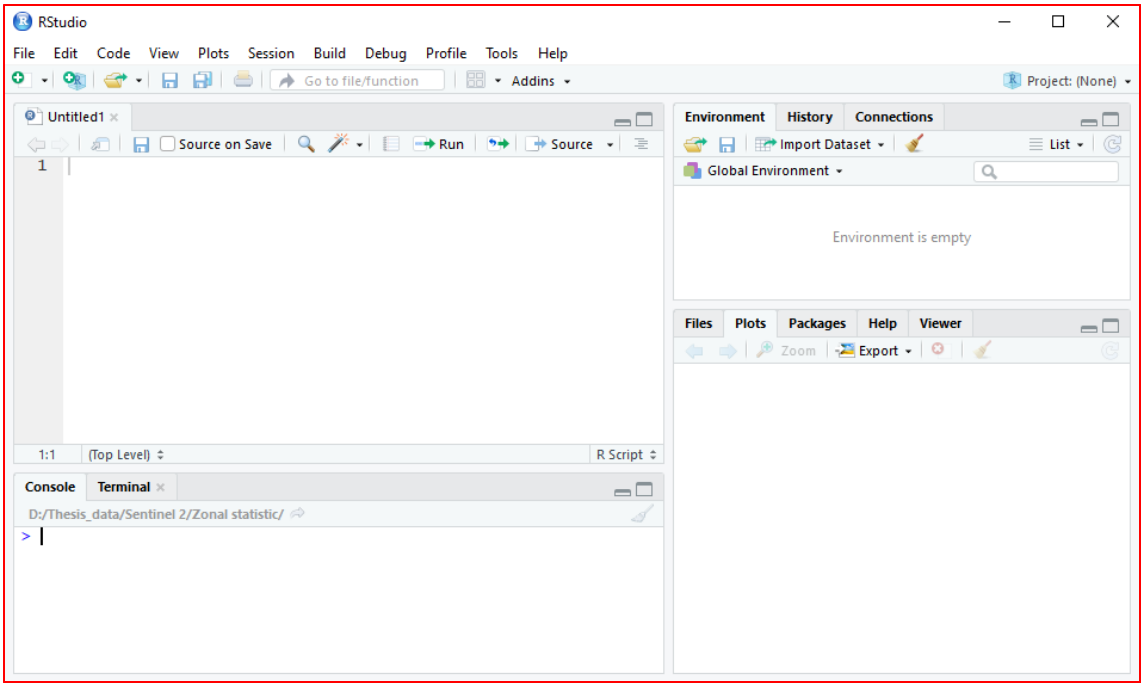

Figure 3.4. *The interface of RStudio version 1.1.456*

3.4. Research Workflow

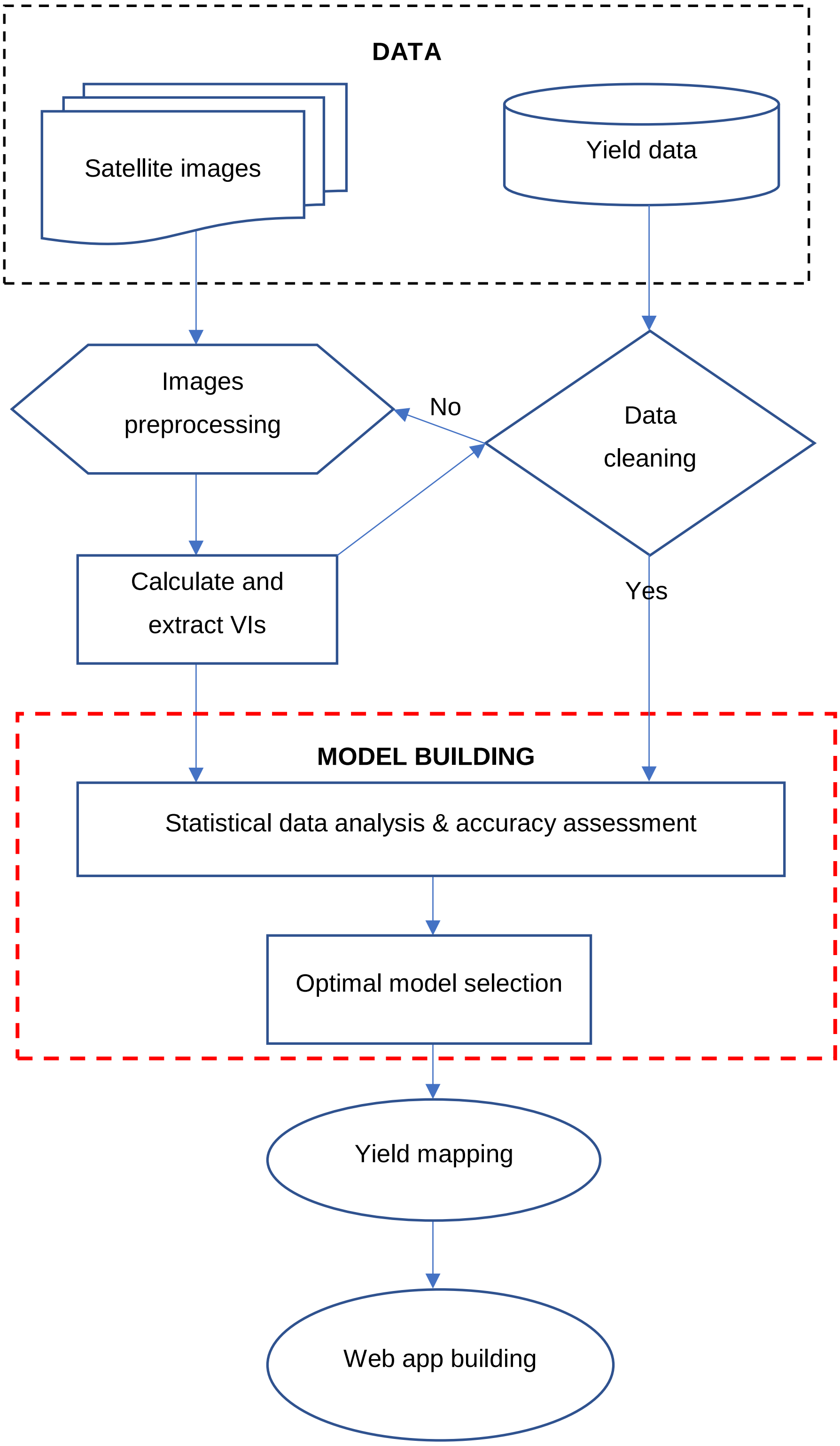

Figure 3.5. *Flowchart of methodology for this study*

This figure is a total overview of the research process and methodology that were applied in this study. The next sections clarify the research question step by step.

3.5. Datasets

In this section, the collected data is described. The datasets of this study include the satellite images and the actual maize yield data. All data is collected in throughout the corn season of 2018. In addition, all datasets were converted and referenced in a projected coordinate system that is the World Geodetic System 84 and the selected projection is Universal Transverse Mercator zone 37N (EPSG:32637 - WGS 84/UTM zone 37N).

3.5.1. Yield data

Raw data were collected from 26 corn fields and then carried on the data cleaning step, i.e., compared with the remote sensing data. There were 8 corn fields removed because the obtained area was too different from the cultivated area and the crop growth cycle was not the same as corn phenology. Finally, the yield data from 18 corn fields are described in detail in Table 3.2 with a total area of 51.3632 ha, whereas the cultivated area is 55.415459 ha.

Table 3.2. *Yield collected data per each corn field*

Map_ID	Area (ha)	Cultivated area (ha)	Actual Yield (t/ha)	Farmer name	Name_ID
1	5.718	5.737422	67.19	Mennan Özkılıç	A
2	1.2966	1.300968	54.14	Selami Babapil	B
3	3.2733	3.718203	59.86	Metin Sarıpül	C
4	3.3	3.311214	73.04	Ayhan Ağver 2	E
5	2	2.624168	53.81	Metin Sarıgül 2	F
6	2.615	2.330036	69.17	Sefa Taşcı 1	G
7	2.4617	2.470088	57	Hamit Tiryaki	H
8	1.5522	2.166867	37.33	Erdal Avcı	K
9	2.51	2.518597	73.88	Esat Kadıoğlu	L
10	2.1883	2.245166	72.68	Zafer Ekrek	M
11	2.6	2.7319	76.34	Ömer Bayram	N
12	5.9216	5.941745	25.76	Tarımsal Araştırma	O
13	0.9243	1.008031	51.33	Kadir Çakıcı 3	Q
14	3.0334	3.043746	78.29	Ömer Bayram 3	S
15	2.0044	1.950061	67.38	Mennan Özkılıc 2	T
16	3.1164	5.626941	37.13	Vahit Oğüs	Y
17	2.348	2.355967	63.29	Murat Çoban	Z

18	4.5	4.334339	56.47	Esat Kadıoğlu 2	W
Total	**51.3632**	**55.415459**			

Figure 3.6 presents some statistical indices of the collected yield data. Specifically, the median is 61.575 t/ha, the maximum and minimum yields are 78.29 t/ha and 25.76 t/ha respectively. In addition, the box plot also shows that 25% of yield data is lower 53.81 t/ha and 75% of yield data is lower 72.68 t/ha.

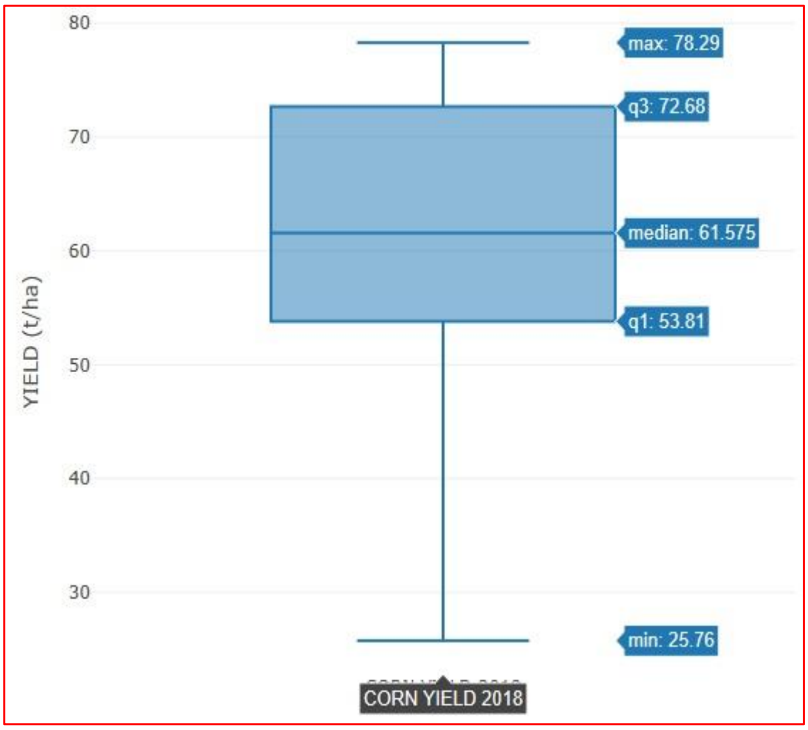

Figure 3.6. *Descriptive statistics of the actual corn yield in 2018*

3.5.2. Satellite data

Based on the crop calendar, the cloud-free satellite images of Landsat-8 and Sentinel-2 for the study area were downloaded. There were 16 Landsat-8 scenes as level-1C that were downloaded from the LandsatLook Viewer website (https://landsatlook.usgs.gov) of the United States Geological Survey (USGS) Landsat image archives. All Landsat 8 images of the study area are at path 171 or 172 and row 32 with the percent of cloud cover from 0 to 42% (Table 3.3).

Table 3.3. *Description of each collected Landsat-8 images*

	Sensor	Path	Row	Cloud cover (%)	Acquisition date	Date of year	Note
1	OLI	172	32	29	01-May-2018	121	Level 1
2	OLI	172	32	20	17-May-2018	137	Level 1
3	OLI	171	32	17	26-May-2018	146	Level 1
4	OLI	171	32	15	11-June-18	162	Level 1
5	OLI	171	32	8	27-June-18	178	Level 1
6	OLI	172	32	30	20-July-18	201	Level 1
7	OLI	171	32	4	29-July-18	210	Level 1
8	OLI	172	32	36	05-August-18	217	Level 1
9	OLI	171	32	42	14-August-18	226	Level 1
10	OLI	172	32	27	21-August-18	233	Level 1
11	OLI	171	32	0	30- August -18	242	Level 1
12	OLI	172	32	9	06-September-18	249	Level 1
13	OLI	171	32	2	15-September-18	258	Level 1
14	OLI	171	32	16	01-October-18	274	Level 1
15	OLI	172	32	16	08-October-18	281	Level 1
16	OLI	171	32	0	17-October-18	290	Level 1

For Sentinel-2 data, a dataset of 29 images as level-2A was used. These scenes were downloaded from the Sentinel Hub website (https://apps.sentinel-hub.com/eo-browser/) of Sinergise is a GIS company. The Sentinel-2 images of the study area are at the tile number T38TKK and the percent of cloud cover from 0 to 28% (Table 3.4).

Table 3.4. *Description of each collected Sentinel-2 images*

	Sensor	Tile number	Cloud cover (%)	Acquisition date	Date of year	Note
1	MSI	T38TKK	12	18-May-18	138	Level 2A
2	MSI	T38TKK	6	07-June-18	158	Level 2A
3	MSI	T38TKK	8	12-June-18	163	Level 2A
4	MSI	T38TKK	28	19-June-18	170	Level 2A
5	MSI	T38TKK	25	24-June-18	175	Level 2A
6	MSI	T38TKK	3	27-June-18	178	Level 2A
7	MSI	T38TKK	0	29-June-18	180	Level 2A
8	MSI	T38TKK	1	02-July-18	183	Level 2A
9	MSI	T38TKK	0	09-July-18	190	Level 2A

10	MSI	T38TKK	0	12-July-18	193	Level 2A
11	MSI	T38TKK	4	19-July-18	200	Level 2A
12	MSI	T38TKK	6	24-July-18	205	Level 2A
13	MSI	T38TKK	10	27-July-18	208	Level 2A
14	MSI	T38TKK	1	01-August-18	213	Level 2A
15	MSI	T38TKK	4	06-August-18	218	Level 2A
16	MSI	T38TKK	3	13-August-18	225	Level 2A
17	MSI	T38TKK	0	16-August-18	228	Level 2A
18	MSI	T38TKK	2	18-August-18	230	Level 2A
19	MSI	T38TKK	3	23-August-18	235	Level 2A
20	MSI	T38TKK	1	26-August-18	238	Level 2A
21	MSI	T38TKK	4	31-August-18	243	Level 2A
22	MSI	T38TKK	0	02-September-18	245	Level 2A
23	MSI	T38TKK	1	05-September-18	248	Level 2A
24	MSI	T38TKK	4	12-September-18	255	Level 2A
25	MSI	T38TKK	11	15-September-18	258	Level 2A
26	MSI	T38TKK	0	25-September-18	268	Level 2A
27	MSI	T38TKK	1	30-September-18	273	Level 2A
28	MSI	T38TKK	3	10-October-18	283	Level 2A
29	MSI	T38TKK	0	15-October-18	288	Level 2A

3.6. Satellite Images Preprocessing

3.6.1. Landsat-8 images

The obtained Landsat-8 images for this study were level-1, which was an ortho-rectified top of atmosphere reflectance. Using the Semi-Automatic Classification Plugin (SCP) for QGIS to convert the sensor digital numbers into the spectral radiance, i.e., the Top Of Atmosphere (TOA) reflectance. This process is executed based on the calibration coefficients from the metadata of the Landsat-8 sensor. Next step, using the Stack raster bands of SCP to create the multi-band image from the single bands (included the visible band and NIR band with 30 m of resolution). Then in the image cropping step, using the R with raster and rgdal packages to write the code for splitting the multi-band image according to the study area.

3.6.2. Sentinel-2 images

The Sentinel-2 data was level-2A. The level-2A products are corrected atmospheric and calculated the Bottom Of Atmosphere (BOA) reflectance. The Sentinel-2 atmospheric correction was based on the algorithm proposed in the Atmospheric/Topographic Correction for Satellite Imagery (Richter & Schläpfer, 2011) and the libRadtran radiative transfer model (Mayer & Kylling, 2005). The level-2A process uses Planet Digital Elevation Model, while cirrus and Bidirectional Reflectance Distribution Function corrections are deactivated (Drusch et al., 2012). Thus, this part only performs the stack raster bands (included the visible band and NIR band with 10 m of resolution) and the image cropping steps that were the same as the Landsat-8 preprocessing.

3.6.3. Calculating and extracting vegetation index

In section 2.1, the basis of yield estimation using remote sensing was explained and the relationship between corn and remote sensing about reflection, absorption, transmission likes any other vegetation. Figure 3.7 illustrates the change in solar energy throughout the maize growth cycle. In the flowering stage, the NIR reflectance is strongest, whereas the Red reflectance is weakest.

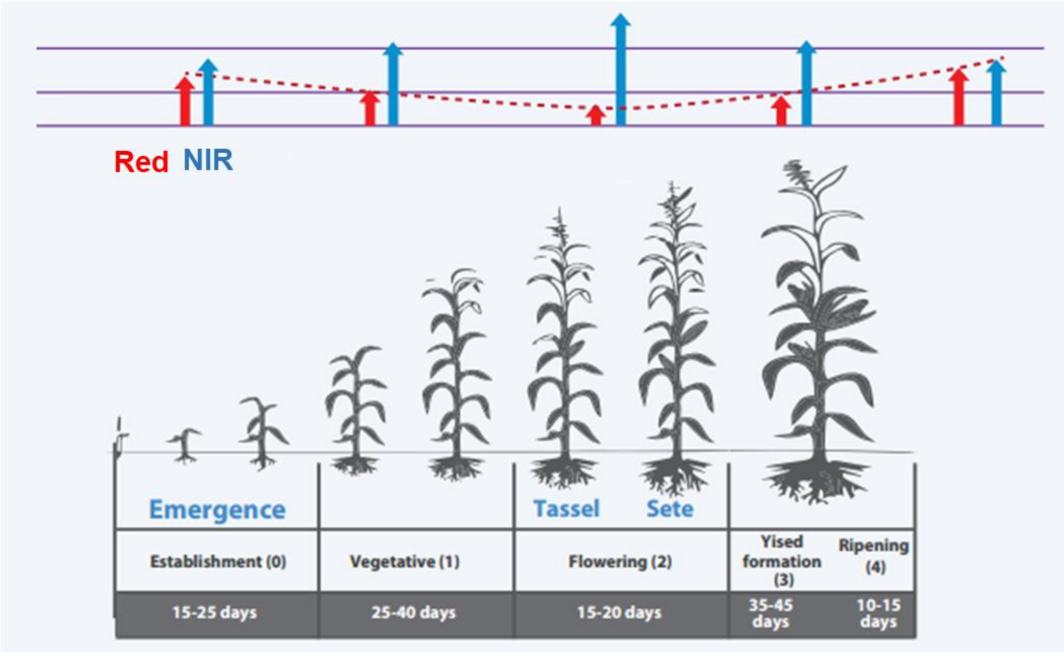

Figure 3.7. *Changing Red and NIR light in the corn growth stage (FAO, 2018)*

Relevant studies were presented in section 2.3 that showed a good correlation between VIs and productivity of corn. Each different index has a different correlation. Based on that groundwork, this research selected the 5 VIs for predicting corn yield, which were NDVI, EVI, SAVI, WDRVI, and GNDVI. These VIs were calculated using the red, green, and near-infrared spectral bands of Landsat-8 and Sentinel-2 imagery with the formula as in the table below.

Table 3.5. *Formulas of the VIs used in this research by each satellite*

Index	*Landsat-8 formula*	*Sentinel-2 formula*	*Reference*
NDVI	$\frac{Band5 - Band4}{Band5 + Band4}$	$\frac{Band8 - Band4}{Band8 + Band4}$	Rouse et al., 1974
EVI	$2.5\frac{Band5 - Band4}{(Band5 + 6Band4 - 7.5Band2) + 1}$	$2.5\frac{Band8 - Band4}{(Band8 + 6Band4 - 7.5Band2) + 1}$	Huete et al., 1997
SAVI	$1.5\ \frac{Band5 - Band4}{Band5 + Band4 + 0.5}$	$1.5\ \frac{Band8 - Band4}{Band8 + Band4 + 0.5}$	Huete, 1988
WDRVI	$\frac{0.1\ Band5 - Band4}{0.1\ Band5 + Band4}$	$\frac{0.1\ Band8 - Band4}{0.1\ Band8 + Band4}$	Gitelson, 2004
GNDVI	$\frac{Band5 - Band3}{Band5 + Band3}$	$\frac{Band8 - Band3}{Band8 + Band3}$	Gitelson et al., 1996

In this step, R was used to calculate these VIs through the raster package (see the code in Appendix 1, 2). Then using the zonal statistic function to extract the mean value of these VIs for each maize field (see the code in Appendix 3). The change in the value of the VIs throughout the corn growth stage is indicated through Figure 3.8, 3.9, 3.10, 3.11, 3.12.

The range of changing value is different for each VI, but generally, the value is low in the sowing stage and gradually increases in the vegetative stage. The high value is maintained stably and reaches its peak value in the flowering stage. After that, the values begin to gradually decline and decrease significantly when it comes to the harvest stage.

Landsat-8 Sentinel-2

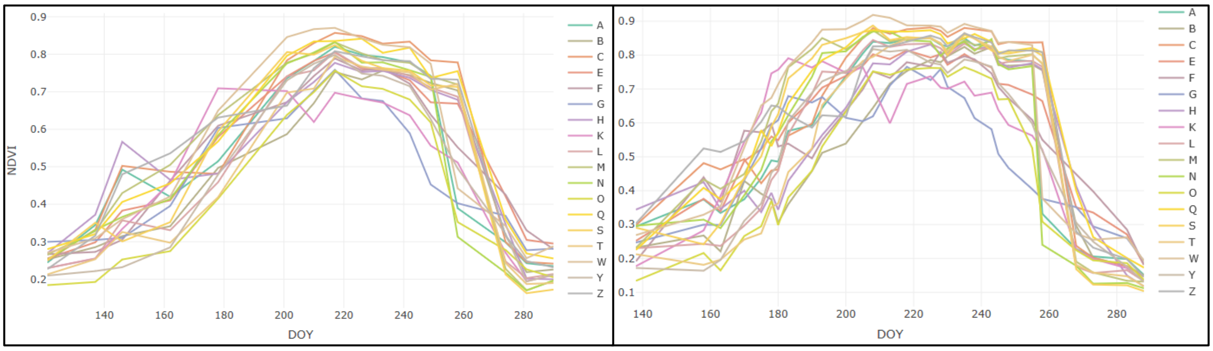

Figure 3.8. *NDVI value of each corn field throughout the season*

The value of NDVI ranges from -1 to 1. The range for green vegetation is between 0.2 to 1. The higher NDVI value correspond to the healthy vegetation.

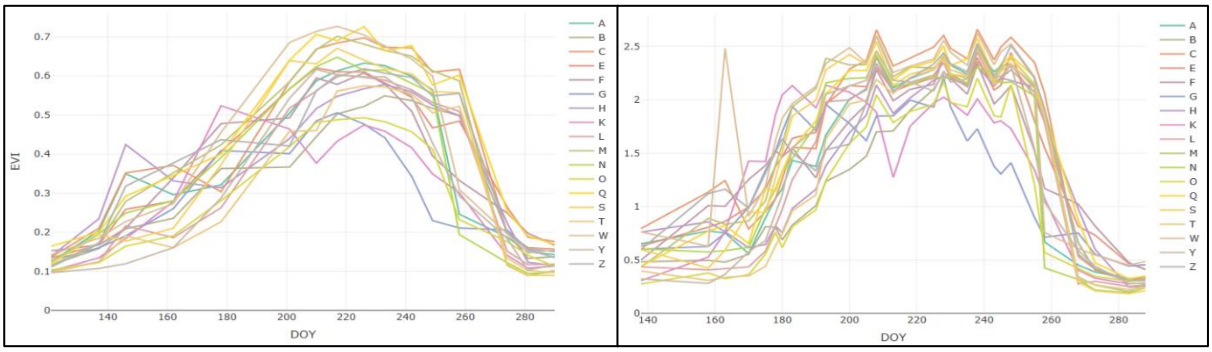

Figure 3.9. *EVI value of each corn field throughout the season*

The EVI is calculated to optimize the vegetation signal through a de-coupling of the canopy background signal and a reduction in atmosphere influences.

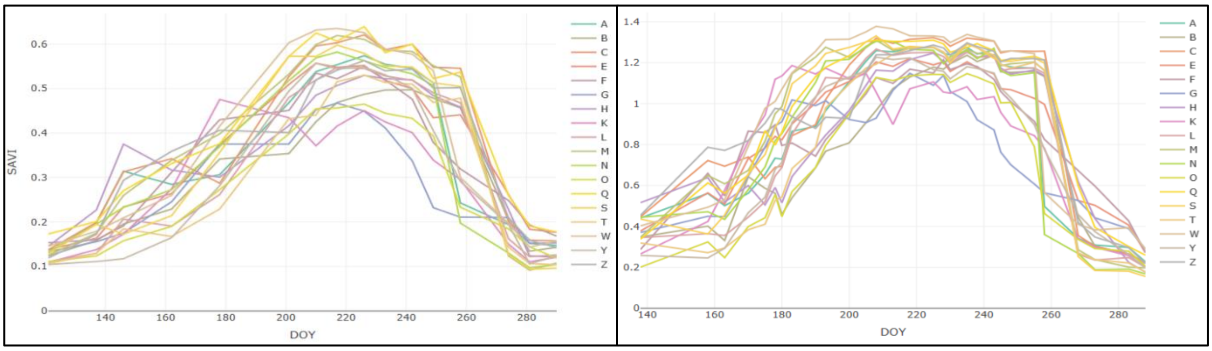

Figure 3.10. *SAVI value of each corn field throughout the season*

The SAVI is a vegetation index that attempts to minimize the influence of soil luminance using a soil luminance correction factor. Thus, the SAVI is often used for monitoring at the sowing stage.

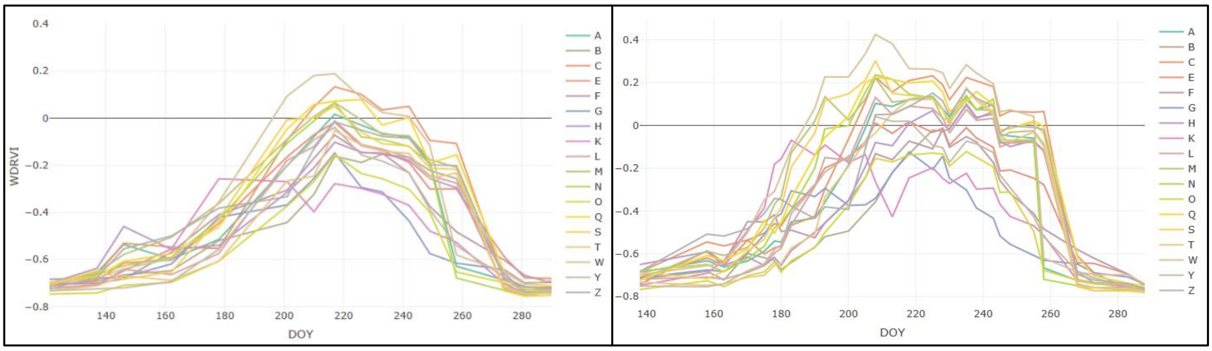

Figure 3.11. *WDRVI value of each corn field throughout the season*

The WDRVI as a way to enhance the dynamic range of the NDVI by using a weighting parameter α to the near infrared reflectance. It is a simple approach to optimize the dynamic range for high biomass environments.

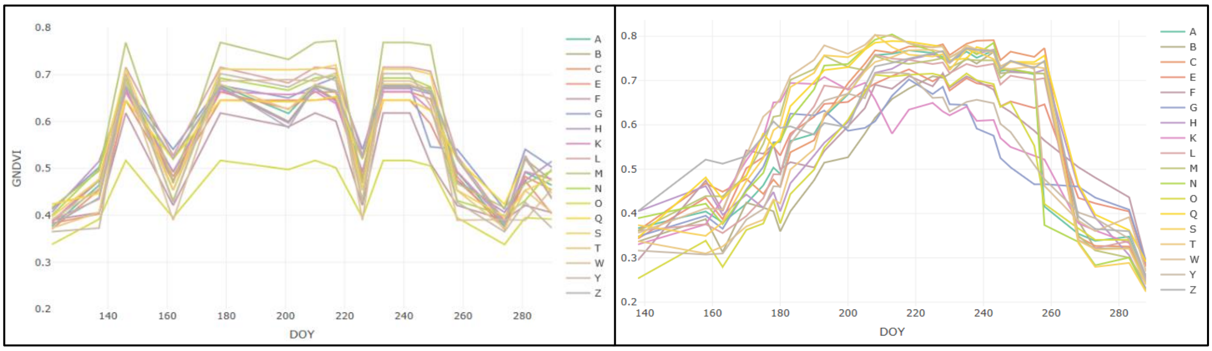

Figure 3.12. *GNDVI value of each corn field throughout the season*

The GNDVI is one of the most regularly used vegetation indices to determine water and nitrogen uptake into the crop canopy. The range of the GNDVI value is from -1 to 1. It helps to optimize irrigation in the field.

3.7. Statistical Analysis Method Selection

3.7.1. Data analysis option

This topic selected the highest VI value, the average VI value throughout the corn growth cycle and the VI value of the first day of the harvest period (258^{th} day of the year) to analyze the correlation with the observed corn yield data in 2018 season. Table 3.6, 3.7, 3.8 and Table 3.9, 3.10, 3.11 show the selected data from Landsat-8 and Sentinel-2, respectively.

Table 3.6. *Maximum VI values for each corn field from Landsat-8 data*

ID	Name_ID	EVI	NDVI	SAVI	WDRVI	GNDVI
1	**A**	0.632947	0.819896	0.573659	0.016976	0.676405
2	**B**	0.549233	0.75637	0.496897	-0.15249	0.673001
3	**C**	0.697536	0.857028	0.620522	0.133684	0.663099
4	**E**	0.620657	0.80498	0.557077	-0.01702	0.649753
5	**F**	0.607461	0.788844	0.549649	-0.07156	0.618235
6	**G**	0.505787	0.758758	0.467397	-0.14762	0.6941
7	**H**	0.578331	0.777075	0.529396	-0.10188	0.670127
8	**K**	0.523886	0.709191	0.475377	-0.25694	0.663775
9	**L**	0.603513	0.806638	0.547288	-0.01104	0.715776
10	**M**	0.701529	0.831926	0.619044	0.065706	0.77229
11	**N**	0.648008	0.832866	0.582008	0.063834	0.697047
12	**O**	0.493061	0.75649	0.464966	-0.15463	0.517052
13	**Q**	0.726082	0.841509	0.638884	0.078907	0.653189
14	**S**	0.670784	0.824468	0.597545	0.050377	0.720481
15	**T**	0.57482	0.793989	0.529968	-0.05245	0.679804
16	**Y**	0.616916	0.798349	0.556729	-0.039	0.702234
17	**Z**	0.618604	0.808106	0.562715	-0.01556	0.675183
18	**W**	0.72696	0.870349	0.635037	0.188665	0.703597

Table 3.7. *Average VI values for each corn field from Landsat-8 data*

ID	Name_ID	EVI	NDVI	SAVI	WDRVI	GNDVI
1	**A**	0.384372	0.5395	0.357214	-0.39941	0.560687
2	**B**	0.343257	0.507732	0.324534	-0.45467	0.567392
3	**C**	0.443564	0.586422	0.401376	-0.31561	0.552034
4	**E**	0.397768	0.554194	0.365826	-0.39359	0.536451
5	**F**	0.378278	0.536673	0.350448	-0.43504	0.504205
6	**G**	0.297321	0.483439	0.283519	-0.50732	0.57935
7	**H**	0.383686	0.544192	0.359933	-0.41749	0.561766
8	**K**	0.303709	0.483685	0.292674	-0.50036	0.558807
9	**L**	0.359601	0.516741	0.337913	-0.42087	0.589799
10	**M**	0.425095	0.562292	0.389209	-0.34764	0.612738
11	**N**	0.372197	0.519481	0.346933	-0.40326	0.5639
12	**O**	0.297441	0.449768	0.28626	-0.51876	0.445554

13	**Q**	0.456349	0.583345	0.416411	-0.33023	0.560357
14	**S**	0.393601	0.53489	0.363889	-0.37663	0.578224
15	**T**	0.333777	0.502081	0.316194	-0.44185	0.545139
16	**Y**	0.337751	0.486711	0.31718	-0.46283	0.54326
17	**Z**	0.400788	0.565483	0.373164	-0.37744	0.563278
18	**W**	0.427675	0.573995	0.388039	-0.32047	0.546595

Table 3.8. *258th day VI values for each corn field from Landsat-8 data*

ID	Name_ID	EVI	NDVI	SAVI	WDRVI	GNDVI
1	**A**	0.24628	0.389407	0.243037	-0.62817	0.491855
2	**B**	0.498527	0.703485	0.456434	-0.25662	0.519803
3	**C**	0.617059	0.778159	0.545597	-0.10774	0.482588
4	**E**	0.484489	0.668234	0.440917	-0.29989	0.473809
5	**F**	0.33265	0.551792	0.319232	-0.48224	0.421121
6	**G**	0.211129	0.402666	0.21096	-0.6152	0.540687
7	**H**	0.498483	0.678501	0.458244	-0.29537	0.473887
8	**K**	0.301267	0.511487	0.295138	-0.52689	0.493395
9	**L**	0.509353	0.68673	0.46799	-0.27513	0.527247
10	**M**	0.587231	0.719316	0.526051	-0.20834	0.467895
11	**N**	0.194	0.31307	0.197545	-0.67836	0.431469
12	**O**	0.232167	0.352523	0.233281	-0.65282	0.395
13	**Q**	0.602261	0.755056	0.536888	-0.15524	0.519784
14	**S**	0.557068	0.71298	0.50471	-0.21723	0.453657
15	**T**	0.522539	0.720974	0.478302	-0.23234	0.453149
16	**Y**	0.292545	0.49559	0.291369	-0.54107	0.427878
17	**Z**	0.555317	0.732438	0.501989	-0.20104	0.52164
18	**W**	0.309389	0.442419	0.300179	-0.58037	0.3895

Table 3.9. *Maximum VI values for each corn field from Sentinel-2 data*

ID	Name_ID	EVI	NDVI	SAVI	WDRVI	GNDVI
1	**A**	2.472845	0.849803	1.274695	0.135399	0.768094
2	**B**	2.357967	0.824151	1.236218	0.094122	0.764811
3	**C**	2.658147	0.881549	1.322313	0.232028	0.791016
4	**E**	2.442005	0.813942	1.220904	0.017996	0.725343
5	**F**	2.397583	0.809048	1.213563	-0.01758	0.716626
6	**G**	2.209907	0.7654	1.148089	-0.12377	0.702657
7	**H**	2.315554	0.839826	1.25973	0.100007	0.772024
8	**K**	2.135061	0.790741	1.186102	-0.06939	0.708245

9	**L**	2.444238	0.844311	1.266457	0.131597	0.758582
10	**M**	2.594808	0.87322	1.30982	0.22247	0.755953
11	**N**	2.417265	0.8694	1.304091	0.236902	0.804218
12	**O**	2.202964	0.764547	1.146811	-0.1219	0.71607
13	**Q**	2.576209	0.873515	1.310263	0.225024	0.789213
14	**S**	2.543372	0.887299	1.330938	0.302704	0.803337
15	**T**	2.515624	0.864814	1.297211	0.17522	0.779602
16	**Y**	2.50458	0.817804	1.226697	0.04153	0.71852
17	**Z**	2.528979	0.86396	1.29593	0.169265	0.772441
18	**W**	2.623175	0.918529	1.377783	0.425303	0.802761

Table 3.10. *Average VI values for each corn field from Sentinel-2 data*

ID	**Name_ID**	**EVI**	**NDVI**	**SAVI**	**WDRVI**	**GNDVI**
1	**A**	1.520348	0.591994	0.887984	-0.29769	0.582097
2	**B**	1.336496	0.534994	0.802484	-0.38396	0.539081
3	**C**	1.736875	0.638638	0.957949	-0.21344	0.605502
4	**E**	1.628086	0.606969	0.910447	-0.31156	0.582041
5	**F**	1.560981	0.585765	0.878641	-0.37431	0.568893
6	**G**	1.363238	0.525679	0.78851	-0.45492	0.537777
7	**H**	1.443848	0.579776	0.869657	-0.33207	0.58025
8	**K**	1.460532	0.574765	0.86214	-0.38349	0.556447
9	**L**	1.468301	0.585104	0.877649	-0.29778	0.583966
10	**M**	1.682245	0.647795	0.971685	-0.19959	0.618324
11	**N**	1.49594	0.596939	0.895402	-0.25693	0.601341
12	**O**	1.192033	0.487256	0.730878	-0.46288	0.520981
13	**Q**	1.670653	0.656235	0.984345	-0.19387	0.636325
14	**S**	1.636528	0.634087	0.951122	-0.19855	0.617285
15	**T**	1.407417	0.56001	0.840008	-0.31808	0.573344
16	**Y**	1.477739	0.556214	0.834315	-0.37281	0.532344
17	**Z**	1.639021	0.644225	0.96633	-0.24418	0.61808
18	**W**	1.811451	0.677295	1.015935	-0.11744	0.637154

Table 3.11. *258th day VI values for each corn field from Sentinel-2 data*

ID	**Name_ID**	**EVI**	**NDVI**	**SAVI**	**WDRVI**	**GNDVI**
1	**A**	0.667802	0.331828	0.497738	-0.66572	0.415674
2	**B**	1.79184	0.755033	1.132541	-0.11603	0.715825
3	**C**	2.058994	0.837711	1.256557	0.064839	0.773356
4	**E**	1.550006	0.664226	0.996331	-0.27683	0.646377

5	**F**	1.16962	0.549868	0.824792	-0.48363	0.56472
6	**G**	0.712612	0.37576	0.563632	-0.62981	0.466249
7	**H**	1.783631	0.757667	1.136492	-0.11936	0.724339
8	**K**	1.075927	0.520899	0.78134	-0.51475	0.521857
9	**L**	1.789619	0.765531	1.148289	-0.12104	0.705516
10	**M**	1.860256	0.774421	1.161624	-0.08682	0.715239
11	**N**	0.424944	0.240176	0.36026	-0.71897	0.37394
12	**O**	0.569737	0.308569	0.46285	-0.67671	0.421567
13	**Q**	1.890108	0.807639	1.21145	-0.0048	0.756447
14	**S**	1.88394	0.798377	1.197558	-0.03785	0.741606
15	**T**	1.828133	0.775639	1.16345	-0.09654	0.727698
16	**Y**	1.039163	0.516881	0.775313	-0.52	0.477638
17	**Z**	1.91537	0.809034	1.213542	-0.01981	0.744488
18	**W**	0.756808	0.376763	0.565141	-0.61989	0.462257

3.7.2. Bayesian Model Averaging method

In this study, Bayesian Model Averaging (BMA) was used to build the maize yield predicting model for the study area. BMA is a comprehensive method to solve model uncertainty in applied science. Based on the idea of Roberts, 1965, in 1978 Leamer expanded and proposed the basic paradigm of BMA. Generally, BMA is applied when there are many statistically reasonable models but lead to different results for the research question (Amini & Parmeter, 2011) or in other words, the impact of the multicollinearity in the multiple linear regression model. According to Amini & Parmeter, 2011 the implementation of BMA for the linear regression model that was used in this research is summarized as follows.

Give a multiple linear regression model with a dependent variable Y, a set of k independent variable X, and a constant β_0:

$$Y = \beta_0 + \beta_1 X_1 + \beta_2 X_2 + \ldots + \beta_k X_k + \varepsilon \quad (1)$$

With k candidate predictors, we will have 2^k variable combinations and thus 2^k models by M_j for j = 1,2,3,4,……2^k. Once the model space has been constructed, the posterior distribution for any coefficient of interest, say β_h, give the data D is

$$\Pr(\beta_h|D) = \sum_{j:\beta_h \in M_j} \Pr(\beta_h|M_j)\Pr(M_j|D) \qquad (2)$$

BMA uses each model's posterior probability, $\Pr(M_j|D)$, as weights. The posterior model probability of M_j is the ratio of its marginal likelihood to the sum of marginal likelihoods over the entire model space and is given by

$$\Pr(M_j|\mathrm{D}) = \Pr(\mathrm{D}|\mathrm{M_j})\frac{\Pr(M_j)}{\Pr(D)} = \Pr(\mathrm{D}|\mathrm{M_j})\frac{\Pr(M_j)}{\sum_{i=0}^{2^k}\Pr(D|M_j)\Pr(M_j)} \quad (3)$$

where

$$\Pr(\mathrm{D}|\mathrm{M_j}) = \int \Pr(\mathrm{D}|\beta^j, M_j)\Pr(\beta^j|M_j)\mathrm{d}\beta^j \quad (4)$$

And β^j is the vector of parameters from model M_j, $\Pr(\beta^j|M_j)$ is a prior probability distribution assigned to the parameters of model M_j, and $\Pr(M_j)$ is the prior probability that M_j is the true model. The estimated posterior means and standard deviations of $\hat{\beta}$=($\hat{\beta}_0, \hat{\beta}_1$, ……,$\hat{\beta}_k$) are then constructed as

$$\mathrm{E}[\hat{\beta}|\mathrm{D}] = \sum_{j=1}^{2^k}\hat{\beta}\Pr\left(M_j\middle|D\right), \quad (5)$$

$$\mathrm{V}[\hat{\beta}|\mathrm{D}] = \sum_{j=1}^{2^k}(Var\left[\beta\middle|\mathrm{D}, M_j\right] + \hat{\beta}^2)\Pr\left(M_j\middle|D\right) - \mathrm{E}[\beta|\mathrm{D}]^{\ 2} \ . \quad (6)$$

In addition, The introduction about BMA was shown in the paper of Hoeting et al., 1999 or Montgomery & Nyhan, 2010.

This method has been built into a package in R by Adrian Raftery, Jennifer Hoeting, Chris Volinsky, Ian Painter, and Ka Yee Yeung, which is the BMA package for linear models, generalized linear models and survival models (Cox regression). In the analysis of this study, the BMA package version 3.18.9 that was published on 14/9/2018 was used with the `bicreg()` function (Raftery et al., 2018).

3.7.3. Model validation and accuracy assessment

In order to choose the useful model for predicting corn yield of the study area, this topic was used the regression coefficients such as p-value, coefficient of determination (R^2), and Bayesian information criterion (BIC) along with the root mean square error (RMSE).

The p-value is calculated to test the statistical significance of each regression. R^2 points out the percent that the model can be predicted and the R^2 is the most important regression coefficient for selecting the optimal mode. The lower the BIC, the better the model is.

The RMSE indicates the degree of dispersion of predicted values from actual values. The formula of RMSE is as follows.

$$\mathrm{RMSE} = \sqrt{\frac{1}{\mathrm{n}} \sum_{i=1}^{n} (y_i - \hat{y}_i)^2} \qquad (7)$$

where y_i is the observed value, $\hat{y}_i$ is the estimated value, and n is the number of the corn field. The unit of RMSE is tons per hectare.

4. RESULTS AND DISCUSSION

4.1. Relationship Between VIs and Actual Yield

4.1.1. VIs obtained from Landsat-8

This section explained the correlation between the observed corn yield and VIs (NDVI, EVI, SAVI, WDRVI, GNDVI) derived from Landsat-8 images. Figure 4.1 shows the correlation between the highest value of the VIs and the corn yield along with the relationship between the highest VIs value together. The GNDVI had a great correlation with corn yield (r=0.65), followed by NDVI and WDRVI with the coefficient of correlation was 0.46, and the lowest was EVI with r = 0.38. Besides, NDVI, EVI, SAVI, and WDRVI had a close relationship with r was over 0.92 that result in these VIs could not appear in the same model because of causing multicollinearity. On the other hand, NDVI and GNDVI had the lowest correlation with r = 0.38 which means that they can enter into the model prediction concurrently.

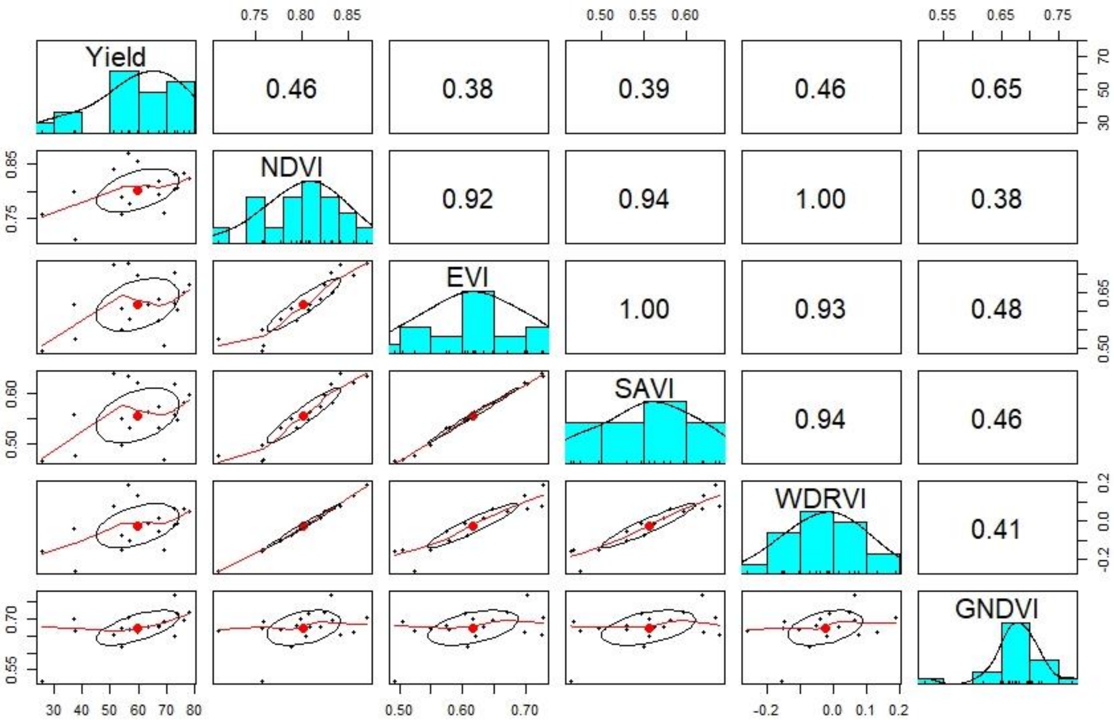

Figure 4.1. *Correlation between the corn yield and the maximum Landsat-8 VI values*

For the mean value of VIs, its correlation with the corn yield was similar to the highest VIs value. Specifically, The GNDVI had a slightly higher correlation with r=0.66

whereas NDVI and the other VIs were lower. Figure 4.2 below clearly presents this difference.

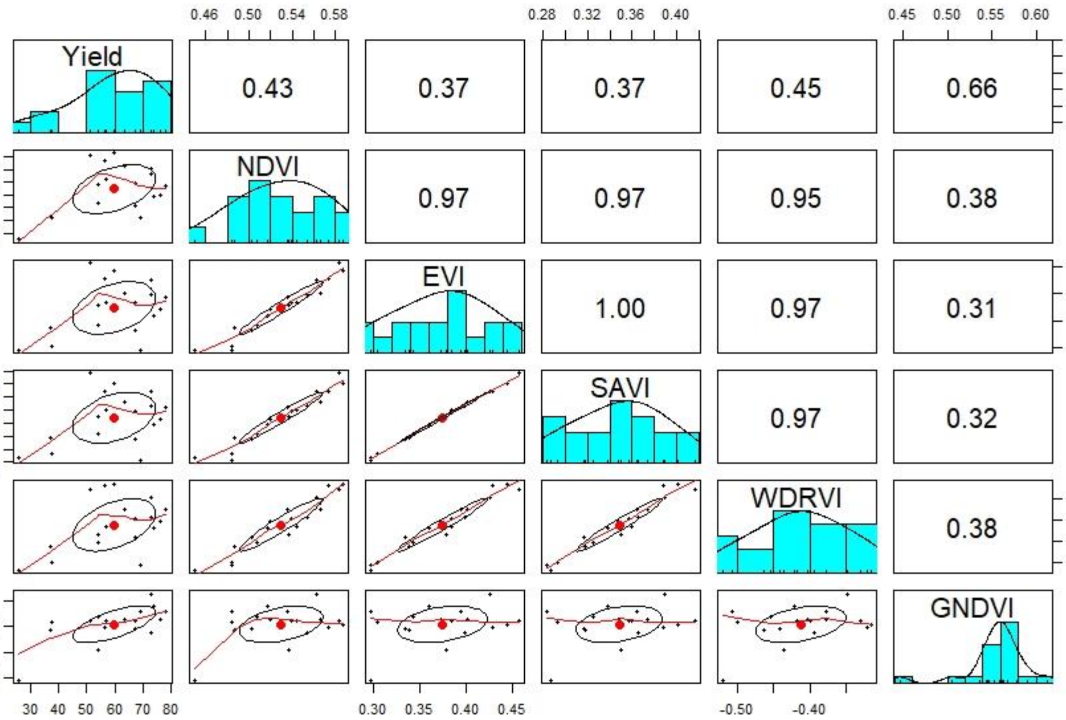

Figure 4.2. *Correlation between the corn yield and the average Landsat-8 VI values*

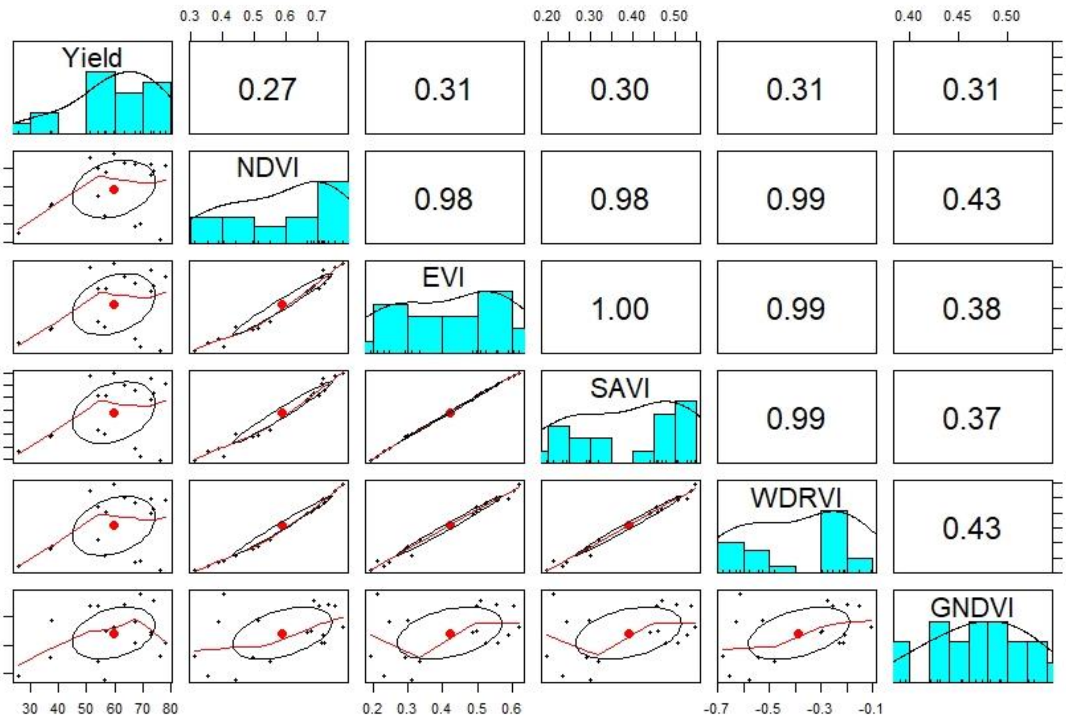

Figure 4.3. *Correlation between the corn yield and the 258th day Landsat-8 VI values*

The relationship of the 258th day VI values with the corn yield that was indicated in Figure 4.3 was very low and it had no statistical significance when building the model by the linear regression method. Thus, the 258th day VI values were not used to build the model in the next step.

4.1.2. VIs obtained from Sentinel-2

The relationship between the VIs value extracted from Sentinel-2 data and the corn yield was described in this part. In general, it was not similar to the correlation between the VIs value derived from Landsat-8 and the corn yield. Particularly, for the maximum VIs value, the NDVI and SAVI had the best correlation with the corn yield (r = 0.48), followed by the WDRVI and GNDVI with r = 0.47, and the lowest correlation was EVI value with r = 0.41. However, when considering the relationship between the VIs together, all of them had a close relationship with each other (r was over 0.68). This correlation pointed out that the VIs could not exist in a multiple linear regression model.

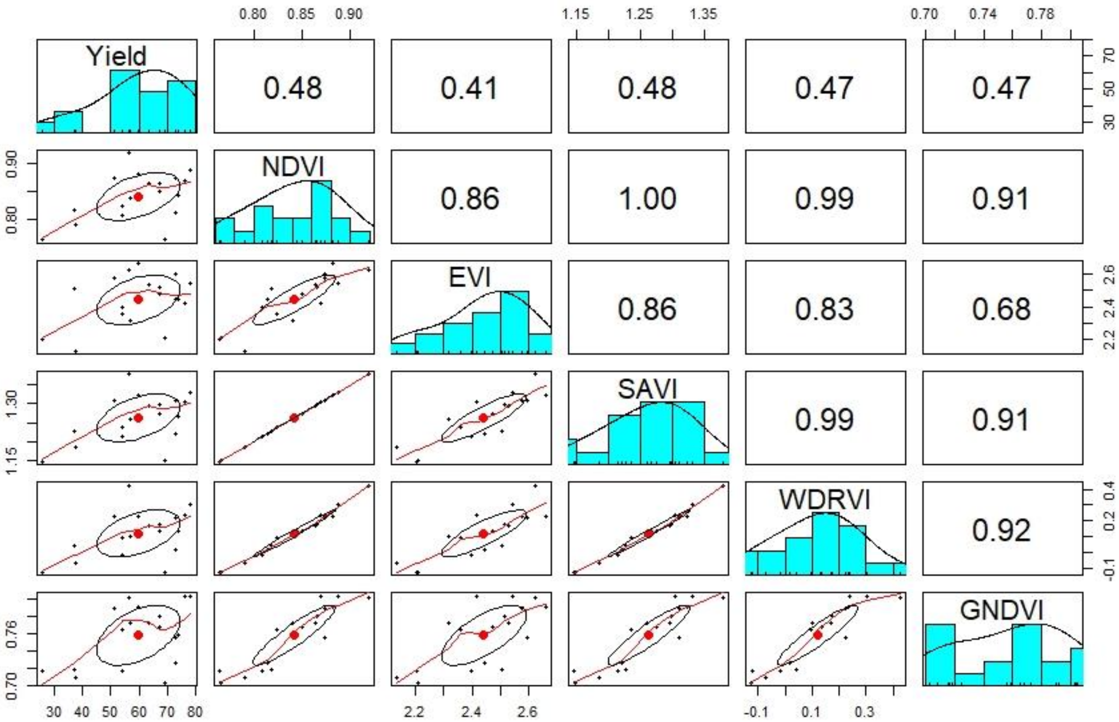

Figure 4.4. *Correlation between the corn yield and the highest Sentinel-2 VI values*

For the mean VI values, the closest correlation to the corn yield was the GNDVI value and the lowest coefficient of correlation was still EVI (r = 0.38), followed by

NDVI, SAVI with r = 0.42, and WDRVI with r = 0.46. The relationship between the VIs value together was so high (over 0.87).

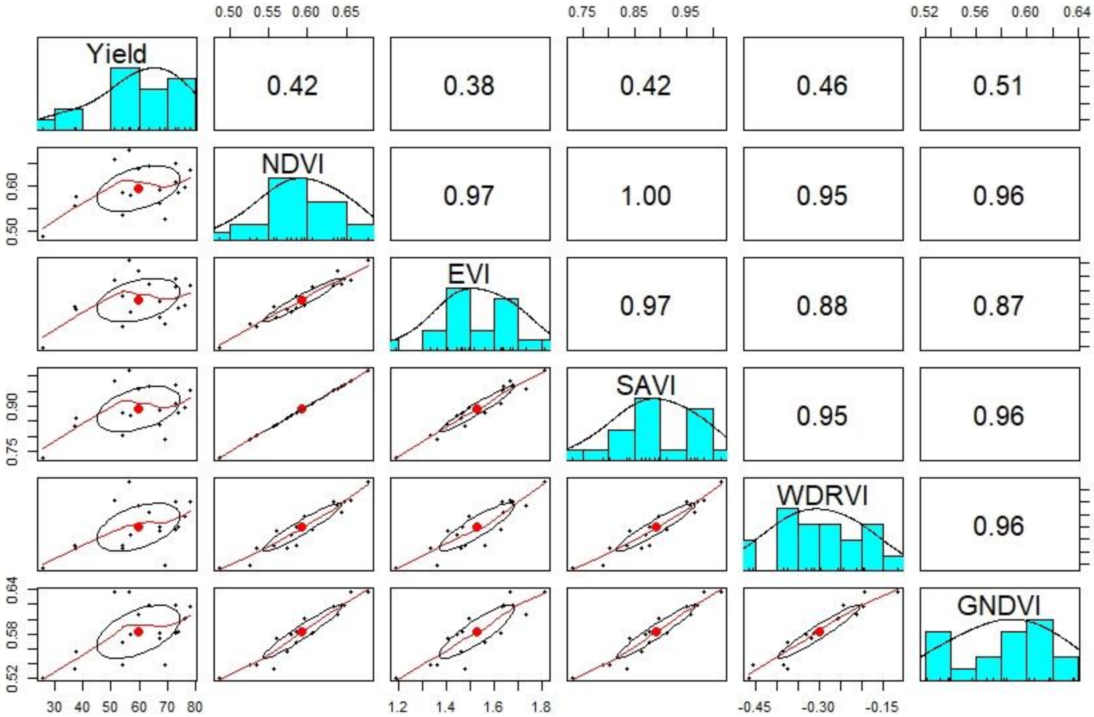

Figure 4.5. *Correlation between the corn yield and the mean Sentinel-2 VI values*

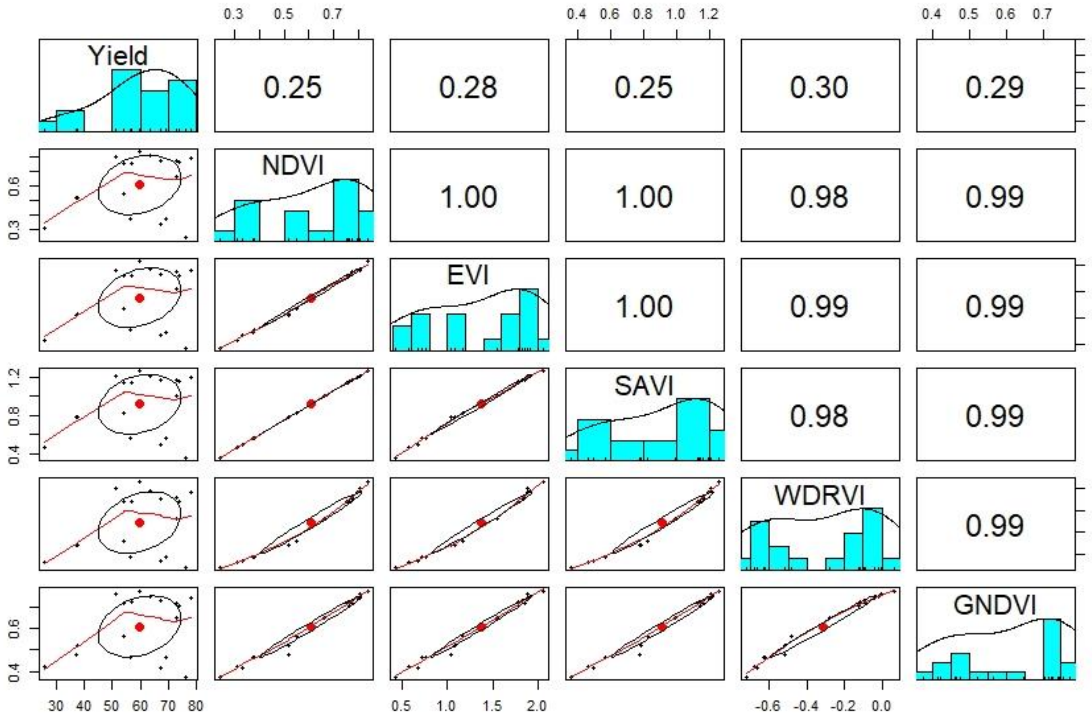

Figure 4.6. *Correlation between the corn yield and the 258th day Sentinel-2 VI values*

Figure 4.6 presents the correlation between the 258th day VI values and the corn yield and it had no statistical significance when building the model by the linear regression method. Thus, the 258th day VI values from Sentinel-2 were not used to build the model in the next step.

Finally, Table 4.1 summarized the coefficient of correlation between the VI values and the corn yield by Landsat-8 and Sentinel-2. The coefficient of correlation of NDVI, EVI, and WDRVI was similar while SAVI and GNDVI had a big difference, especially, the coefficient of correlation of GNDVI derived from Landsat-8 is much higher than GNDVI derived from Sentinel-2.

Table 4.1. *Coefficient of correlation between the VI values and the corn yield*

VI values	**Maximum**		**Mean**		**Minimum**	
Satellite	Landsat-8	Sentinel-2	Landsat-8	Sentinel-2	Landsat-8	Sentinel-2
NDVI	0.46	0.48	0.43	0.42	0.27	0.25
EVI	0.38	0.41	0.37	0.38	0.31	0.28
SAVI	0.39	0.48	0.37	0.42	0.30	0.25
WDRVI	0.46	0.47	0.45	0.46	0.31	0.30
GNDVI	0.65	0.47	0.66	0.51	0.31	0.29

4.2. Possible Model Selection

After analyzing the correlation of each selected data with the actual yield, the highest VI value and the average value are eligible to build a predicting model for the study area. In this step, the `bicreg()` function in the package BMA was used to determine possible models (see the code in appendix 4).

For the highest Landsat-8 VI values, the result of BMA analysis selected 18 models and the best 5 models, defined by lowest BIC and largest posterior probability, are shown in Table 4.2. The cumulative posterior probability of these models is 0.53.

Table 4.2. *BMA results showing the 5 best models for the highest Landsat-8 VI values*

	p!=0	SD	model 1	model 2	model 3	model 4	model 5
Intercept	100	358.65	-65.539	-252.312	-238.436	-121.28	-46.772
NDVI	49.6	454.42	.	360.837	374.369	92.624	.
EVI	40.1	290.76	.	-175.32	.	.	.
SAVI	34.7	389.63	.	.	-230.635	.	.
WDRVI	37.2	156.25	.	.	.	.	30.177
GNDVI	98.2	64.75	185.572	193.637	186.787	158.081	158.806
nVar			1	3	3	2	2
R^2			0.42	0.572	0.558	0.475	0.465
BIC			-6.929	-6.611	-6.044	-5.817	-5.476
post prob			0.148	0.127	0.095	0.085	0.072

p!=0: Probability of independent variables affects corn yield

SD: Standard deviation

nVar: Number of variables

post prob: Posterior probability

Based on the evaluation metrics of the model mentioned in section 3.7.3, model 1 seemed to be the best fit model because it had the lowest BIC with -6.93 and the highest posterior probability with 14.8%. Moreover, this model explained 42% of the variance of the actual corn yield. Besides, when considering model 2, although BIC (-6.61) and posterior probability (12.7%) were slightly lower than model 1, it explained 57.2% of the variance of the actual corn yield by 3 variables (NDVI, EVI, GNDVI). The 3 remaining models had the regression coefficients were much lower. As the evidence above, model 1 and model 2 were selected to be the optimal model for estimating corn yield from the highest Landsat-8 VI values.

The result of BMA analysis for the mean Landsat-8 VI values chose 13 models and the best 5 models are displayed in Table 4.3 with the cumulative posterior probability of these models is 0.74.

Table 4.3. *BMA results showing the 5 best models for the mean Landsat-8 VI values*

	p!=0	SD	model 1	model 2	model 3	model 4	model 5
Intercept	100	117.74	-93.537	-50.68	-118.168	-101.278	-103.743
NDVI	25.4	126.71	.	.	81.914	.	.
EVI	23.3	264.18	.	.	.	55.761	.
SAVI	23.3	316.61	.	.	.	.	66.745
WDRVI	30.2	108.55	.	54.785	.	.	.
GNDVI	100	85.46	276.619	240.033	242.783	252.918	253.063
nVar			1	2	2	2	2
R^2			0.44	0.486	0.479	0.47	0.468
BIC			-7.547	-6.185	-5.971	-5.654	-5.58
post prob			0.271	0.137	0.123	0.105	0.101

In this analysis, model 1 had the lowest BIC with -7.55 and the highest posterior probability with 27.1%. These coefficients were so different from the other models and only with 1 variable (GNDVI), it explained 44% of the variance of the actual corn yield. Hence, model 1 was optimal model for estimating corn yield from the mean Landsat-8 VI values.

With selected Sentinel-2 VI values, there were 4 models were selected from the BMA analysis of the highest VI values. These models had a cumulative posterior probability of 1. Table 4.4 shows the regression coefficients of 4 models in details.

Table 4.4. *BMA results showing the 5 best models for the highest Sentinel-2 VI values*

	p!=0	SD	model 1	model 2	model 3	model 4
Intercept	100	102.30	-79.95	59.67	-151.80	-159.50
NDVI	77.7	8.60E+06	165.90	.	1.20E+07	1.18E+07
SAVI	24.5	5.73E+06	.	.	-8.02E+06	-7.84E+06
GNDVI	4.9	53.83	.	.	.	74.5
WDRVI	0	0.00	.	.	.	.
EVI	0	0.00	.	.	.	.
nVar			1	0	2	3
R^2			0.227	0	0.264	0.269
BIC			-1.74	0.00	0.26	3.02
post prob			0.532	0.223	0.195	0.049

The best fit model of this result was model 1 because it had the lowest BIC with -1.74 and the highest posterior probability with 53.2% and it explained 22.7% of the variance of the actual corn yield by 1 variable (NDVI).

For the mean Sentinel-2 VI values, the result of BMA analysis selected 5 models with the cumulative posterior probability of 1, are shown in Table 4.5.

Table 4.5. *BMA results showing the 5 best models for the mean Sentinel-2 VI values*

	p!=0	SD	model 1	model 2	model 3	model 4	model 5
Intercept	100	134.20	-63.48	59.67	-161.10	-128.00	-55.93
GNDVI	83.9	230.40	211.30	.	350.60	528.20	482.40
WDRVI	26	67.81	.	.	-54.59	-13.88	71.25
NDVI	10.5	5.36E+06	.	.	.	-209.50	2.05E+07
SAVI	4.5	3.57E+06	.	.	.	.	-1.37E+07
EVI	0	0.00	.	.	.	.	.
nVar			1	0	2	3	4
R^2			0.261	0	0.272	0.31	0.395
BIC			-2.56	0.00	0.07	1.99	2.53
post prob			0.579	0.161	0.155	0.06	0.045

Model 1 had the lowest BIC with -2.56 and the highest posterior probability with 57.9% and it explained 26.1% of the variance of the actual corn yield by 1 variable (GNDVI). The model of best fit in this analysis appeared to be model 1 because it’s coefficient value had a big difference with the other models.

In summary, there were 3 models were built for predicting corn yield from the BMA analysis of the selected Landsat-8 VI values and 2 models from the BMA analysis of the selected Sentinel-2 VI values (Table 4.6).

4.3. Accuracy Assessment and Optimal Model Selection

After determining the possible models by the BMA method, the RMSE was computed to compare the accuracy between the possible models and validate the optimal models for predicting corn yield. The lower the RMSE, the better model is. The calculation results (Table 4.6) showed that the highest RMSE came from model 2 that was built from the highest Landsat-8 VI values with RMSE of 9.38 t/ha and the lowest RMSE was 12.61 t/ha of model 4 that was built from the highest Sentinel-2 VI values.

The correlation between actual and predicted yield of the possible models was expressed visually through Figure 4.7 and Figure 4.8.

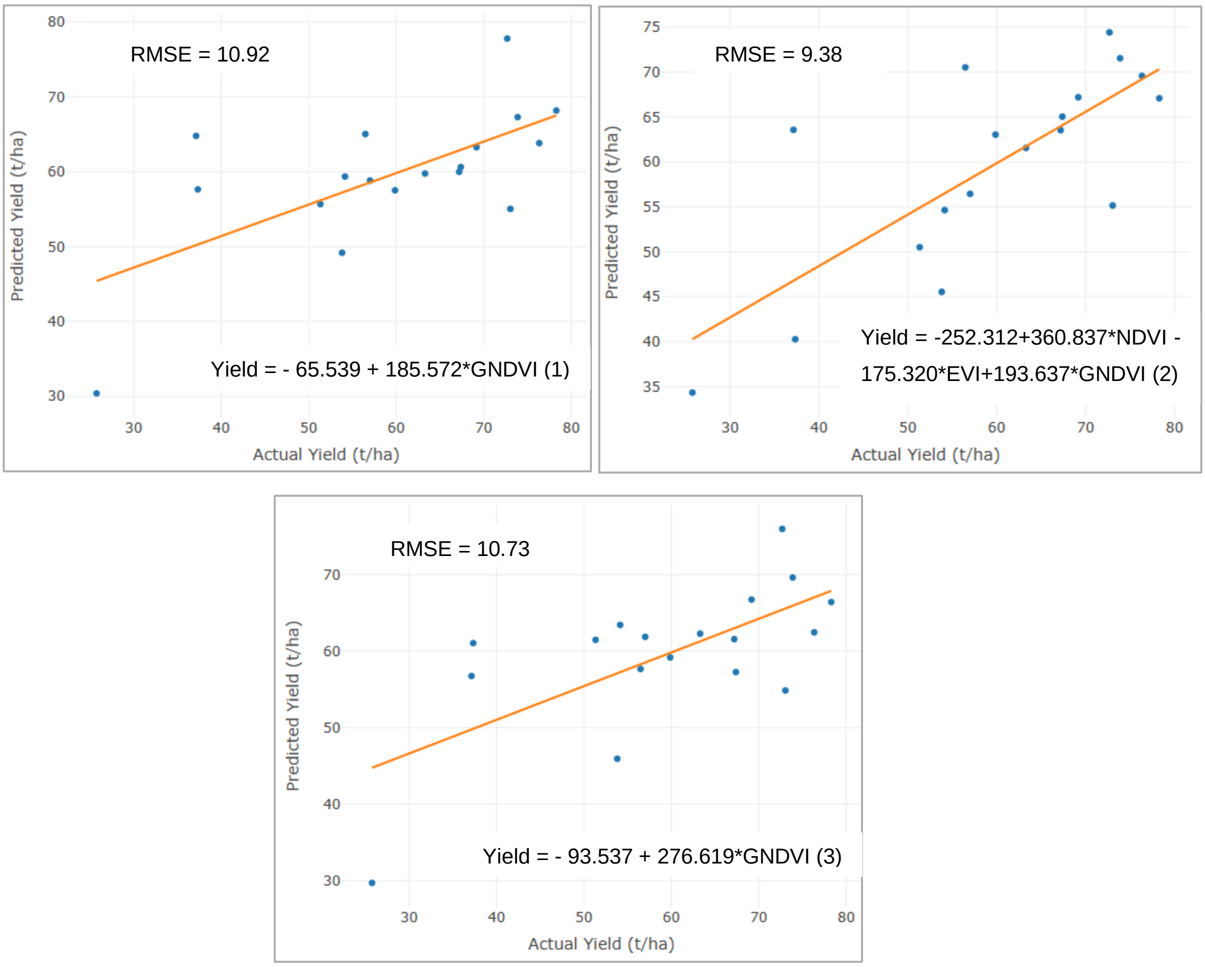

Figure 4.7. *Correlation between actual and predicted yield for possible model from Landsat-8 VI values.*

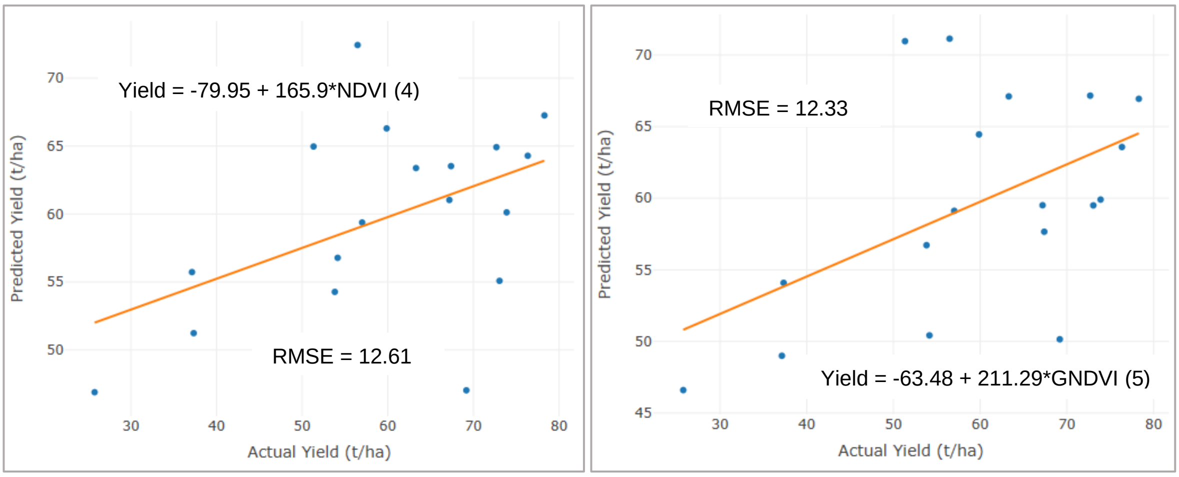

Figure 4.8. *Correlation between actual and predicted yield for the possible model from Sentinel-2 VI values.*

Table 4.6. *Model validation indicators for each possible models*

Satellite		Possible model	RMSE (t/ha)	R^2	p-value
Landsat-8	1	Yield = - 65.539 + 185.572*GNDVI	10.92	0.42	0.0036
	2	Yield = -252.312+360.837*NDVI - 175.320*EVI+193.637*GNDVI	9.38	0.57	0.00028
	3	Yield = - 93.537 + 276.619*GNDVI	10.73	0.44	0.0027
Sentinel-2	4	Yield = -79.95 + 165.9*NDVI	12.61	0.23	0.046
	5	Yield = -63.48 + 211.29*GNDVI	12.33	0.26	0.030

Finally, based on the RMSE value, 2 optimal models which were validated as model 2 (RMSE = 9.38) for Landsat-8 and model 5 (RMSE = 12.33) for Sentinel-2.

4.4. Yield Mapping

Based on the optimal maize yield forecasting model, the maps of corn yield forecast for the study area were established from Landsat-8 image (Figure 4.9) and Sentinel-2 image (Figure 4.10).

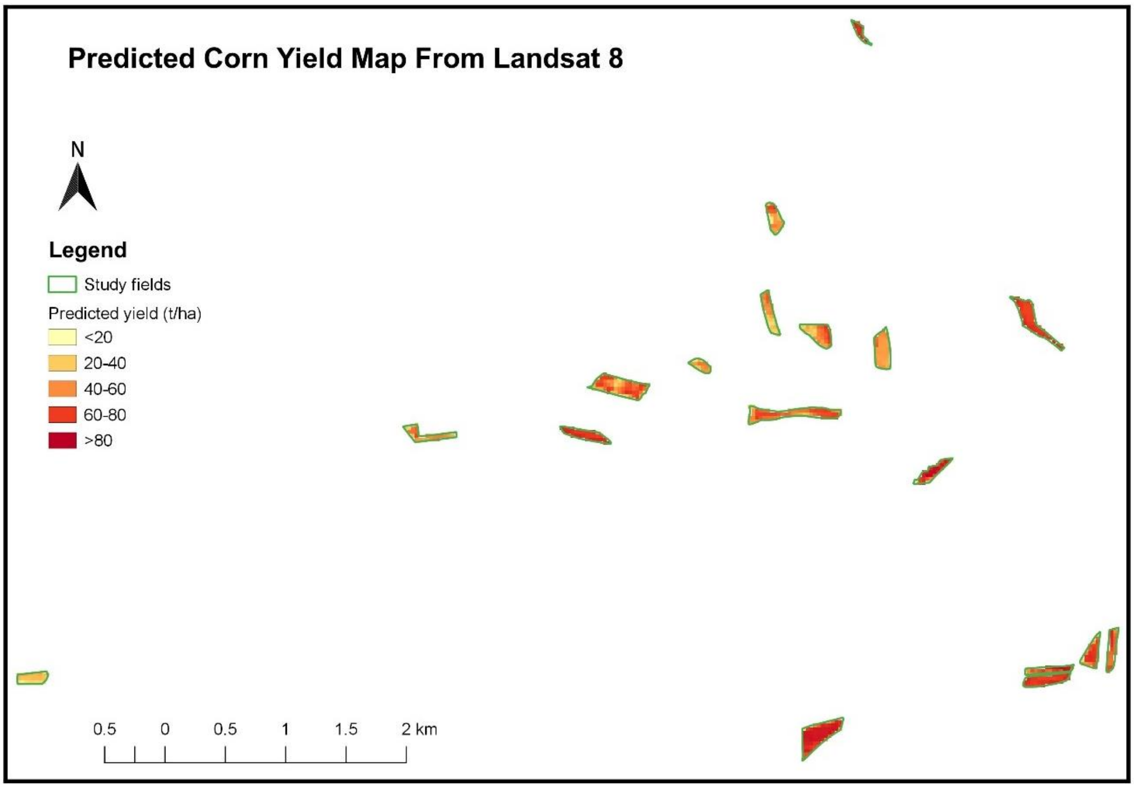

Figure 4.9. *Map of predicted corn yields was built from Landsat-8 image*

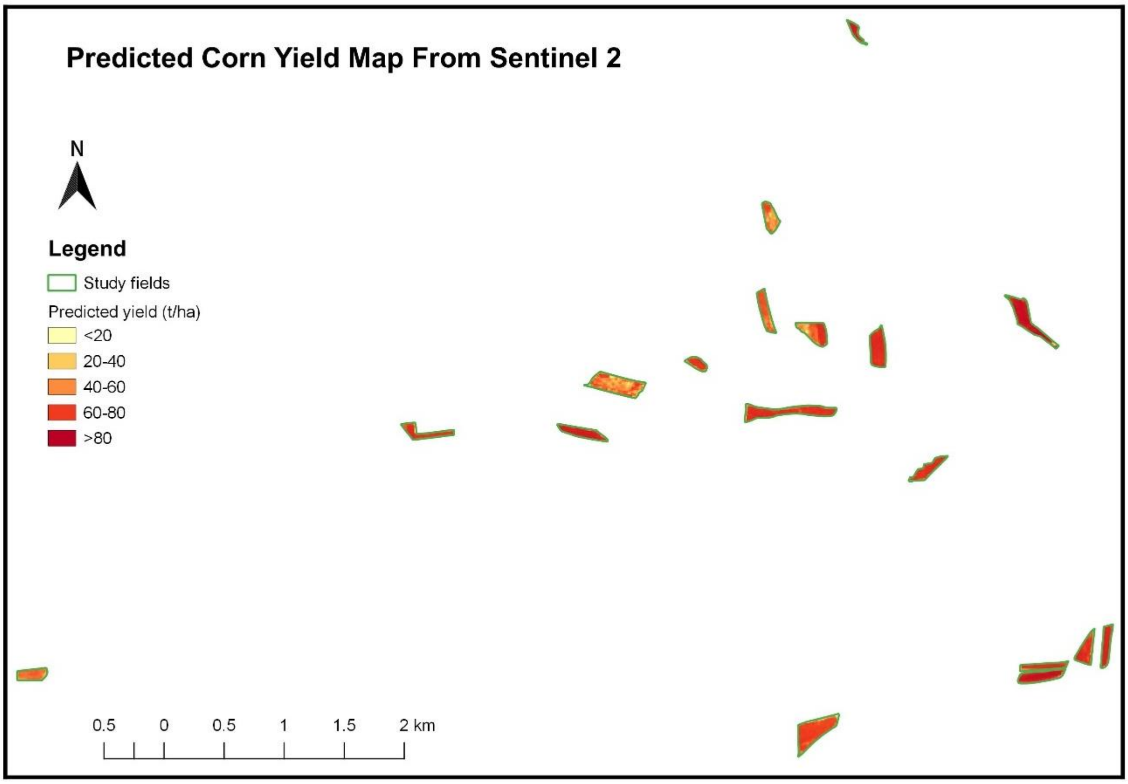

Figure 4.10. *Map of predicted corn yields was built from Sentinel-2 image*

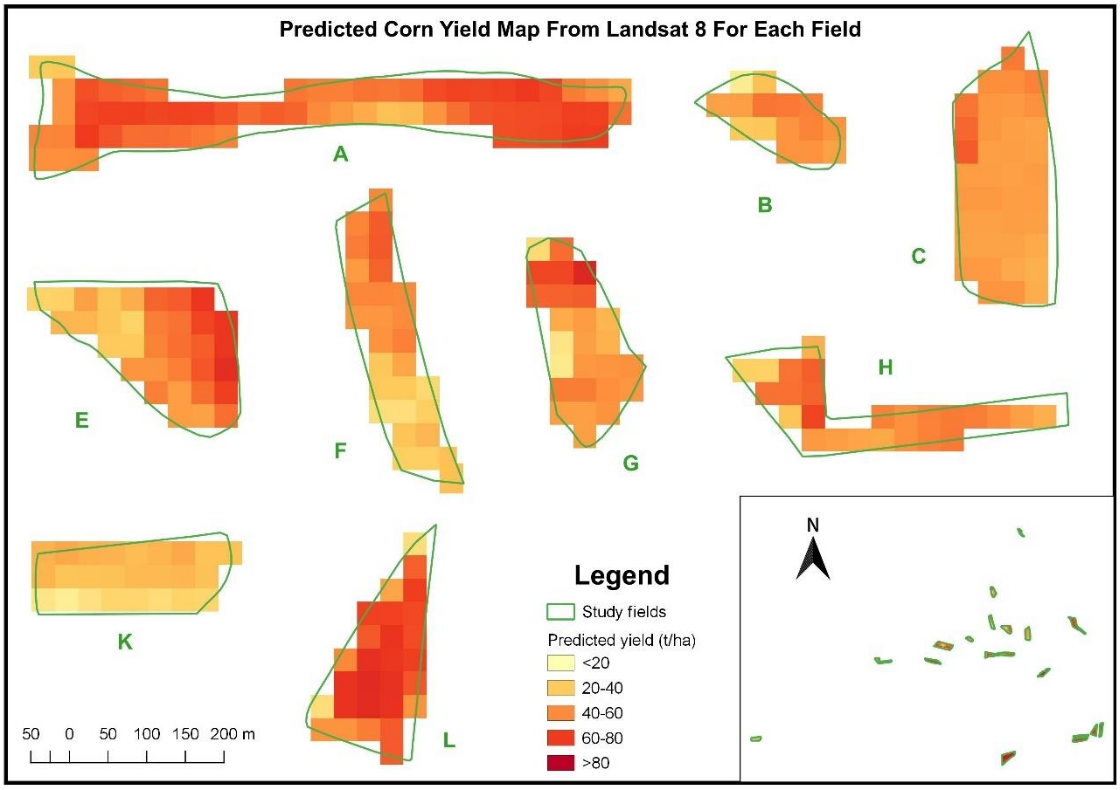

Figure 4.11. *Map of predicted corn yield was built from Landsat-8 image for each field*

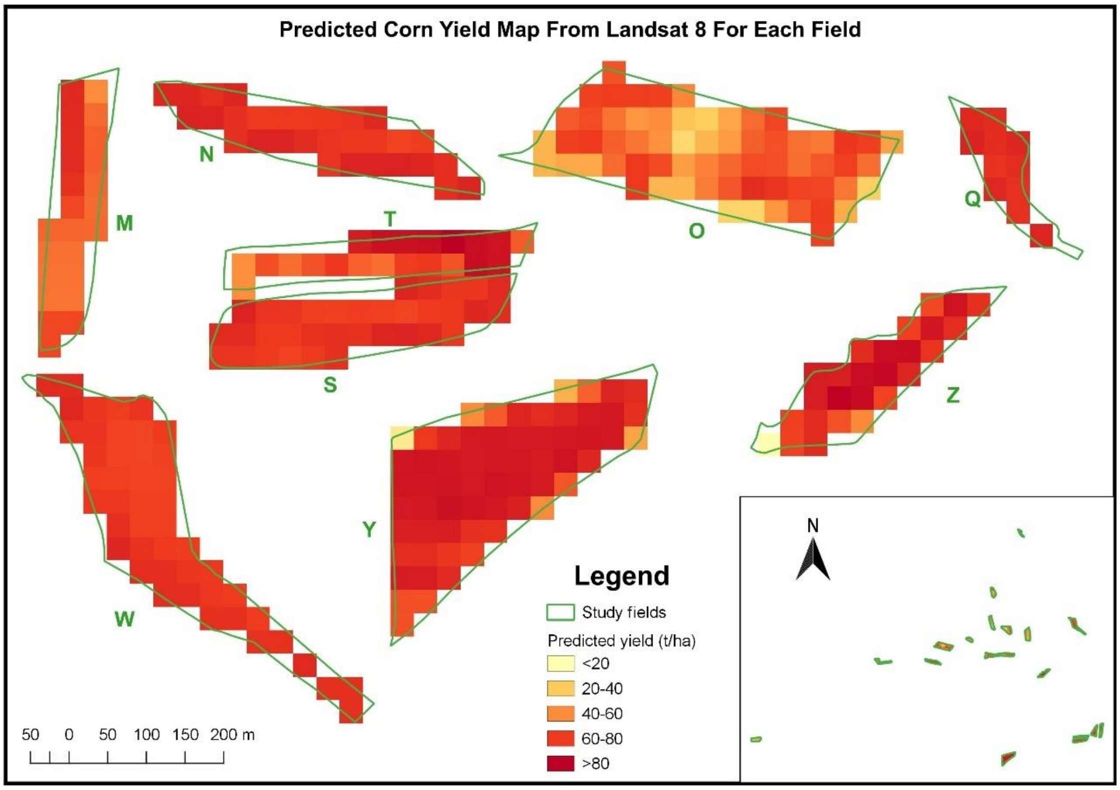

Figure 4.12. *Map of predicted corn yield was built from Landsat-8 image for each field*

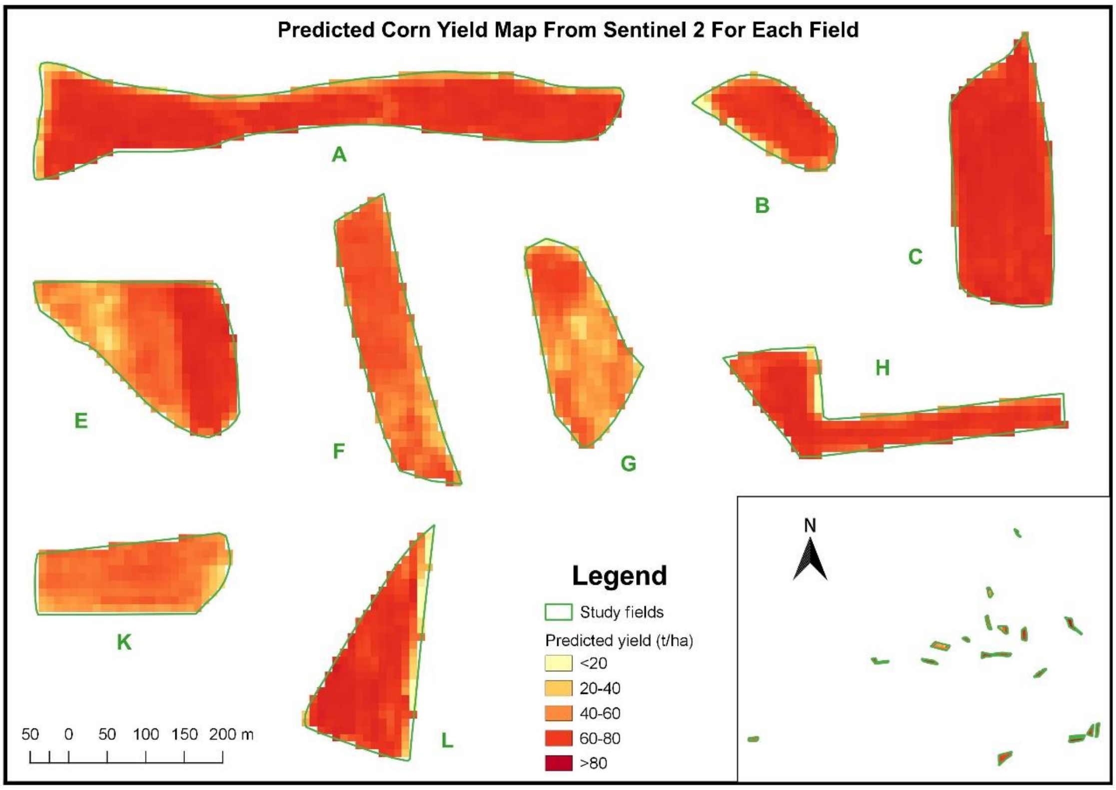

Figure 4.13. *Map of predicted corn yield was built from Sentinel-2 image for each field*

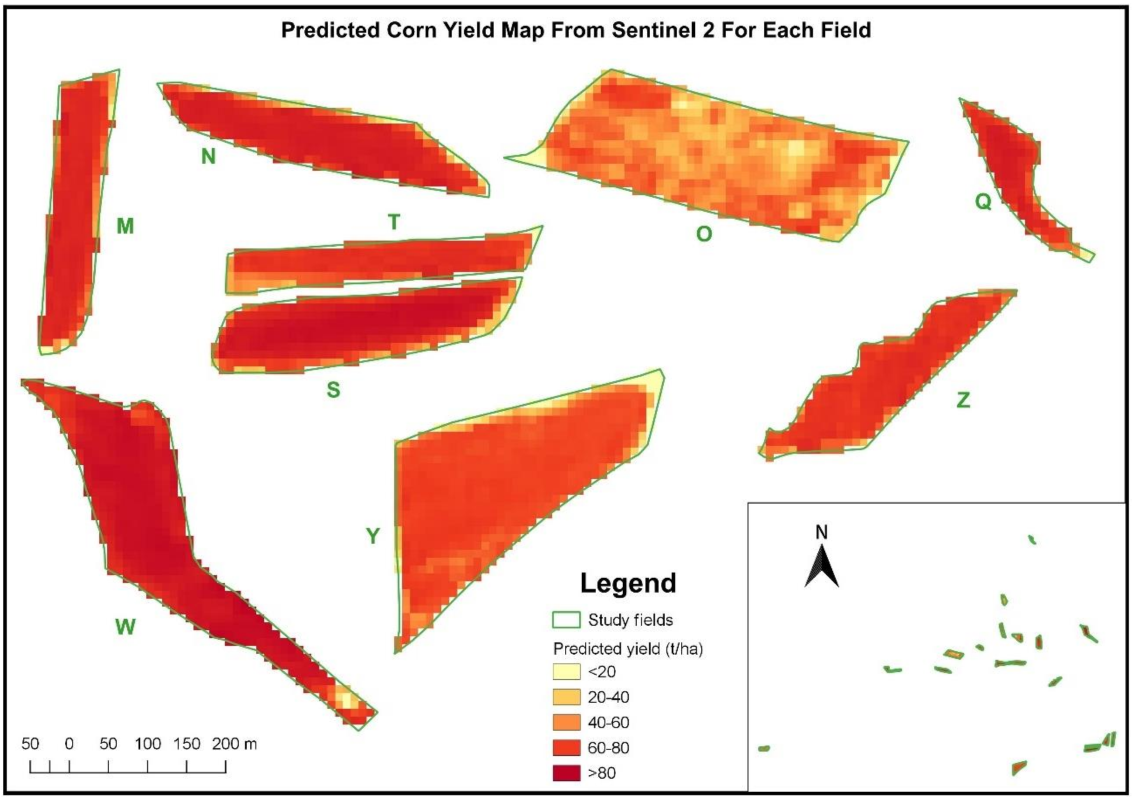

Figure 4.14. *Map of predicted corn yield was built from Sentinel-2 image for each field*

The map visually presented the predicted corn yield by each pixel value for each corn field. The results are shown in detail through Figure 4.11, 4.12, 4.13, 4.14. In this section, the research used R software with rgdal and raster packages to extract VI value and convert them to points. Then QGIS was used to create and edit the map of predicted corn yield for the study area.

4.5. Building Web Application

The web application is an interactive tool that provides information about the development status, the disease risk of corn through the VIs, the predicting yield before harvest. Based on that information, farmers can adjust fertilizer, irrigation system appropriately and timely in order to enhance corn productivity and making a specific plan for harvesting time. In this section, the topic used R software with rgdal, raster, shiny, shinydashboard, plotly, datasets, dplyr, and leaflet packages to build the web application (see the code in Appendix 5).

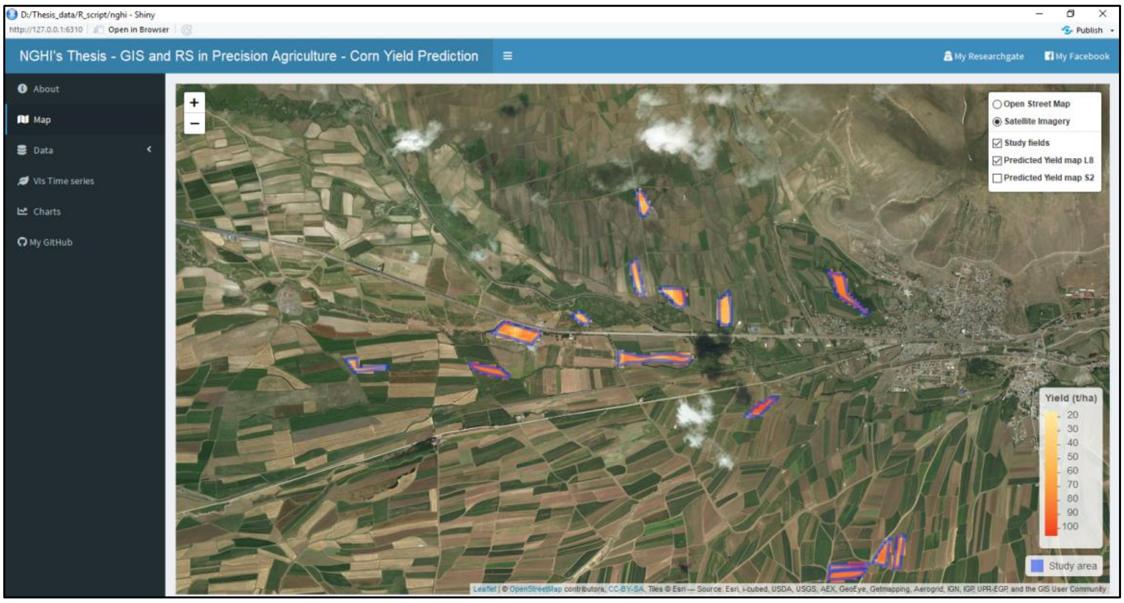

Figure 4.15. *Interactive interface of the web application*

5. CONCLUSION AND RECOMMENDATION

5.1. Conclusions

Through answering the research questions in section 1.2, the research purpose of the topic was gradually clarified. The following conclusions are learned from this study:

- The literature part summarized and gave an overview of the application of remote sensing technology in corn yield prediction. Furthermore, it was a valuable literature review to assess and analyse the advantages and disadvantages of historical remote sensing data for estimating corn yield objectively by specific platforms (satellite, airborne, UAV, and ground-based).

- The research built 2 models for predicting corn yield from Landsat-8 and Sentinel-2 image data respectively by the linear regression method. The BMA method which was applied in this study expressed the trust in the validation and the accuracy assessment of the models.

- The analysis results of the selected VI values demonstrated that the GNDVI had the highest correlation with the actual corn yield and it appeared into both optimal predicting models. Besides, the study result also showed that for Landsat-8 data, the maximum value of VIs had a great relationship to the actual corn yield. Meanwhile, the VIs derived from Sentinel-2 image is the mean value. Generally, the forecasting model was built from Landsat-8 image had a higher accuracy than it was built from Sentinel-2.

Finally, this study proved the efficiency and capability of open-source software in spatial analysis, data analysis, building statistical models and building visually interactive web applications.

5.2. Recommendations

- Input data is very important so that the cleaning data step is essential. In this study, because the observed maize yield data limited only in the 2018 season, it is necessary to get more corn yield data of previous years, especially, the 2019 season to test the accuracy of the optimal models. It is recommended to select the study area in the area specializing in corn cultivation to make sure the quality of the actual corn yield data.

- Some researches used the non-linear regression method (Cai, 2017; Inman, 2007; Peng, 2011; Vergara-Díaz, 2016), convolutional neural network (Russello, 2018; Sabini et al., 2017; You, 2017), artificial neural network (Jiang et al., 2004), and deep learning (Kim & Lee, 2016; Kuwata & Shibasaki, 2015) to build the crop yield predicting model with higher accuracy. Therefore, these methods should be studied and applied to the study area. In addition, using data fusion from different platforms or combining remote sensing data and Crop Simulation Models to improve the accuracy of the forecasting model.

- Some other input variables such as EVI2, TSAVI, NDWI, SAVI2, WDVI, TVI, and so on; meteorological data such as temperature, moisture, and rainfall; soil indices such as soil moisture, and soil erosion should be considered to optimize the current model and build the new useful models for the study area.

- The web application can be developed into a real-time monitoring and predicting system in the future.

REFERENCES

Aase, J. K., & Siddoway, F. H. (1981). Spring wheat yield estimates from spectral reflectance measurements Spring wheat yield estimates from spectral reflectance measurements. *IEEE Transactions on Geoscience and Remote Sensing*, *19*(2), 78–84.

Abiy, W. Z., & Suryabhagavan, K. V. (2016). Remote Sensing and GIS Based Spectro-Agrometeorological Maize Yield Forecast Model for South Tigray Zone, Ethiopia. *Journal of Geographic Information System*, *08*(02), 282–292. https://doi.org/10.4236/jgis.2016.82024

Aguate, F. M., Trachsel, S., González Pérez, L., Burgueño, J., Crossa, J., Balzarini, M., … de los Campos, G. (2017). Use of hyperspectral image data outperforms vegetation indices in prediction of maize yield. *Crop Science*, *57*(5), 2517–2524. https://doi.org/10.2135/cropsci2017.01.0007

Amini, S. M., & Parmeter, C. F. (2011). Bayesian model averaging in R. *Journal of Economic and Social Measurement*, *36*(4), 253–287.

Asrar, G., Kanemasu, E. T., Jackson, R. D., & Pinter, P. J., J. (1985). Estimation of total above-ground phytomass production using remotely sensed data. *Remote Sens. Environ.*, *17*, 211–220.

Atzberger, C. (2013). Advances in remote sensing of agriculture: Context description, existing operational monitoring systems and major information needs. *Remote Sensing*, *5*(2), 949–981. https://doi.org/10.3390/rs5020949

Awan, S. (2016). A review of the past, present and future of precision agriculture in the UK. Agriculture and Horticulture Development Board, Stoneleigh Park, Kenilworth CV8 2TL.

Bach, H. (1998). Yield estimation of corn based on multitemporal LANDSAT-TM data as input for an agrometeorological model. *Pure and Applied Optics (Print Edition) (United Kingdom)*, *7*(4), 809–825. https://doi.org/10.1088/0963-9659/7/4/017

Badu-Apraku, áB, Hunter, R. B., & Tollenaar, M. (1983). Effect of temperature during grain filling on whole plant and grain yield in maize (Zea mays L.). *Canadian Journal of Plant Science*, *63*(2), 357–363.

Baez-Gonzalez, A. D., Kiniry, J. R., Maas, S. J., Tiscareno, M. L., Macias C., J., Mendoza, J. L., … Manjarrez, J. R. (2005). Large-Area Maize Yield Forecasting

Using Leaf Area Index Based Yield Model. *Agronomy Journal*, *97*, 418–425. https://doi.org/10.2134/agronj2005.0418

Ban, H. Y., Kim, K. S., Park, N. W., & Lee, B. W. (2017). Using MODIS data to predict regional corn yields. *Remote Sensing*, *9*(1). https://doi.org/10.3390/rs9010016

Baret, F. (1995). Use of spectral reflectance variation to retrieve canopy biophysical characteristics. *In Advances in Environmental Remote Sensing(M. Darson and S. Plummer, Eds.), John Wiley and Sons, Inc.*, 33–51.

Basso, B., Cammarano, D., & Carfagna, E. (2013). Review of Crop Yield Forecasting Methods and Early Warning Systems. The First Meeting of the Scientific Advisory Committee of the Global Strategy to Improve Agricultural and Rural Statistics.

Basu, S. K., & Kumar, N. (2014). *Modelling and Simulation of Diffusive Processes: Methods and Applications*. https://doi.org/10.1007/978-3-319-05657-9

Battude, M., Al Bitar, A., Morin, D., Cros, J., Huc, M., Marais Sicre, C., … Demarez, V. (2016). Estimating maize biomass and yield over large areas using high spatial and temporal resolution Sentinel-2 like remote sensing data. *Remote Sensing of Environment*, *184*, 668–681. https://doi.org/10.1016/j.rse.2016.07.030

Bauer, M. E., & Cipra, J. E. (1973). Identification of agricultural crops by computer processing of ERTS MSS data. Purdue Univ. Retrieved from http://docs.lib.purdue.edu/larstech/20

Bausch, W. C., Halvorson, A. D., & Cipra, J. (2008). Quickbird satellite and ground-based multispectral data correlations with agronomic parameters of irrigated maize grown in small plots. *Biosystems Engineering*, *101*(3), 306–315. https://doi.org/10.1016/j.biosystemseng.2008.09.011

Becker, R. ., Chambers, J. M., & Wilks, A. R. (1988). *The New S Language*. London, UK: Chapman & Hall.

Best, R. G., & Harlan, J. C. (1985). Spectral estimation of green leaf area index of oats. *Remote Sens. Environ.*, *17*, 27–36.

Black, T. A., Chen, J.-M., Lee, X., & Sagar, R. M. (1991). Characteristics of shortwave and longwave irradiances under a Douglas-fir forest stand. *Canadian Journal of Forest Research*, *21*(7), 1020–1028.

Bognár, P., Ferencz, C., Pásztor, S., Molnár, G., Timár, G., Hamar, D., … Ferencz, O. E. (2011). Yield forecasting for wheat and corn in Hungary by satellite remote sensing. *International Journal of Remote Sensing*, *32*(17), 4759–4767.

https://doi.org/10.1080/01431161.2010.493566

Bolton, D. K., & Friedl, M. A. (2013). Forecasting crop yield using remotely sensed vegetation indices and crop phenology metrics. *Agricultural and Forest Meteorology*, *173*, 74–84. https://doi.org/10.1016/j.agrformet.2013.01.007

Bu, H., Sharma, L. K., Denton, A., & Franzen, D. W. (2017). Comparison of satellite imagery and ground-based active optical sensors as yield predictors in sugar beet, spring wheat, corn, and sunflower. *Agronomy Journal*, *109*(1), 299–308. https://doi.org/10.2134/agronj2016.03.0150

Cai, Y., Moore, K., Pellegrini, A., Elhaddad, A., Lessel, J., Townsend, C., … Semret, N. (2017). Crop yield predictions -high resolution statistical model for intra-season forecasts applied to corn in the US. *American Geophysical Union, Fall Meeting 2017*.

Cairns, J. E., Araus, J. L., Ordoñez, R., Sanchez, C., & Vargas, M. (2012). Dissecting Maize Productivity: Ideotypes Associated with Grain Yield under Drought Stress and Well-watered Conditions. *Journal of Integrative Plant Biology*, *54*(12), 1007–1020. https://doi.org/10.1111/j.1744-7909.2012.01156.x

Campbell, J. B. (1996). *Introduction to remote sensing. Second edition*. The Guilford Press: New York, NY.

Campbell, J. B. (2007). *Introduction to Remote Sensing: Fourth Edition*. The Guilford Press: New York, NY.

Candiago, S., Remondino, F., De Giglio, M., Dubbini, M., & Gattelli, M. (2015). Evaluating multispectral images and vegetation indices for precision farming applications from UAV images. *Remote Sensing*, *7*(4), 4026–4047. https://doi.org/10.3390/rs70404026

Casanova, D., Epema, G. F., & Goudriaan, J. (1998). Monitoring rice reflectance at field level for estimating biomass and LAI. *Field Crops Research*, *55*(1), 83–92. https://doi.org/https://doi.org/10.1016/S0378-4290(97)00064-6

Cassman, K. G. (1999). Ecological intensification of cereal production systems: Yield potential, soil quality, and precision agriculture. *Proc. Natl. Acad. Sci.*, *96*, 5952–5959.

Chang, J., Dalsted, K., O'Neill, M., Clay, S., & Clay, D. E. (2003). Corn (L.) Yield Prediction Using Multispectral and Multidate Reflectance. *Agronomy Journal*, *95*, 1447–1453. https://doi.org/10.2134/agronj2003.1447

Chen, J. M., & Black, T. A. (1992). Defining leaf area index for non-flat leaves. *Plant, Cell & Environment*, *15*(4), 421–429.

Chen, K., Wu, A., Applied, N., Chen, L. Y., & Chang, W. (2010). FORMOSAT-2 Mission : Current Status and Contributions to Earth Observations. *Proceedings of the IEEE*, *98*(5), 878–891. https://doi.org/10.1109/JPROC.2009.2035355

Chivasa, W., Mutanga, O., & Biradar, C. (2017). Application of remote sensing in estimating maize grain yield in heterogeneous African agricultural landscapes: a review. *International Journal of Remote Sensing*, *38*(23), 6816–6845. https://doi.org/10.1080/01431161.2017.1365390

Christoph Hormann. (2016). Satellite comparison update. Retrieved June 3, 2019, from http://blog.imagico.de/satellite-comparison-update/

Colewell, R. N. (1956). Determining the prevalence of certain cereal crop diseases by means of aerial photography. *Hilgardia*, *26*, 223–286.

Curran, P. J. (1983). Multispectral remote sensing for the estimation of green leaf area index. *Phil. Trans. Roy. Soc. London Ser.*, *A309*, 257–270.

Delia Báez-González, A., Chen, P., Tiscareño-López, M., & Srinivasan, R. (2002). *Using Satellite and Field Data with Crop Growth Modeling to Monitor and Estimate Corn Yield in Mexico*. *Crop Science - CROP SCI* (Vol. 42). https://doi.org/10.2135/cropsci2002.1943

Doraiswamy, P. (2004). Crop condition and yield simulations using Landsat and MODIS. *Remote Sensing of Environment*, *92*(4), 548–559. https://doi.org/10.1016/j.rse.2004.05.017

Doraiswamy, P. C., Moulin, S., Cook, P. W., & Stern, A. (2003). Crop Yield Assessment from Remote Sensing. *Photogrammetric Engineering & Remote Sensing*, *69*(6), 665–674. https://doi.org/10.14358/pers.69.6.665

Doraiswamy, P. C., Sinclair, T. R., Hollinger, S., Akhmedov, B., Stern, A., & Prueger, J. (2005). Application of MODIS derived parameters for regional crop yield assessment. *Remote Sensing of Environment*, *97*(2), 192–202. https://doi.org/10.1016/j.rse.2005.03.015

Drusch, M., Del Bello, U., Carlier, S., Colin, O., Fernandez, V., Gascon, F., … Martimort, P. (2012). Sentinel-2: ESA's optical high-resolution mission for GMES operational services. *Remote Sensing of Environment*, *120*, 25–36.

Dupuis, I., & Dumas, C. (1990). Influence of temperature stress on in vitro fertilization and heat shock protein synthesis in maize (Zea mays L.) reproductive tissues. *Plant Physiology*, *94*(2), 665–670.

Durgun, Y., Gobin, A., Gilliams, S., Duveiller, G., & Tychon, B. (2016). Testing the Contribution of Stress Factors to Improve Wheat and Maize Yield Estimations Derived from Remotely-Sensed Dry Matter Productivity. *Remote Sensing*, *8*(3). https://doi.org/10.3390/rs8030170

Fang, H., Liang, S., & Hoogenboom, G. (2011). Integration of MODIS LAI and vegetation index products with the CSM-CERES-Maize model for corn yield estimation. *International Journal of Remote Sensing*, *32*(4), 1039–1065. https://doi.org/10.1080/01431160903505310

Fang, H., Teasdale, J., Cavigelli, M., Liang, S., & Hoogenboom, G. (2008). Corn-yield estimation through assimilation of remotely sensed data into the CSM-CERES-Maize model. *International Journal of Remote Sensing*, *29*(10), 3011–3032. https://doi.org/10.1080/01431160701408386

FAO, IFAD, UNICEF, W. and W. (2018). *The State of Food Security and Nutrition in the World 2018. Building climate resilience for food security and nutrition. Rome, FAO. Licence: CC BY-NC-SA 3.0 IGO*. https://doi.org/10.1093/cjres/rst006

FAO. (2017). *Review of the available Remote sensing tools, products, methodologies and data to improve crop production forecasts*.

FAO. (2018). *Country-level ASIS: an agricultural drought monitoring system*. Retrieved from http://www.fao.org/publications/card/en/c/CA0986EN

Ferencz, C., Bognár, P., Lichtenberger, J., Hamar, D., Tarcsai†, G., Timár, G., … Ferencz-Árkos, I. (2004). Crop yield estimation by satellite remote sensing. *International Journal of Remote Sensing*, *25*(20), 4113–4149. https://doi.org/10.1080/01431160410001698870

Fernandez-Ordonez, Y. M., & Soria-Ruiz, J. (2017). Maize crop yield estimation with remote sensing and empirical models. *2017 IEEE International Geoscience and Remote Sensing Symposium (IGARSS)*. https://doi.org/10.1109/igarss.2017.8127638

Fieuzal, R., Marais Sicre, C., & Baup, F. (2017). Estimation of corn yield using multi-temporal optical and radar satellite data and artificial neural networks. *International Journal of Applied Earth Observation and Geoinformation*, *57*, 14–23. https://doi.org/10.1016/j.jag.2016.12.011

Fischer, W. A., Hemphill, W. R., & Kover, A. (1976). Progress in remote sensing (1972–

1976). *Photogrammetria*, *32*(2), 33–72.

Fonseca, A. E., & Westgate, M. E. (2005). Relationship between desiccation and viability of maize pollen. *Field Crops Research*, *94*(2–3), 114–125.

Franzen, D., Sharma, L., & Bu, H. (2014). *Active optical sensor algorithm for corn yield prediction and corn side dress nitrogen rate aid*. *NDSU Extension Publication* (Vol. SF1176-5).

Freeman, K. W., Girma, K., Arnall, D. B., Mullen, R. W., Martin, K. L., Teal, R. K., & Raun, W. R. (2007). By-plant prediction of corn forage biomass and nitrogen uptake at various growth stages using remote sensing and plant height. *Agronomy Journal*, *99*(2), 530–536. https://doi.org/10.2134/agronj2006.0135

Funk, C., & Budde, M. E. (2009). Phenologically-tuned MODIS NDVI-based production anomaly estimates for Zimbabwe. *Remote Sensing of Environment*, *113*(1), 115–125. https://doi.org/10.1016/j.rse.2008.08.015

Gao, F., Anderson, M., Daughtry, C., & Johnson, D. (2018). Assessing the Variability of Corn and Soybean Yields in Central Iowa Using High Spatiotemporal Resolution Multi-Satellite Imagery. *Remote Sensing*, *10*(9). https://doi.org/10.3390/rs10091489

Geipel, J., Link, J., & Claupein, W. (2014). Combined spectral and spatial modeling of corn yield based on aerial images and crop surface models acquired with an unmanned aircraft system. *Remote Sensing*, *6*(11), 10335–10355. https://doi.org/10.3390/rs61110335

Global Strategy to Improve Agricultural and Rural Statistics. (2015). Cost – Effectiveness of Remote Sensing for Agricultural Statistics in Developing and Emerging Economies.

Guan, K., Wu, J., Kimball, J. S., Anderson, M. C., Frolking, S., Li, B., … Lobell, D. B. (2017). The shared and unique values of optical, fluorescence, thermal and microwave satellite data for estimating large-scale crop yields. *Remote Sensing of Environment*, *199*, 333–349. https://doi.org/10.1016/j.rse.2017.06.043

Guindin-Garcia, N. (2011). *Estimating maize grain yield from crop biophysical parameters using remote sensing*. *ProQuest Dissertations and Theses*. The University of Nebraska - Lincoln, Ann Arbor. Retrieved from https://search.proquest.com/docview/824023600?accountid=7181

Guindin-garcia, N., Arkebauer, T. J., Shanahan, J., Weiss, A., Guindin-garcia, N., Gitelson, A. A., … Weiss, A. (2012). An evaluation of MODIS 8- and 16-day composite products for monitoring maize green leaf area index monitoring maize green leaf area index. *Agricultural and Forest Meteorology*, *161*, 15–25. https://doi.org/10.1016/j.agrformet.2012.03.012

Hatfield, J L. (1983). Remote sensing estimators of potential and actual crop yield. *Remote Sensing of Environment*, *13*(4), 301–311.

Hatfield, Jerry L., Asrar, G., & Kanemasu, E. T. (1984). Intercepted photosynthetically active radiation estimated by spectral reflectance. *Remote Sensing of Environment*, *14*, 65–75.

Hatfield, Jerry L, & Dold, C. (2018). Climate Change Impacts on Corn Phenology and Productivity. In *Corn-Production and Human Health in Changing Climate*. IntechOpen.

Hayes, M. J., & Decker, W. L. (1996). Using NOAA AVHRR data to estimate maize production in the United States Corn Belt. *International Journal of Remote Sensing*, *17*(16), 3189–3200. https://doi.org/10.1080/01431169608949138

Herrero, M. P., & Johnson, R. R. (1980). High Temperature Stress and Pollen Viability of Maize 1. *Crop Science*, *20*(6), 796–800.

Hoeting, J. A., Madigan, D., Raftery, A. E., & Volinsky, C. T. (1999). Bayesian model averaging: a tutorial. *Statistical Science*, 382–401.

Hoogenboom, G., White, J. W., & Messina, C. D. (2004). From genome to crop: integration through simulation modeling. *Field Crops Research*, *90*(1), 145–163.

Horie, T., Yajima, M., & Nakagawa, H. (1992). Yield forecasting. *Agricultural Systems*, *40*(1–3), 211–236.

Http-1. (n.d.). No Title. Retrieved April 14, 2019, from https://tr.climate-data.org/asya/tuerkiye/erzurum/pasinler-30509/#climate-graph

Http-2. (n.d.). No Title. Retrieved April 15, 2019, from https://ipad.fas.usda.gov/rssiws/al/crop_calendar/images/metu_tu_calendar.png

Idso, S B, Hatfield, J. L., Reginato, R. J., & Jackson, R. D. (1978). Wheat yield estimation by albedo measurement. *Remote Sensing of Environment*, *7*(3), 273–276.

Idso, Sherwood B, Jackson, R. D., & Reginato, R. J. (1977). Remote-sensing of crop yields. *Science*, *196*(4285), 19–25.

Ihaka, R., & Gentleman, R. (1996). R: a language for data analysis and graphics. *Journal of Computational and Graphical Statistics*, *5*(3), 299–314.

Ines, A. V. M., Das, N. N., Hansen, J. W., & Njoku, E. G. (2013). Assimilation of remotely sensed soil moisture and vegetation with a crop simulation model for maize yield prediction. *Remote Sensing of Environment*, *138*, 149–164. https://doi.org/10.1016/j.rse.2013.07.018

Inman, D., Khosla, R., Reich, R. M., & Westfall, D. G. (2007). Active remote sensing and grain yield in irrigated maize. *Precision Agriculture*, *8*(4–5), 241–252. https://doi.org/10.1007/s11119-007-9043-z

Jaafar, H. H., & Ahmad, F. A. (2015). Crop yield prediction from remotely sensed vegetation indices and primary productivity in arid and semi-arid lands. *International Journal of Remote Sensing*, *36*(18), 4570–4589. https://doi.org/10.1080/01431161.2015.1084434

Jackson R.D. (1986). Remote sensing of biotic and abiotic plant stress. *Annual Review of Phytopathology*, *24*, 265–286.

Jégo, G., Pattey, E., & Liu, J. (2012). Using Leaf Area Index, retrieved from optical imagery, in the STICS crop model for predicting yield and biomass of field crops. *Field Crops Research*, *131*, 63–74. https://doi.org/10.1016/j.fcr.2012.02.012

Jensen, J. R. (2009). *Remote sensing of the environment: An earth resource perspective 2/e*. Pearson Education India.

Jewel, N. (1989). An evaluation of multi-date SPOT data for agriculture and land use mapping in the United Kingdom. *International Journal of Remote Sensing*, *10*, 939–951.

Jiang, D., Yang, X., Clinton, N., & Wang, N. (2004). An artificial neural network model for estimating crop yields using remotely sensed information. *International Journal of Remote Sensing*, *25*(9), 1723–1732.

Jin, X., Kumar, L., Li, Z., Feng, H., Xu, X., Yang, G., & Wang, J. (2018). A review of data assimilation of remote sensing and crop models. *European Journal of Agronomy*, *92*(October 2017), 141–152. https://doi.org/10.1016/j.eja.2017.11.002

Johnson, D. M. (2014). An assessment of pre- and within-season remotely sensed variables for forecasting corn and soybean yields in the United States. *Remote Sensing of Environment*, *141*, 116–128. https://doi.org/10.1016/j.rse.2013.10.027

Johnson, D. M. (2016). A comprehensive assessment of the correlations between field crop yields and commonly used MODIS products. *International Journal of Applied Earth Observation and Geoinformation*, *52*, 65–81. https://doi.org/10.1016/j.jag.2016.05.010

Johnson, M. D., Hsieh, W. W., Cannon, A. J., Davidson, A., & Bédard, F. (2016). Crop yield forecasting on the Canadian Prairies by remotely sensed vegetation indices and machine learning methods. *Agricultural and Forest Meteorology*, *218–219*, 74–84. https://doi.org/10.1016/j.agrformet.2015.11.003

Jovanovic, D., Sabo, F., Govedarica, M., & Marinkovic, B. (2014). Crop yield estimation in 2014 for Vojvodina using methods of remote sensing. *Ratarstvo i Povrtarstvo*, *51*(3), 145–153. https://doi.org/10.5937/ratpov51-6712

Kalaitzidis, C., & Zianis, D. (2009). A review of multispectral vegetation indices for biomass estimation. *Imagin[e,g] Europe*, 201–208. https://doi.org/10.3233/978-1-60750-494-8-201

Kasampalis, D. A., Alexandridis, T. K., Deva, C., Challinor, A., Moshou, D., & Georgios Zalidis. (2018). Contribution of Remote Sensing on Crop Models: A Review. *Journal of Imaging*, *4*(52), 19. https://doi.org/10.3390/jimaging4040052

Kern, A., Barcza, Z., Marjanović, H., Árendás, T., Fodor, N., Bónis, P., … Lichtenberger, J. (2018). Statistical modelling of crop yield in Central Europe using climate data and remote sensing vegetation indices. *Agricultural and Forest Meteorology*, *260–261*(February), 300–320. https://doi.org/10.1016/j.agrformet.2018.06.009

Khanal, S., Fulton, J., Klopfenstein, A., Douridas, N., & Shearer, S. (2018). Integration of high resolution remotely sensed data and machine learning techniques for spatial prediction of soil properties and corn yield. *Computers and Electronics in Agriculture*, *153*(July), 213–225. https://doi.org/10.1016/j.compag.2018.07.016

Kim, N., & Lee, Y. W. (2016). Machine learning approaches to corn yield estimation using satellite images and climate data: a case of Iowa State. *J. Korean Soc. Surv. Geod. Photogramm. Cartogr.*, *34*(4), 383–390.

Kiniry, J. R., & Bonhomme, R. (1991). Predicting maize phenology. *Predicting Crop Phenology*, *11*, 5–131.

Kogan, F., Salazar, L., & Roytman, L. (2012). Forecasting crop production using satellite-based vegetation health indices in Kansas, USA. *International Journal of Remote Sensing*, *33*(9), 2798–2814. https://doi.org/10.1080/01431161.2011.621464

Kogan, F., Yang, B., Xianfeng, J., Zhiyuan, P., & Wei, G. (2005). Modelling corn production in China using AVHRR-based vegetation health indices. *International Journal of Remote Sensing*, *26*(11), 2325–2336. https://doi.org/10.1080/01431160500034235

Kuwata, K., & Shibasaki, R. (2015). Estimating crop yields with deep learning and remotely sensed data. In *2015 IEEE International Geoscience and Remote Sensing Symposium (IGARSS)* (pp. 858–861). IEEE.

L. Wiegand, C., & J. Richardson, A. (1990). *Use of Spectral Vegetation Indices to Infer Leaf Area, Evapotranspiration and Yield: I. Rationale. Agronomy Journal - AGRON J* (Vol. 82). https://doi.org/10.2134/agronj1990.00021962008200030037x

Lambert, M. J., Traoré, P. C. S., Blaes, X., Baret, P., & Defourny, P. (2018). Estimating smallholder crops production at village level from Sentinel-2 time series in Mali's cotton belt. *Remote Sensing of Environment*, *216*(September 2017), 647–657. https://doi.org/10.1016/j.rse.2018.06.036

Lang, A. R. G. (1991). Application of some of Cauchy's theorems to estimation of surface areas of leaves, needles and branches of plants, and light transmittance. *Agricultural and Forest Meteorology*, *55*(3–4), 191–212.

Leamer, E. E. (1978). *Specification searches: Ad hoc inference with nonexperimental data* (Vol. 53). John Wiley & Sons Incorporated.

Lewis, J. E., Rowland, J., & Nadeau, A. (1998). Estimating maize production in Kenya using NDVI: Some statistical considerations. *International Journal of Remote Sensing*, *19*(13), 2609–2617. https://doi.org/10.1080/014311698214677

Li, A., Liang, S., Wang, A., & Qin, J. (2007). Estimating Crop Yield from Multi-temporal Satellite Data Using Multivariate Regression and Neural Network Techniques. *Photogrammetric Engineering & Remote Sensing*, *73*(10), 1149–1157. https://doi.org/10.14358/pers.73.10.1149

Li, Y., Chen, C., Zhang, G., Wang, J., Zhou, Q., & Zhou, J. (2014). Assimilating remote sensing information into a coupled hydrology-crop growth model to estimate regional maize yield in arid regions. *Ecological Modelling*, *291*, 15–27. https://doi.org/10.1016/j.ecolmodel.2014.07.013

Liang, S., Li, X., & Wang, J. B. T.-A. R. S. (Eds.). (2012). Chapter 11 - Leaf Area Index. In *Advanced Remote Sensing* (pp. 347–381). Boston: Academic Press. https://doi.org/https://doi.org/10.1016/B978-0-12-385954-9.00011-3

Liebisch, F., Kirchgessner, N., Schneider, D., Walter, A., & Hund, A. (2015). Remote, aerial phenotyping of maize traits with a mobile multi-sensor approach. *Plant Methods*, *11*(1). https://doi.org/10.1186/s13007-015-0048-8

Lillesaeter, O. (1982). Spectral reflectance of partly transmitting leaves: laboratory measurements and mathematical modeling. *Remote Sensing of Environment*, *12*(3), 247–254.

Lillesand, T. M., & Kiefer, R. (1994). *Remote sensing and image interpretation. 3rd edition*.

Link, J., Senner, D., & Claupein, W. (2013). Developing and evaluating an aerial sensor platform (ASP) to collect multispectral data for deriving management decisions in precision farming. *Computers and Electronics in Agriculture*, *94*, 20–28. https://doi.org/10.1016/j.compag.2013.03.003

Liu, J., Pattey, E., Miller, J. R., McNairn, H., Smith, A., & Hu, B. (2010). Estimating crop stresses, aboveground dry biomass and yield of corn using multi-temporal optical data combined with a radiation use efficiency model. *Remote Sensing of Environment*, *114*(6), 1167–1177. https://doi.org/10.1016/j.rse.2010.01.004

Lobell, D B, & Asner, G. P. (2003). Comparison of earth observing-1 ali and landsat etm+ for crop identification and yield prediction in mexico. *IEEE Transactions on Geoscience and Remote Sensing*, *41*(6), 1277–1282. https://doi.org/10.1109/tgrs.2003.812909

Lobell, David B. (2013). The use of satellite data for crop yield gap analysis. *Field Crops Research*, *143*, 56–64. https://doi.org/10.1016/j.fcr.2012.08.008

Lobell, David B, Asner, G. P., Ortiz-Monasterio, J. I., & Benning, T. L. (2003). Remote sensing of regional crop production in the Yaqui Valley, Mexico: estimates and uncertainties. *Agriculture, Ecosystems & Environment*, *94*(2), 205–220. https://doi.org/https://doi.org/10.1016/S0167-8809(02)00021-X

Lobell, David B, Thau, D., Seifert, C., Engle, E., & Little, B. (2015). A scalable satellite-based crop yield mapper. *Remote Sensing of Environment*, *164*, 324–333. https://doi.org/10.1016/j.rse.2015.04.021

Maresma, Á., Ariza, M., Lloveras, J., Martínez-Casasnovas, J., & Martínez, E. (2016). Analysis of Vegetation Indices to Determine Nitrogen Application and Yield Prediction in Maize (Zea mays L.) from a Standard UAV Service. *Remote Sensing*, *8*(12), 973. https://doi.org/10.3390/rs8120973

Maresma, Á., Lloveras, J., & Martínez-Casasnovas, J. A. (2018). Use of multispectral airborne images to improve in-season nitrogen management, predict grain yield and estimate economic return of maize in irrigated high yielding environments. *Remote Sensing*, *10*(4), 1–19. https://doi.org/10.3390/rs10040543

Martin, K. L., Mullen, R. W., Phillips, S. B., Raun, W. R., Melchiori, R., Schepers, J. S., … Desta, K. (2005). Plant-to-Plant Variability in Corn Production. *Agronomy Journal*, *97*, 1603–1611. https://doi.org/10.2134/agronj2005.0129

Martin, K. L., Raun, W. R., Chung, B., Stone, M. L., Arnall, D. B., Solie, J. B., … Girma, K. (2007). Expression of Variability in Corn as Influenced by Growth Stage Using Optical Sensor Measurements. *Agronomy Journal*, *99*(2), 384. https://doi.org/10.2134/agronj2005.0268

Martin, K., Raun, W., & Solie, J. (2012). By-plant prediction of corn grain yield using optical sensor readings and measured plant height. *Journal of Plant Nutrition*, *35*(9), 1429–1439. https://doi.org/10.1080/01904167.2012.684133

Mayer, B., & Kylling, A. (2005). The libRadtran software package for radiative transfer calculations-description and examples of use. *Atmospheric Chemistry and Physics*, *5*(7), 1855–1877.

McCree, K. J. (1971). The action spectrum, absorptance and quantum yield of photosynthesis in crop plants. *Agricultural Meteorology*, *9*, 191–216. https://doi.org/https://doi.org/10.1016/0002-1571(71)90022-7

Mkhabela, M. S., Mkhabela, M. S., & Mashinini, N. N. (2005). Early maize yield forecasting in the four agro-ecological regions of Swaziland using NDVI data derived from NOAA's-AVHRR. *Agricultural and Forest Meteorology*, *129*(1–2), 1–9. https://doi.org/10.1016/j.agrformet.2004.12.006

Mladenova, I. E., Mueller, R., Hain, C. R., Anderson, M. C., Bolten, J. D., Crow, W. T., & Johnson, D. M. (2017). Intercomparison of Soil Moisture, Evaporative Stress, and Vegetation Indices for Estimating Corn and Soybean Yields Over the U.S. *IEEE Journal of Selected Topics in Applied Earth Observations and Remote Sensing*, *10*(4), 1328–1343. https://doi.org/10.1109/jstars.2016.2639338

Monmonier, M. (2002). Aerial photography at the Agricultural Adjustment Administration: Acreage controls, conservation. *Photogrammetric Engineering & Remote Sensing*, *68*, 1257–1261.

Montgomery, J. M., & Nyhan, B. (2010). Bayesian model averaging: Theoretical developments and practical applications. *Political Analysis*, *18*(2), 245–270.

Moyroud, N., & Portet, F. (2018). Introduction to QGIS. *QGIS and Generic Tools*, *1*, 1–17.

Muchow, R. C., Sinclair, T. R., & Bennett, J. M. (1990). Temperature and solar radiation effects on potential maize yield across locations. *Agronomy Journal*, *82*(2), 338–343.

Mulla, D. J. (2013). Twenty five years of remote sensing in precision agriculture: Key advances and remaining knowledge gaps. *Biosystems Engineering*, *114*(4), 358–371. https://doi.org/10.1016/j.biosystemseng.2012.08.009

Myneni, R. B., Hoffman, S., Knyazikhin, Y., Privette, J. L., Glassy, J., Tian, Y., … Smith, G. R. (2002). Global products of vegetation leaf area and fraction absorbed PAR from year one of MODIS data. *Remote Sensing of Environment, 83*(1–2), 214–231.

National Agricultural Statistics Service. (2005). History of Remote Sensing for Crop Acreage. Retrieved from http://www.nass.usda.gov/Surveys/Remotely_Sensed_Data_Crop_Acreage/index.asphttp://www.nass.usda.gov/Surveys/Remotely_Sensed_Data_Crop_Acreage/index.asp

Nellis, M. D., Price, K. P., & Rundquist, D. (2009). Remote Sensing of Cropland Agriculture In: The SAGE Handbook of Remote Sensing. *Papers in Natural Resources, 217*. https://doi.org/10.4135/9780857021052

Ngie, A., & Ahmed, F. (2018). Estimation of Maize grain yield using multispectral satellite data sets (SPOT 5) and the random forest algorithm. *South African Journal of Geomatics, 7*(1). https://doi.org/10.4314/sajg.v7i1.2

Pan, G., Sun, G. J., & Li, F. M. (2009). Using QuickBird imagery and a production efficiency model to improve crop yield estimation in the semi-arid hilly Loess Plateau, China. *Environmental Modelling and Software*, *24*(4), 510–516. https://doi.org/10.1016/j.envsoft.2008.09.014

Pan, Z., Huang, J., Zhou, Q., Wang, L., & Cheng, Y. (2015). International Journal of Applied Earth Observation and Geoinformation Mapping crop phenology using NDVI time-series derived from HJ-1 A / B data. *International Journal of Applied Earth Observations and Geoinformation*, *34*, 188–197. https://doi.org/10.1016/j.jag.2014.08.011

Panda, S. S., Ames, D. P., & Panigrahi, S. (2010). Application of vegetation indices for agricultural crop yield prediction using neural network techniques. *Remote Sensing*, *2*(3), 673–696. https://doi.org/10.3390/rs2030673

Paul J. Pinter, J., Hatfield, J. L., Schepers, J. S., Barnes, E. M., Moran, M. S., Daughtry, C. S. T., & Upchurch, D. R. (2003). Remote Sensing for Crop Management.

Photogrammetric Engineering & Remote Sensing, *69*(6), 647–664.

Pearson, R. L., Miller, L. D., & Tucker, C. J. (1976). Hand-held spectral radiometer to estimate gramineous biomass. *Applied Optics*, *15*(2), 416–418.

Peng, Y., & Gitelson, A. A. (2011). Application of chlorophyll-related vegetation indices for remote estimation of maize productivity. *Agricultural and Forest Meteorology*, *151*(9), 1267–1276. https://doi.org/10.1016/j.agrformet.2011.05.005

Peralta, N. R., Assefa, Y., Du, J., Barden, C. J., & Ciampitti, I. A. (2016). Mid-season high-resolution satellite imagery for forecasting site-specific corn yield. *Remote Sensing*, *8*(10). https://doi.org/10.3390/rs8100848

Petersen, L. K. (2018). Real-time prediction of crop yields from MODIS relative vegetation health: A continent-wide analysis of Africa. *Remote Sensing*, *10*(11), 1–31. https://doi.org/10.3390/rs10111726

Peterson, D. L., Spanner, M. A., Running, S. W., & Teuber, K. B. (1987). Relationship of thematic mapper simulator data to leaf area index of temperate coniferous forest. *Remote Sens. Environ.*, *22*, 323–341.

Pinter, Jr., P. J., Jackson, R. D., Idso, S. B., & Reginato, R. J. (1981). Multidate spectral reflectances as predictors of yield in water stressed wheat and barley. *International Journal of Remote Sensing*, *2*(1), 43–48.

Prasad, A. K., Chai, L., Singh, R. P., & Kafatos, M. (2006). Crop yield estimation model for Iowa using remote sensing and surface parameters. *International Journal of Applied Earth Observation and Geoinformation*, *8*(1), 26–33. https://doi.org/10.1016/j.jag.2005.06.002

Prasad, S., Bruce, L. M., & Chanussot, J. (2011). *Optical Remote Sensing - Advances in Signal Processing and Exploitation Techniques* (3rd ed.). Augmented Vision and Reality. https://doi.org/10.1007/978-3-642-14212-3

Price, J. C., & Bausch, J. C. (1995). Leaf area index estimation from visible and near-infrared reflectance data. *Remote Sens. Environ.*, *52*, 55–65.

Qi, J., Kerr, Y. H., Moran, M. S., Weltz, M., Huete, A. R., & Sorooshian, S. (2000). Leaf Area Index Estimates Using Remotely Sensed Data and BRDF Models in a Semiarid Region. *Remote Sensing of Environment*, *73*, 18–30. https://doi.org/10.1016/S0034-4257(99)00113-3

Quarmby, N. A., Milnes, M., Hindle, T. L., & Silleos, N. (1993). The use of multi-temporal NDVI measurements from AVHRR data for crop yield estimation and prediction. *International Journal of Remote Sensing*, *14*(2), 199–210. https://doi.org/10.1080/01431169308904332

Raftery, A., Hoeting, J., Volinsky, C., Painter, I., Yeung, K. Y., Sevcikova, M. H., & Suggests, M. (2018). Package 'BMA.' Version.

Ransom, J., & Enders, G. J. (2013). Corn growth and management quick guide. *North Dakota State University, Fargo, North Dakota*.

Reginato, R. J., Idso, S. B., & Jackson, R. D. (1978). Estimating forage crop production – Technique adaptable to remote-sensing. *Remote Sensing of Environment*, *7*(1), 77–80.

Richter, R., & Schläpfer, D. (2011). Atmospheric/topographic correction for satellite imagery: ATCOR-2/3 User Guide. *DLR IB*, 501–565.

Roberts, H. V. (1965). Probabilistic prediction. *Journal of the American Statistical Association*, *60*(309), 50–62.

Rojas, O. (2007). Operational maize yield model development and validation based on remote sensing and agro-meteorological data in Kenya. *International Journal of Remote Sensing*, *28*(17), 3775–3793. https://doi.org/10.1080/01431160601075608

Rorie, R. L., Karcher, D. E., Longer, D. E., Purcell, L. C., King, C. A., Mozaffari, M., & Marsh, M. C. (2011). Association of "Greenness" in Corn with Yield and Leaf Nitrogen Concentration. *Agronomy Journal*, *103*(2), 529–535. https://doi.org/10.2134/agronj2010.0296

Ross, J. (1981). 1.3 Phytometric methods. *The Radiation Regime and Architecture of Plant Stands; Kluwer Academic Publishers: Holand*, 42–44.

Russello, H. (2018). *Convolutional Neural Networks for Crop Yield Prediction using Satellite Images*. University of Amsterdam. Retrieved from https://esc.fnwi.uva.nl/thesis/centraal/files/f1570224447.pdf

Sabini, M., Rusak, G., & Ross, B. (2017). *Understanding Satellite-Imagery-Based Crop Yield Predictions*. Technical Report. Stanford University. http://cs231n. stanford. edu/reports ….

Sakamoto, T., Gitelson, A. A., & Arkebauer, T. J. (2013). MODIS-based corn grain yield estimation model incorporating crop phenology information. *Remote Sensing of Environment*, *131*, 215–231. https://doi.org/10.1016/j.rse.2012.12.017

Sakamoto, T., Gitelson, A. A., & Arkebauer, T. J. (2014). Near real-time prediction of U.S. corn yields based on time-series MODIS data. *Remote Sensing of Environment*, *147*, 219–231. https://doi.org/10.1016/j.rse.2014.03.008

Salazar, L., Kogan, F., & Roytman, L. (2008). Using vegetation health indices and partial least squares method for estimation of corn yield. *International Journal of Remote Sensing*, *29*(1), 175–189. https://doi.org/10.1080/01431160701271974

Sankaran, S., Khot, L. R., Espinoza, C. Z., Jarolmasjed, S., Sathuvalli, V. R., Vandemark, G. J., … Pavek, M. J. (2015). Low-altitude, high-resolution aerial imaging systems for row and field crop phenotyping: A review. *European Journal of Agronomy*, *70*, 112–123. https://doi.org/10.1016/j.eja.2015.07.004

Schwalbert, R. A., Amado, T. J. C., Nieto, L., Varela, S., Corassa, G. M., Horbe, T. A. N., … Ciampitti, I. A. (2018). Forecasting maize yield at field scale based on high-resolution satellite imagery. *Biosystems Engineering*, *171*, 179–192. https://doi.org/10.1016/j.biosystemseng.2018.04.020

Seelan, S. K., Laguette, S., Casady, G. M., & Seielstad, G. A. (2003). Remote sensing applications for precision agriculture: A learning community approach. *Remote Sensing of Environment*, *88*(1–2), 157–169. https://doi.org/10.1016/j.rse.2003.04.007

Senay, G. B., Ward, A. D., Lyon, J. G., Fausey, N. R., & Nokes, S. E. (1998). Manipulation of high spatial resolution aircraft remote sensing data for use in site-specific farming. *American Society of Agricultural Engineers*, *41*(2), 489–495.

Senthilnath, J., Kandukuri, M., Dokania, A., & Ramesh, K. N. (2017). Application of UAV imaging platform for vegetation analysis based on spectral-spatial methods. *Computers and Electronics in Agriculture*, *140*, 8–24. https://doi.org/10.1016/j.compag.2017.05.027

Shanahan, J. F., Major, D. J., Tringe, J. M., Francis, D. D., Wilhelm, W. W., Schepers, J. S., … Varvel, G. E. (2001). Use of Remote-Sensing Imagery to Estimate Corn Grain Yield. *Agronomy Journal*, *93*, 583–589. https://doi.org/10.2134/agronj2001.933583x

Shao, Y., Campbell, J. B., Taff, G. N., & Zheng, B. (2015). An analysis of cropland mask choice and ancillary data for annual corn yield forecasting using MODIS data. *International Journal of Applied Earth Observation and Geoinformation*, *38*, 78–87. https://doi.org/10.1016/j.jag.2014.12.017

Sharma, L. K., Bu, H., & Franzen, D. W. (2016). Comparison of two ground-based active-optical sensors for in-season estimation of corn (Zea mays, L.) yield. *Journal of*

Plant Nutrition, *39*(7), 957–966. https://doi.org/10.1080/01904167.2015.1109109

Sharma, L. K., Bu, H., Franzen, D. W., & Denton, A. (2016). Use of corn height measured with an acoustic sensor improves yield estimation with ground based active optical sensors. *Computers and Electronics in Agriculture*, *124*, 254–262. https://doi.org/10.1016/j.compag.2016.04.016

Sharma, L. K., & Franzen, D. W. (2014). Use of corn height to improve the relationship between active optical sensor readings and yield estimates. *Precision Agriculture*, *15*(3), 331–345. https://doi.org/10.1007/s11119-013-9330-9

Sharma, L.K., Bali, S. K., Franzen, D. W., Baldwin, P., & Zaeen, A. A. (2018). Use of Rainfall Data to Improve Ground-Based Active Optical Sensors Yield Estimates. *Agronomy Journal*, *110*(4), 1561. https://doi.org/10.2134/agronj2017.12.0696

Sharma, Lakesh K., Bu, H., Denton, A., & Franzen, D. W. (2015). Active-optical sensors using red NDVI compared to red edge NDVI for prediction of corn grain yield in north Dakota, U.S.A. *Sensors (Switzerland)*, *15*(11), 27832–27853. https://doi.org/10.3390/s151127832

Shaver, T. M., Khosla, R., & Westfall, D. G. (2015). Utilizing normalized difference vegetation indices (NDVI) and in-season crop and soil variables to estimate corn grain yield, (April). Retrieved from http://fluidfertilizer.org/wp-content/uploads/2016/05/T-M-Shaver-and-Raj-Khosla-1.pdf

Sibley, A. M., Grassini, P., Thomas, N. E., Cassman, K. G., & Lobell, D. B. (2014). Testing remote sensing approaches for assessing yield variability among maize fields. *Agronomy Journal*, *106*(1), 24–32. https://doi.org/10.2134/agronj2013.0314

Sivasankar, T., Kumar, D., Srivastava, H. S., & Patel, P. (2018). Advances in Radar Remote Sensing of Agricultural Crops : A Review. *Advanced Science Engineering Information Technology*, *8*(4), 1126–1137.

Slonecker, T., Lacerte, M. J., & Garofalo, D. (1999). Airborne: The Value of Historic Imagery. Earth Observation Magazine. Retrieved from http://www.eomonline.com/Common/Archives/1999julaug/99julaug_airborne.html

Smith, W. K., Schoettle, A. W., & Cui, M. (1991). Importance of the method of leaf area measurement to the interpretation of gas exchange of complex shoots. *Tree Physiology*, *8*(2), 121–127.

Solari, F., Shanahan, J., Ferguson, R., Schepers, J., & Gitelson, A. (2008). Active sensor reflectance measurements of corn nitrogen status and yield potential. *Agronomy*

Journal, *100*(3), 571–579. https://doi.org/10.2134/agronj2007.0244

Song, X., Wang, J., & Huang, W. (2010). Winter wheat growth and grain protein uniformity monitoring through remotely sensed data. In *Proc.SPIE* (Vol. 7824). Retrieved from https://doi.org/10.1117/12.865162

Soria-Ruíz, J., & Fernández-Ordoñez, Y. (2003). Prediction of Corn Yield in Mexico Using Vegetation Indices from NOAA-AVHRR Satellite Images and Degree-days. *Geocarto International*, *18*(4), 33–42. https://doi.org/10.1080/10106040308542287

Soria-Ruíz, J., Fernández-Ordoñez, Y., & Granados-Ramírez, R. (2004). Methodology for prediction of corn yield using remote sensing satellite data in Central Mexico. *Investigaciones Geográficas*, *55*, 61–78. https://doi.org/http://dx.doi.org/10.14350/rig.30111

Soria-Ruiz, J., Fernandez-Ordonez, Y., McNairm, H., & Bugden-Storie, J. (2007). Corn monitoring and crop yield using optical and RADARSAT-2 images. *International Geoscience and Remote Sensing Symposium (IGARSS)*, (August), 3655–3658. https://doi.org/10.1109/IGARSS.2007.4423638

Spitkó, T., Nagy, Z., Zsubori, Z. T., Szőke, C., Berzy, T., Pintér, J., & Marton, C. L. (2016). Connection between normalized difference vegetation index and yield in maize. *Plant, Soil and Environment*, *62*(7), 293–298. https://doi.org/10.17221/676/2015-PSE

Stafford, J. V. (2000). Implementing precision agriculture in the 21st century. *Journal of Agricultural and Engineering Research*, *76*(3), 267–275. https://doi.org/10.1006/jaer.2000.0577

Sun, C., Liu, Y., Zhao, S., Zhou, M., & Yang, Y. (2016). International Journal of Applied Earth Observation and Geoinformation Classification mapping and species identification of salt marshes based on a short-time interval NDVI time-series from HJ-1 optical imagery. *International Journal of Applied Earth Observations and Geoinformation*, *45*, 27–41. https://doi.org/10.1016/j.jag.2015.10.008

Teal, R. K., Walsh, O., Arnall, D. B., Freeman, K. W., Raun, W. R., Tubana, B., & Girma, K. (2006). In-Season Prediction of Corn Grain Yield Potential Using Normalized Difference Vegetation Index. *Agronomy Journal*, *98*(6), 1488. https://doi.org/10.2134/agronj2006.0103

Team, R. C. (2013). R: A language and environment for statistical computing.

Tenkorang, F., & Lowenberg-doboer, J. (2008). On-Farm Profitability of Remote Sensing in Agriculture History of Remote Sensing in. *The Journal of Terrestrial Observation Volume*, *1*(1), 50–59.

Thomas, J. R., & Gerbermann, A. H. (1977). Yield-reflectance relations in cabbage. *Photogrammetric Engineering & Remote Sensing*, *43*(10), 1257–1266.

Thomas, J. R., Wiegand, C. L., & Myers, V. I. (1967). Reflectance of cotton leaves and its relation to yields. *Agronomy Journal*, *59*, 551–554.

Tucker, C.J., Holben, B. N., Elgin, J. H., & McMurtrey, J. E. (1980). Relationship of spectral data to grain yield variation. Photogram. *Photogram. Eng. Remote Sens.*, *45*, 600–608.

Tucker, C.J., J.H. Elgin, J., & III, J. E. M. (1979). Temporal spectral measurements of corn and soybean crops. *Photogrammetric Engineering & Remote Sensing*, *45*(5), 643–653.

Tucker, C.J., Townshend, J. R. G., & Goef, T. E. (1985). African land cover classification using satellite data. *Science*, *227*, 110.

Tucker, Compton J. (1979). Red and photographic infrared linear combinations for monitoring vegetation. *Remote Sensing of Environment*, *8*(2), 127–150. https://doi.org/https://doi.org/10.1016/0034-4257(79)90013-0

Tucker, Compton J, Holben, B. N., Elgin, J. H., & McMurtrey, J. E. (1981). Remote sensing of total dry-matter accumulation in winter wheat. *Remote Sensing of Environment*, *11*, 171–189. https://doi.org/https://doi.org/10.1016/0034-4257(81)90018-3

Ulaby, F. ., & Dobson, M. C. (1989). *Handbook of Radar Scattering Statistics for Terrain*. Artech House.

Unganai, L. S., & Kogan, F. N. (1998). Drought Monitoring and Corn Yield Estimation in Southern Africa from AVHRR Data. *Remote Sensing of Environment*, *63*(3), 219–232. https://doi.org/https://doi.org/10.1016/S0034-4257(97)00132-6

Veloso, A., Mermoz, S., Bouvet, A., Le Toan, T., Planells, M., Dejoux, J. F., & Ceschia, E. (2017). Understanding the temporal behavior of crops using Sentinel-1 and Sentinel-2-like data for agricultural applications. *Remote Sensing of Environment*, *199*, 415–426. https://doi.org/10.1016/j.rse.2017.07.015

Vergara-Díaz, O., Zarco-Tejada, P., Prasanna, B. M., Hornero, A., Zaman-Allah, M. A., Cairns, J. E., … Masuka, B. (2016). A Novel Remote Sensing Approach for Prediction of Maize Yield Under Different Conditions of Nitrogen Fertilization.

Frontiers in Plant Science, *7*(666), 1–13. https://doi.org/10.3389/fpls.2016.00666

Vina, A., Gitelson, A. A., Rundquist, D. C., Keydan, G., Leavitt, B., & Schepers, J. (2004). Monitoring maize (Zea mays)Phenology with Remote sensing. *Agronomy Journal*, *96*, 1139–1147.

Wahab, I., Hall, O., & Jirström, M. (2018). Remote Sensing of Yields: Application of UAV Imagery-Derived NDVI for Estimating Maize Vigor and Yields in Complex Farming Systems in Sub-Saharan Africa. *Drones*, *2*(3), 28. https://doi.org/10.3390/drones2030028

Walker, G. K., & Hatfield, J. L. (1979). Test of the stress-degree-day concept using multiple planting dates of red kidney beans. *Agronomy Journal*, *71*(6), 967–971.

Wang, J., Li, X., Lu, L., & Fang, F. (2013). Estimating near future regional corn yields by integrating multi-source observations into a crop growth model. *European Journal of Agronomy*, *49*, 126–140. https://doi.org/10.1016/j.eja.2013.03.005

Watson, D. J. (1947). Comparative Physiological Studies on the Growth of Field Crops: I. Variation in Net Assimilation Rate and Leaf Area between Species and Varieties, and within and between Years. *Annals of Botany*, *11*(1), 41–76. https://doi.org/10.1093/oxfordjournals.aob.a083148

Wiegand, C. L., Gerbermann, A. H., Gallo, K. P., Blad, B. L., & Dusek, D. (1990). Multisite analyses of spectral-biophysical data for corn. *Remote Sens. Environ.*, *33*, 1–16.

Wiegand, C. L., Richardson, A. J., & Kanemasu, E. T. (1979). *Leaf Area Index Estimates for Wheat from LANDSAT and Their Implications for Evapotranspiration and Crop Modeling1*. *Agronomy Journal - AGRON J* (Vol. 71). https://doi.org/10.2134/agronj1979.00021962007100020027x

Wójtowicz, M., Wójtowicz, A., & Piekarczyk, J. (2016). Application of Remote Sensing in Agriculture. *Communications in Biometry and Crop Science*, *11*(1), 31–50.

Xin, Q., Gong, P., Yu, C., Yu, L., Broich, M., Suyker, A. E., & Myneni, R. B. (2013). A production efficiency model-based method for satellite estimates of corn and soybean yields in the midwestern US. *Remote Sensing*, *5*(11), 5926–5943. https://doi.org/10.3390/rs5115926

Xue, J., & Su, B. (2017). Significant Remote Sensing Vegetation Indices: A Review of Developments and Applications. *Journal of Sensors*, *2017*, 1–17. https://doi.org/10.1155/2017/1353691

Yang, G., Yang, X., Zhang, X., Li, Z., Liu, J., Zhu, D., … Huang, Y. (2017). Unmanned Aerial Vehicle Remote Sensing for Field-Based Crop Phenotyping: Current Status and Perspectives. *Frontiers in Plant Science*, *8*(June). https://doi.org/10.3389/fpls.2017.01111

Yao, F., Tang, Y., Wang, P., & Zhang, J. (2015). Estimation of maize yield by using a process-based model and remote sensing data in the Northeast China Plain. *Physics and Chemistry of the Earth, Parts A/B/C, 87–88*, 142–152. https://doi.org/10.1016/j.pce.2015.08.010

You, J., Li, X., Low, M., Lobell, D., & Ermon, S. (2017). Deep gaussian process for crop yield prediction based on remote sensing data. In *Thirty-First AAAI Conference on Artificial Intelligence*.

Yu, B., & Shang, S. (2017). Multi-year mapping of maize and sunflower in hetao irrigation district of china with high spatial and temporal resolution vegetation index series. *Remote Sensing*, *9*(8). https://doi.org/10.3390/rs9080855

Zaman-Allah, M., Vergara, O., Araus, J. L., Tarekegne, A., Magorokosho, C., Zarco-Tejada, P. J., … Cairns, J. (2015). Unmanned aerial platform-based multi-spectral imaging for field phenotyping of maize. *Plant Methods*, *11*(1), 1–10. https://doi.org/10.1186/s13007-015-0078-2

Zarco-Tejada, P. J., Berjon, A., R.Lopez-Lozano, Miller, J. R., Martın, P., Cachorro, V., … A. (2005). Assessing vineyard condition with hyperspectral indices : Leaf and canopy reflectance simulation in a row-structured discontinuous canopy. *Remote Sensing of Environment*, *99*, 271–287. https://doi.org/10.1016/j.rse.2005.09.002

Zhang, C., & Kovacs, J. M. (2012). The application of small unmanned aerial systems for precision agriculture: A review. *Precision Agriculture*, *13*(6), 693–712. https://doi.org/10.1007/s11119-012-9274-5

Zhao, Y., Chen, S., & Shen, S. (2013). Assimilating remote sensing information with crop model using Ensemble Kalman Filter for improving LAI monitoring and yield estimation. *Ecological Modelling*, *270*, 30–42. https://doi.org/10.1016/j.ecolmodel.2013.08.016

Zheng, G., & Moskal, L. M. (2009). Retrieving Leaf Area Index (LAI) Using Remote Sensing: Theories, Methods and Sensors. *Sensors*, *9*, 2719–2745. https://doi.org/10.3390/s90402719

APPENDIX

Appendix 1. *The code in R to calculate NDVI from Landsat-8 images*

```
setwd("D:/Thesis_data/Landsat/cut")
library(raster)
library(rgdal)

L0105 = brick("1-5.tif")
L0110 = brick("1-10.tif")
L0508 = brick("5-8.tif")
L0609 = brick("6-9.tif")
L0810 = brick("8-10.tif")
L1106 = brick("11-6.tif")
L1408 = brick("14-8.tif")
L1509 = brick("15-9.tif")
L1705 = brick("17-5.tif")
L1710 = brick("17-10.tif")
L2007 = brick("20-7.tif")
L2108 = brick("21-8.tif")
L2605 = brick("26-5.tif")
L2706 = brick("27-6.tif")
L2907 = brick("29-7.tif")
L3008 = brick("30-8.tif")

red = L0105[[3]]
nir = L0105[[4]]
ndvi = (nir - red)/(nir + red)
setwd("D:/Thesis_data/Landsat/NDVI")
writeRaster(ndvi,filename = "1-5.tif",format="GTiff",overwrite=TRUE)

red = L0110[[3]]
nir = L0110[[4]]
ndvi = (nir - red)/(nir + red)
writeRaster(ndvi,filename = "1-10.tif",format="GTiff",overwrite=TRUE)

red = L0508[[3]]
nir = L0508[[4]]
ndvi = (nir - red)/(nir + red)
writeRaster(ndvi,filename = "5-8.tif",format="GTiff",overwrite=TRUE)

red = L0609[[3]]
nir = L0609[[4]]
ndvi = (nir - red)/(nir + red)
writeRaster(ndvi,filename = "6-9.tif",format="GTiff",overwrite=TRUE)
```

The code in R to calculate EVI, SAVI, WDRVI, GNDVI was written similarly to NDVI.

Appendix 2. *The code in R to calculate NDVI from Sentinel-2 images*

```
setwd("D:/Thesis_data/Sentinel 2/cut")
library(raster)
library(rgdal)

L0108 = brick("1-8.tif")
L0207 = brick("2-7.tif")
L0209 = brick("2-9.tif")
L0509 = brick("5-9.tif")
L0608 = brick("6-8.tif")
L0706 = brick("7-6.tif")
L0907 = brick("9-7.tif")
L1010 = brick("10-10.tif")
L1206 = brick("12-6.tif")
L1207 = brick("12-7.tif")
L1209 = brick("12-9.tif")
L1308 = brick("13-8.tif")
L1509 = brick("15-9.tif")
L1510 = brick("15-10.tif")
L1608 = brick("16-8.tif")
L1805 = brick("18-5.tif")
L1808 = brick("18-8.tif")
L1906 = brick("19-6.tif")
L1907 = brick("19-7.tif")
L2108 = brick("21-8.tif")
L2308 = brick("23-8.tif")
L2406 = brick("24-6.tif")
L2407 = brick("24-7.tif")
L2509 = brick("25-9.tif")
L2608 = brick("26-8.tif")
L2706 = brick("27-6.tif")
L2707 = brick("27-7.tif")
L2906 = brick("29-6.tif")
L2907 = brick("29-7.tif")
L3009 = brick("30-9.tif")
L3108 = brick("31-8.tif")

red = L0108[[3]]
nir = L0108[[4]]
ndvi = (nir - red)/(nir + red)

setwd("D:/Thesis_data/Sentinel 2/NDVI")
writeRaster(ndvi,filename = "1-8.tif",format="GTiff",overwrite=TRUE)
```

The code in R to calculate EVI, SAVI, WDRVI, GNDVI was written similarly to NDVI.

Appendix 3. *The code in R to extract Landsat-8 NDVI value by zonal statistic function*

```r
setwd("D:/Thesis_data/Landsat/NDVI")
library(raster)
library(rgdal)

L0105 = raster("1-5.tif")
L0110 = raster("1-10.tif")
L0508 = raster("5-8.tif")
L0609 = raster("6-9.tif")
L0810 = raster("8-10.tif")
L1106 = raster("11-6.tif")
L1408 = raster("14-8.tif")
L1509 = raster("15-9.tif")
L1705 = raster("17-5.tif")
L1710 = raster("17-10.tif")
L2007 = raster("20-7.tif")
L2108 = raster("21-8.tif")
L2605 = raster("26-5.tif")
L2706 = raster("27-6.tif")
L2907 = raster("29-7.tif")
L3008 = raster("30-8.tif")

shp = readOGR("D:/CAO HOC/Hoc ky 2 2017-2018 Turkey/Precision AG/Data/field border","field")

z0105 = extract(L0105, shp, fun = mean, df = T, na.rm = T)
z0110 = extract(L0110, shp, fun = mean, df = T, na.rm = T)
z0508 = extract(L0508, shp, fun = mean, df = T, na.rm = T)
z0609 = extract(L0609, shp, fun = mean, df = T, na.rm = T)
z0810 = extract(L0810, shp, fun = mean, df = T, na.rm = T)
z1106 = extract(L1106, shp, fun = mean, df = T, na.rm = T)
z1408 = extract(L1408, shp, fun = mean, df = T, na.rm = T)
z1509 = extract(L1509, shp, fun = mean, df = T, na.rm = T)
z1705 = extract(L1705, shp, fun = mean, df = T, na.rm = T)
z1710 = extract(L1710, shp, fun = mean, df = T, na.rm = T)
z2007 = extract(L2007, shp, fun = mean, df = T, na.rm = T)
z2108 = extract(L2108, shp, fun = mean, df = T, na.rm = T)
z2605 = extract(L2605, shp, fun = mean, df = T, na.rm = T)
z2706 = extract(L2706, shp, fun = mean, df = T, na.rm = T)
z2907 = extract(L2907, shp, fun = mean, df = T, na.rm = T)
z3008 = extract(L3008, shp, fun = mean, df = T, na.rm = T)

dfall = Reduce(function(x, y) merge(x, y, all=TRUE), list(z0105,z1705,z2605,z1106,z2706,z2007,
                                                          z2907,z0508,z1408,z2108,z3008,z0609,
                                                          z1509,z0110,z0810,z1710))

write.csv(dfall, file="D:/Thesis_data/Landsat/Zonal statistic/NDVI.csv")
```

The code for the others VIs and VIs derived from Sentinel-2 image were similar.

Appendix 4. *The code in R to make the correlation plots and select possible models by BMA package from the Landsat-8 VI values*

```
setwd("D:/Thesis_data/Landsat/Zonal statistic")
library(psych)

MAX = read.csv("L_MAX_n.csv",header = T)
MEAN = read.csv("L_MEAN_n.csv",header = T)
HAR = read.csv("L_HARVEST_n.csv",header = T)

attach(MAX)
dd = cbind(Yield, NDVI, EVI, SAVI, WDRVI, GNDVI)
pairs.panels(dd)

attach(MEAN)
dd = cbind(Yield, NDVI, EVI, SAVI, WDRVI, GNDVI)
pairs.panels(dd)

attach(HAR)
dd = cbind(Yield, NDVI, EVI, SAVI, WDRVI, GNDVI)
pairs.panels(dd)

# Build model by BMA ----------------------------------------------------

library(BMA)
attach(MAX)
X = cbind(NDVI,EVI,SAVI,WDRVI,GNDVI)
Y = MAX$Yield
Model = bicreg(X,Y, strict = F, OR = 20)
summary(Model)
write.csv(summary(Model), file = "D:/Thesis_data/Landsat/Zonal statistic/Model/L_MAX_n.csv")

attach(MEAN)
X = cbind(NDVI,EVI,SAVI,WDRVI,GNDVI)
Y = MEAN$Yield
Model = bicreg(X,Y, strict = F, OR = 20)
summary(Model)
write.csv(summary(Model), file = "D:/Thesis_data/Landsat/Zonal statistic/Model/L_MEAN_n.csv")

attach(HAR)
X = cbind(NDVI,EVI,SAVI,WDRVI,GNDVI)
Y = HAR$Yield
Model = bicreg(X,Y, strict = F, OR = 20)
summary(Model)
write.csv(summary(Model), file = "D:/Thesis_data/Landsat/Zonal statistic/Model/L_HAR_n.csv")
```

For Sentinel-2 data, the code was similar.

Appendix 5. *The code in R to build the interactive web application*

```
library(shiny)
library(shinydashboard)
library(plotly)
library(datasets)
library(dplyr)
library(leaflet)
library(rgdal)
library(raster)

L_MAX_n <- read.csv("L_MAX_n.csv",stringsAsFactors = F,header = T)
S_MAX_n <- read.csv("S_MAX_n.csv",stringsAsFactors = F,header = T)
S_index <- read.csv("S_index_2.csv",stringsAsFactors = F,header = T)
L_index <- read.csv("L_index_2.csv",stringsAsFactors = F,header = T)

f = readOGR("field_84.shp",layer = "field_84",GDAL1_integer64_policy = T)
y1 = raster("yield_L.tif")
y2 = raster("yield_S.tif")

pal = colorNumeric(c("#ffeda0", "#feb24c", "#f03b20"), values(y2), na.color = "transparent")
pal1 = colorNumeric(c("#ffeda0", "#feb24c", "#f03b20"), values(y1), na.color = "transparent")

ui <- dashboardPage(
  dashboardHeader(title = "NGHI's Thesis - GIS and RS in Precision Agriculture - Corn Yield Prediction",
                  titleWidth = 700,
                  tags$li(class="dropdown",tags$a(href="https://www.researchgate.net/profile/Nghi_Do",
                                                  icon("user-secret"),"My Researchgate",target="_blank")),
                  tags$li(class="dropdown",tags$a(href="https://www.facebook.com/nghi.rex",
                                                  icon("facebook-square"),"My Facebook",target="_blank"))
                  ),
  dashboardSidebar(
    sidebarMenu(
      menuItem(text = "About",tabName ="about",icon=icon("info-circle")),
      menuItem("Map",tabName = "map",icon = icon("map")),
      menuItem("Data",icon = icon("database"),
               menuSubItem("Landsat8 Index",tabName = "landsat8",icon = icon("rocket")),
               menuSubItem("Sentinel2 Index",tabName = "sentinel2",icon = icon("plane"))),
      menuItem("VIs Time series",tabName = "VI",icon = icon("leaf")),
      menuItem("Charts",tabName = "charts",icon = icon("line-chart")),
      menuItem("My GitHub",href = "https://github.com/tannghi91",
               icon = icon("github")))
  ),

  dashboardBody(
    tabItems(
      tabItem(tabName = "about",
              fluidRow(imageOutput("pic"),
              fluidRow(box(h3("Hi everyone,"),
                       h3("I am a master science candidate of the Department
                          of Remote Sensing and Geographical Information Systems,
                          Eskisehir Technical University, Eskisehir, Turkey."),
                       h3("I am working as a lecturer at the Department of
                          Geography and Land administration, Quy Nhon University,
                          Binh Dinh, Vietnam."),
                       h3("My current research interests are GIS analysis,
                          Spatial analysis, Remote sensing and Data science."),width=12)))),
      tabItem(tabName = "map",leafletOutput("ymap", height = 733)),
      tabItem(tabName = "landsat8",dataTableOutput("mydata1")),
      tabItem(tabName = "sentinel2",dataTableOutput("mydata2")),
      tabItem(tabName = "charts",
              fluidRow(box(title = "LANDSAT8 SCATTER PLOT BOX",plotlyOutput("plot1",height = 300),
                           status = "danger",solidHeader = T),
                       box(title = "SENTINEL2 SCATTER PLOT BOX",plotlyOutput("plot3",height = 300),
                           status = "success",solidHeader = T),
                       fluidRow(box(title = " L8 PARAMETER BOX",uiOutput("inputpara"),
                                    width=3,status = "warning",solidHeader = T),
                                box(title = "YIELD 2018 PLOT BOX",plotlyOutput("plot2",height = 270),
                                    status = "info",solidHeader = T),
                                box(title = "S2 PARAMETER BOX",uiOutput("inputpara1"),
                                    width=3,status = "warning",solidHeader = T))
                       )
              ),
      tabItem(tabName = "VI",
              fluidRow(box(title = "LANDSAT8 VEGETATION INDEX BOX",plotlyOutput("plot4",height = 350),
                           status = "danger",solidHeader = T),
                       box(title = "SENTINEL2 VEGETATION INDEX BOX",plotlyOutput("plot5",height = 350),
                           status = "success",solidHeader = T),
                       fluidRow(box(title = " L8 PARAMETER BOX",uiOutput("inputpara2"),
                                    width=6,status = "warning",solidHeader = T),
                                box(title = "S2 PARAMETER BOX",uiOutput("inputpara3"),
                                    width=6,status = "warning",solidHeader = T))
              )
      )
    )
  )
)
```

```r
# Define server logic required to draw a histogram
server <- function(input, output) {
  output$mydata1 <- renderDataTable({
    L_MAX_n
  })
  output$pic <- renderImage({return(list(src="avatar.png",contentType=("image/png"),
                                       height=390))},deleteFile = F)
  output$mydata2 <- renderDataTable({
    S_MAX_n
  })
  output$plot1 <- renderPlotly({
    plot_ly(data=L_MAX_n,
            x=(L_MAX_n[,input$xaxis]),
            y=~Yield,
            type = "scatter",
            mode = "markers")%>%
      add_lines(y=~fitted(lm(Yield~(L_MAX_n[,input$xaxis]))),
                line=list(color="red"),showlegend = F)%>%
      layout(xaxis = list(title="Vegetation Index"),
             yaxis = list(title="Yield (t/ha)"))
  })
  output$plot2 <- renderPlotly({
    plot_ly(data=L_MAX_n, x=~Name_ID, y=~Yield, type="bar")%>%
      layout(xaxis = list(title="Study fields"),
             yaxis = list(title="Yield (t/ha)"))
  })
  output$plot3 <- renderPlotly({
    plot_ly(data=S_MAX_n,
            x=(S_MAX_n[,input$xaxis1]),
            y=~Yield,
            type = "scatter",
            mode = "markers")%>%
      add_lines(y=~fitted(lm(Yield~(S_MAX_n[,input$xaxis1]))),
                line=list(color="red"),showlegend = F)%>%
      layout(xaxis = list(title="Vegetation Index"),
             yaxis = list(title="Yield (t/ha)"))
  })
  output$plot4 <- renderPlotly({
    plot_ly(data=L_index,x=~DOY,y=(L_index[,input$yaxis1]),type = "scatter",
            mode = 'lines',color = ~Field)%>%
      layout(yaxis= list(title="Vegetation Index"),
             xaxis= list(title="Day of Year"))
  })
```

```r
  output$plot5 <- renderPlotly({
    plot_ly(data=S_index,x=~DOY,y=(S_index[,input$yaxis2]),type = "scatter",
            mode = 'lines',color = ~Field)%>%
      layout(yaxis= list(title="Vegetation Index"),
             xaxis= list(title="Day of Year"))
  })
  output$inputpara <- renderUI({
    selectInput(inputId = "xaxis","Select the X variable",
                choices = names(L_MAX_n),selected = "NDVI")
  })
  output$inputpara1 <- renderUI({
    selectInput(inputId = "xaxis1","Select the X variable",
                choices = names(S_MAX_n),selected = "NDVI")
  })
  output$inputpara2 <- renderUI({
    selectInput(inputId = "yaxis1","Select the Vegetation Index",
                choices = names(L_index),selected = "NDVI")
  })
  output$inputpara3 <- renderUI({
    selectInput(inputId = "yaxis2","Select the Vegetation Index",
                choices = names(S_index),selected = "NDVI")
  })
```